

Award Number: W81XWH-12-1-0604

TITLE: Deciphering the Adaptive Immune Response to Ovarian Cancer

PRINCIPAL INVESTIGATOR:

Brad H. Nelson, Ph.D.

CONTRACTING ORGANIZATION:

British Columbia Cancer Agency,  
2410 Lee Avenue,  
Victoria BC V8R 6V5  
Canada

REPORT DATE:

October 2013

TYPE OF REPORT:

Annual

PREPARED FOR: U.S. Army Medical Research and Materiel Command  
Fort Detrick, Maryland 21702-5012

DISTRIBUTION STATEMENT: Approved for Public Release;  
Distribution Unlimited

The views, opinions and/or findings contained in this report are those of the author(s) and should not be construed as an official Department of the Army position, policy or decision unless so designated by other documentation.

<b>REPORT DOCUMENTATION PAGE</b>			Form Approved OMB No. 0704-0188		
Public reporting burden for this collection of information is estimated to average 1 hour per response, including the time for reviewing instructions, searching existing data sources, gathering and maintaining the data needed, and completing and reviewing this collection of information. Send comments regarding this burden estimate or any other aspect of this collection of information, including suggestions for reducing this burden to Department of Defense, Washington Headquarters Services, Directorate for Information Operations and Reports (0704-0188), 1215 Jefferson Davis Highway, Suite 1204, Arlington, VA 22202-4302. Respondents should be aware that notwithstanding any other provision of law, no person shall be subject to any penalty for failing to comply with a collection of information if it does not display a currently valid OMB control number. <b>PLEASE DO NOT RETURN YOUR FORM TO THE ABOVE ADDRESS.</b>					
<b>1. REPORT DATE (DD-MM-YYYY)</b> Oct 2013		<b>2. REPORT TYPE</b> Annual		<b>3. DATES COVERED (From - To)</b> Sept 30, 2012- Sept 29, 2013	
<b>4. TITLE AND SUBTITLE</b> Deciphering the Adaptive Immune Response to Ovarian Cancer			<b>5a. CONTRACT NUMBER</b>		
			<b>5b. GRANT NUMBER</b> W81XWH-12-1-0604		
			<b>5c. PROGRAM ELEMENT NUMBER</b>		
<b>6. AUTHOR(S)</b> Brad H. Nelson, Ph.D. bnelson@bccancer.bc.ca			<b>5d. PROJECT NUMBER</b>		
			<b>5e. TASK NUMBER</b>		
			<b>5f. WORK UNIT NUMBER</b>		
<b>7. PERFORMING ORGANIZATION NAME(S) AND ADDRESS(ES)</b>  British Columbia Cancer Agency, 2410 Lee Avenue, Victoria BC V8R 6V5 Canada			<b>8. PERFORMING ORGANIZATION REPORT NUMBER</b>		
<b>9. SPONSORING / MONITORING AGENCY NAME(S) AND ADDRESS(ES)</b> US Army Medical Research and Material Command Fort Detrick, Maryland 21702-5012			<b>10. SPONSOR/MONITOR'S ACRONYM(S)</b>		
			<b>11. SPONSOR/MONITOR'S REPORT NUMBER(S)</b>		
<b>12. DISTRIBUTION / AVAILABILITY STATEMENT</b> Approved for public release; distribution unlimited					
<b>13. SUPPLEMENTARY NOTES</b>					
<b>14. ABSTRACT</b> The presence of CD8+ tumor-infiltrating lymphocytes (CD8+ TIL) has been associated with increased patient survival in ovarian cancer. We discovered that this effect is even stronger when CD8+ TIL are found together with CD20+ B cells and CD4+FoxP3+ T cells. We hypothesized that CD20+ TIL contribute to tumor immunity by presenting antigens to CD4+ and CD8+ TIL. To test this, we are attempting to identify the tumor antigens recognized by CD20+ TIL. As a first step, this year we developed methods to clone immunoglobulin molecules from individual CD20+ TIL by single-cell reverse-transcriptase PCR. We also hypothesized that a subset of CD4+FoxP3+ TIL produces effector cytokines that enhance CD8+ TIL responses. This year, we developed methods to profile T cell receptors (TCR) from tumor-infiltrating T cells, which will facilitate future TCR cloning and antigen identification, as originally proposed. Overall, this project is progressing on schedule and is yielding innovative methods and publishable results that lead toward a better understanding of the mechanisms used by the immune system to control the progression of ovarian cancer.					
<b>15. SUBJECT TERMS</b> Tumor immunology, immunotherapy, ovarian cancer, antibody, T cell, tumor antigen					
<b>16. SECURITY CLASSIFICATION OF:</b>			<b>17. LIMITATION OF ABSTRACT</b>  UU	<b>18. NUMBER OF PAGES</b>  50	<b>19a. NAME OF RESPONSIBLE PERSON</b> USAMRMC
<b>a. REPORT</b> U	<b>b. ABSTRACT</b> U	<b>c. THIS PAGE</b> U			<b>19b. TELEPHONE NUMBER (include area code)</b>

## Table of Contents

	<u>Page</u>
<b>Introduction.....</b>	<b>4</b>
<b>Body.....</b>	<b>4</b>
<b>Key Research Accomplishments.....</b>	<b>7</b>
<b>Reportable Outcomes.....</b>	<b>8</b>
<b>Conclusion.....</b>	<b>11</b>
<b>References.....</b>	<b>11</b>
<b>Appendices.....</b>	<b>12</b>
<b>Supporting Data.....</b>	<b>12</b>
<b>Figures.....</b>	<b>13</b>

**W81XWH-12-1-0604 (OC110435) Annual Report, Oct 2013**

PI: Brad H. Nelson, Ph.D.

Co-PIs: Rob Holt, Ph.D., John Webb Ph.D., Peter Watson, M.D.

Title of Project: Deciphering the Adaptive Immune Response to Ovarian Cancer

**INTRODUCTION:**

Tumor-infiltrating CD8+ T cells are strongly associated with increased survival in ovarian cancer. However, they do not work in isolation. We discovered that two other types of immune cell play an important supportive role: B cells and helper T cells (specifically, helper T cells that express a protein called FoxP3). We made this discovery by performing a systematic analysis of immune cells in ovarian cancer. We found that killer T cells are often found in small clusters together with B cells and helper T cells. Importantly, we found that patients whose tumors have these combinations of immune cells have better survival rates than patients whose tumors contain killer T cells alone. This tells us that T cells and B cells work together to attack tumors. These findings have powerful clinical implications: to enhance the immune response to ovarian cancer, we need to enhance the activity of all three types of immune cell, rather than killer T cells alone.

To explain these observations, we hypothesized that B cells serve as “organizers” that help to draw T cells into the tumor. In addition, B cells might present tumor proteins to the T cells to facilitate tumor recognition. We further hypothesized that FoxP3 helper T cells might produce cytokines that help to excite the killer T cells. To test these hypotheses, we proposed to determine which tumor proteins (antigens) are recognized by B cells and FoxP3 helper T cells in ovarian cancer. By identifying these antigens, we will be able to create new molecular tools to elucidate how the immune system recognizes and attacks ovarian cancer. The study has four tasks:

Task 1. To identify tumor antigens recognized by CD20+ TIL.

Task 2. To identify tumor antigens recognized by CD4+FoxP3+ TIL.

Task 3. To determine whether tumor-infiltrating B cells and T cells recognize the same antigens.

Task 4. To assess the functional phenotype of antigen-specific CD4+FoxP3+ TIL.

Significance: The immune system has a profound influence on survival from ovarian cancer. With better understanding of the immune response, it will be possible to design new treatments such as vaccines that enhance tumor immunity and increase patient survival. We envision our work will lead to a major re-think about cancer vaccines: instead of simply trying to activate killer T cells, we also need to find effective ways to activate their team mates, the B cells and FoxP3+ helper T cells.

**BODY:****Task 1. To identify tumor antigens recognized by CD20+ TIL.**

In this task, we proposed to identify the antigens recognized by the 3 most abundant CD20+ TIL clones from each of 3 ovarian cancer patients. To accomplish this, we proposed to clone immunoglobulin G (IgG) molecules from individual CD20+ TIL. These will be used to identify the corresponding antigens using three different approaches: candidate antigen assays, cDNA library screening, and mass spectrometry.

**Progress to date:****Generating IgG and TCR profiles from ovarian tumor specimens**

To identify the 3 most abundant IgG (for Task 1) and TCR clones (for Task 2) in each patient's tumor, we are using deep sequencing methods developed in the Holt lab. Our approach for deep sequence analysis of T cell receptor (TCR) beta chain diversity has been previously described (1, 2), and we have recently made adaptations to enable B cell receptor (BCR) heavy chain profiling and sample multiplexing, as described below. For the present investigation, we isolated total RNA from bulk ascites from the three HGSC ovarian cancer study subjects at three different timepoints (the time of primary disease, at first recurrence, and at second recurrence). First strand cDNA was synthesized from total RNA using either TCR beta chain or BCR heavy chain gene-specific primers, and this cDNA was then used as template to amplify the CDR3 sequences from each receptor population by PCR. The CDR3 region is the site of VDJ recombination and is the most highly variable and thus most informative region for the purpose of profiling repertoire diversity. The PCR primers were tagged with unique, 6 base pair, error tolerant barcode sequences. A different barcode was used for each individual sample. The CDR3 amplicons were then subjected to several additional rounds of nested PCR using primers tailed with Illumina adapter sequences necessary for annealing to the Illumina flow cell surface for massively parallel sequencing. The samples were pooled and sequenced using a single flow cell and the Illumina miSeq platform. Sequence data was then de-convoluted based on the barcode identifiers, and the TCR and BCR CDR3 sequences were filtered to remove low quality reads, then clustered using standard bioinformatic methods. Clustering was done to determine the number of distinct CDR3 sequences present in each sample, which reflects the diversity of distinct T-cell and B-cell clonotypes with the original ascites specimens. Prior to reverse transcription and PCR each sample was spiked with RNA from a single, known clonotype in order to monitor PCR and sequence error rates and the efficiency of sequence recovery.

So far, we have filtered and analyzed the sequence data derived from specimens taken from each of the three timepoints for one of the three study subjects. We obtained over 30,000 total TCR beta chain CDR3 sequences from each of these three samples, and over 15,000 total BCR heavy chain CDR3 sequences from each of these same three samples. These collapsed, upon clustering, into a much smaller number of distinct sequences. Specifically there were 1,598 distinct TCR sequences and 688 distinct BCR sequences observed per sample. However, as expected, the majority of these unique sequences were "singletons", representing rare clonotypes, with the bulk of the accumulated sequence data from each sample represented approximately 30 clonotypes per sample. Thus the ascites repertoires are polyclonal, but not to the same extent as peripheral blood, where previously we have been able to detect over a million distinct sequences from a single sample by deep sequencing. Interestingly, 18 of the BCR clonotypes were detectable at all three timepoints, albeit with varying abundance, but the TCR clonotypes were much more sample specific, with only one TCR clonotype being present in all three samples.

**Amplification of matched IgG heavy and light chains by single-cell RT-PCR**

Single cell sorting and PCR amplification of matched immunoglobulin (Ig) heavy and light chains from tumor-infiltrating B lymphocytes is being accomplished via the methods of Tiller et al. (3). Single B cells are isolated based on their surface expression of CD19, CD20 and IgG using a BD Influx cell sorter. Individual cells are sorted directly into single wells of 96-well PCR plates. Reverse transcription is accomplished directly within the sorting plate, which yields cDNA corresponding to the original single cell. This cDNA is then split equally between four separate PCR reactions, one each for the variable portions of Ig heavy, kappa, and lambda, and

one for the control housekeeping gene GAPDH. The variable portions of the immunoglobulin genes are then amplified by sequential nested multiplex PCR using primer sets known to amplify all human variable and joining gene segments and containing restriction enzyme cut sites to facilitate downstream molecular cloning. To date we have successfully amplified matched pairs of Ig genes from B cells isolated from the tumors of three high-grade serous ovarian cancer patients (Figure 1). Roughly 70% of all sorting wells yield amplification of at least one B cell-specific gene product, while about 10-25% yield matched pairs of heavy and light chains. In total, we have successfully amplified 28 pairs of Ig genes from the 3 patients.

#### Cloning of CDR3 regions into IgG expression vectors

Molecular cloning of the PCR amplified variable portions of matched heavy and light chain genes derived from single sorted tumor infiltrating B cells is accomplished by standard techniques. All pairs that have been amplified have subsequently been cloned into appropriate expression vectors containing the signal sequence and constant portions of the corresponding germline immunoglobulin chain (heavy, kappa, lambda). Once inserted into these expression vectors, the DNA sequence of each immunoglobulin chain is determined by Sanger sequencing. Sequences for each of the pairs of heavy and light chains have been obtained (Figure 2). We are currently evaluating the prevalence of each immunoglobulin heavy sequence by sequencing samples prepared by conventional RT-PCR of bulk tumor preparations.

#### Preparation of recombinant IgG (rIgG)

To produce recombinant IgG, two expression vectors encoding cloned matched heavy and light chain variable portions are co-transfected into log-phase 293T cells. This transient transfection is accomplished by a calcium phosphate precipitation method. After seven days in culture, the supernatant is harvested and assessed for the presence of rIgG by human IgG-specific western blot. Fully assembled IgG molecules (~150 kDa) are observed in the supernatant of 80-90% of culture transfected with different pairs of expression vectors (Figure 3) under non-reducing conditions. To isolate rIgG from the culture supernatant, it is concentrated and run over protein G sepharose columns. Captured IgG molecules are eluted at low pH and the resulting eluate is neutralized and desalted. Further concentration and assessment of purity is accomplished by BCA assay and additional western blot analysis. To date, 11 recombinant antibodies have successfully been expressed in vitro from 14 different matched Ig pairs. Based on this, we expect to have an 80% success rate in the production of rIgG from the remaining cloned Ig pairs.

#### **Task 2. To identify tumor antigens recognized by CD4+FoxP3+ TIL.**

We proposed to clone TCR molecules from CD4+FoxP3+ tumor-infiltrating T cells from the 3 ovarian cancer patients described above. Cloned TCR's will be expressed in a hybridoma cell line, which in turn will be used to identify the underlying antigens using a candidate approach and/or cDNA library screening.

#### **Progress to date:**

#### Amplification of paired TCR-alpha and -beta CDR3 regions by single-cell RT-PCR

We are developing single-cell analytical methods for profiling CDR3 sequences from paired alpha and beta subunits. To date, large-scale T-cell repertoire analysis has been limited to interrogation of a single TCR subunit, usually the beta chain, per sequencing run (as described for Task 1). Recently, however, the potential for pairwise Illumina sequencing of  $\alpha\beta$ TCRs has been demonstrated, by means of alpha and beta chain fusion PCR executed within single cell containing droplets of water in oil emulsions (4). Using this approach, hundreds of  $\alpha\beta$ TCR sequences could be identified from starting populations of greater than 1 million total

cells. Likewise, it was recently demonstrated that thousands of immunoglobulin heavy and light chain pairs can be obtained by bead capture of single B-cell mRNA followed by linkage PCR in single bead-containing emulsion droplets (5). While the yield of each of these approaches is modest, they represent important advances towards the goal of deep, cheap and fast profiling of dimeric antigen receptors. We have been pursuing pairwise sequencing of  $\alpha\beta$ TCRs and have established a unique method for fusion of  $\alpha\beta$ TCR cDNAs during reverse transcription. We have demonstrated this approach using bulk RNA from Jurkat cells, which are a T cell line expressing a defined  $\alpha\beta$ TCR (Figure 4). We are working to adapt this system to a single cell microfluidics platform in order to establish a robust single cell assay amenable to deep sequencing on the Illumina platform. In future, this assay will allow us to move from deep TCR sequence profiling data directly to receptor reconstitution (using TCR expression vectors we now have in hand, generously provided by our colleague Klaus Dornmair, Univ. of Munich) and then antigen screening. Thus, we are making excellent progress in terms of developing the necessary technology to complete Task 2.

**Task 3. To determine whether tumor-infiltrating B cells and T cells recognize the same antigens.**

Once we have identified cognate antigens for the predominant CD8+ (from the original IDEA proposal), CD20+ (Task 1) and CD4+FoxP3+ (Task 2) TIL, we proposed to assess the extent to which these antigen sets overlap. If the antigens recognized by CD20+ TIL are also recognized by CD8+ or CD4+ TIL, this would support our hypothesis that CD20+ TIL can serve as APC in the tumor environment.

**Progress to date:**

This task is not scheduled to start until Year 2.

**Task 4. To assess the functional phenotype of antigen-specific CD4+FoxP3+ TIL.**

CD4+FoxP3+ TIL show great functional heterogeneity in EOC, which makes it difficult to draw definitive conclusions about their role in the tumor environment. With knowledge of their cognate antigens, we will be able to clarify this issue by assessing the functional phenotype of individual CD4+FoxP3+ T cell clones as opposed to bulk cell preparations. We proposed to do this by constructing MHC class II tetramers, which bind specifically to CD4+ T cells expressing TCRs relevant to a particular antigen.

**Progress to date:**

This task is not scheduled to start until Year 2.

**KEY RESEARCH ACCOMPLISHMENTS:**

1. We published a key manuscript describing the results of the original IDEA award: Castellarin M, Milne K, Zeng T, Tse K, Mayo M, Zhao Y, Webb JR, Watson PH, Nelson BH, Holt RA. Clonal evolution of high-grade serous ovarian carcinoma from primary to recurrent disease. *J Pathol.* 2013 Mar;229(4):515-24. doi:10.1002/path.4105. Epub 2012 Nov 29. PubMed PMID: 22996961. (**Appendix A**)
- A second key manuscript from the original IDEA award is under revision at *Clinical Cancer Research* (with an enthusiastic invitation to re-submit): Wick, D., Webb, J.R., Nielsen, J.S., Martin, S., Kroeger, D.R., Milne, K., Castellarin, M., Twumasi-Boateng, K., Watson, P.H., Holt, R.H., Nelson, B.H. 2013. Surveillance of the tumor mutanome by T cells during progression from primary to recurrent ovarian cancer. *Clin Cancer Res*, in revision.

- As listed below, in 2012-2013 our team published 9 other manuscripts with direct relevance to this project, and 16 with indirect relevance.
- Task 1: Illumina-based IgG profiling has been completed for 3 patients at 3 time points.
- Task 1: Robust methods have been developed to amplify matched IgG heavy and light chains by single-cell RT-PCR.
- Task 1: Robust methods have been developed to clone CDR3 regions into IgG expression vectors.
- Task 1: Robust methods have been developed to prepare recombinant IgG (rlgG).
- Task 2: Illumina-based profiling of TCRs has been completed for 3 patients at 3 time points; the next step is to do this for the CD4+CD25+ subset.
- Task 2: Robust methods have been developed to amplify paired TCR-alpha and -beta CDR3 regions by single-cell RT-PCR; the next step is to insert these into expression vectors and transfect murine T cell hybridoma cells.

## REPORTABLE OUTCOMES:

### Manuscripts with direct relevance published by the team in 2012/2013:

1. Castellarin M, Milne K, Zeng T, Tse K, Mayo M, Zhao Y, Webb JR, Watson PH, Nelson BH, Holt RA. Clonal evolution of high-grade serous ovarian carcinoma from primary to recurrent disease. *J Pathol.* 2013 Mar;229(4):515-24. doi:10.1002/path.4105. Epub 2012 Nov 29. PubMed PMID: 22996961. (**Appendix A**)
2. Nielsen JS, Sahota RA, Milne K, Kost SE, Nesslinger NJ, Watson PH, Nelson BH. CD20+ tumor-infiltrating lymphocytes have an atypical CD27- memory phenotype and together with CD8+ T cells promote favorable prognosis in ovarian cancer. *Clin Cancer Res.* 2012 Jun 15;18(12):3281-92. doi: 10.1158/1078-0432.CCR-12-0234. Epub 2012 May 2. PubMed PMID: 22553348. (**Appendix B**)
3. deLeeuw RJ, Kost SE, Kakal JA, Nelson BH. The prognostic value of FoxP3+ tumor-infiltrating lymphocytes in cancer: a critical review of the literature. *Clin Cancer Res.* 2012 Jun 1;18(11):3022-9. doi: 10.1158/1078-0432.CCR-11-3216. Epub 2012 Apr 17. Review. PubMed PMID: 22510350. (**Appendix C**)
4. Nielsen JS, Nelson BH. Tumor-infiltrating B cells and T cells: Working together to promote patient survival. *Oncoimmunology.* 2012 Dec 1;1(9):1623-1625. PubMed PMID: 23264915; PubMed Central PMCID: PMC3525624.
5. Watson CT, Steinberg KM, Huddleston J, Warren RL, Malig M, Schein J, Willsey AJ, Joy JB, Scott JK, Graves TA, Wilson RK, Holt RA, Eichler EE, Breden F. Complete haplotype sequence of the human immunoglobulin heavy-chain variable, diversity, and joining genes and characterization of allelic and copy-number variation. *Am J Hum Genet.* 2013 Apr 4;92(4):530-46. doi: 10.1016/j.ajhg.2013.03.004. Epub 2013 Mar 28. PubMed PMID: 23541343; PubMed Central PMCID: PMC3617388.
6. Warren RL, Choe G, Freeman DJ, Castellarin M, Munro S, Moore R, Holt RA. Derivation of HLA types from shotgun sequence datasets. *Genome Med.* 2012 Dec 10;4(12):95. [Epub ahead of print] PubMed PMID: 23228053; PubMed Central PMCID: PMC3580435.
7. Milne K, Alexander C, Webb JR, Sun W, Dillon K, Kalloger SE, Gilks CB, Clarke B, Köbel M, Nelson BH. Absolute lymphocyte count is associated with survival in ovarian cancer

independent of tumor-infiltrating lymphocytes. *J Transl Med.* 2012 Feb 27;10:33. doi: 10.1186/1479-5876-10-33. PubMed PMID: 22369276; PubMed Central PMCID: PMC3310776.

8. Nelson BH. Killer T cells to the rescue in ovarian cancer. *Gynecol Oncol.* 2012 Feb;124(2):178-9. doi: 10.1016/j.ygyno.2011.12.434. PubMed PMID: 22264602.
9. Woodsworth D., Castellarin M., Holt R.A. 2013. Sequence analysis of T-cell repertoires in health and disease. *Genome Medicine, in press.*
10. Webb, J.R., Milne, K., Watson, P.H., deLeeuw, R.D., and Nelson, B.H. 2013. Tumor-infiltrating lymphocytes expressing the tissue resident memory marker CD103 are associated with increased survival in high-grade serous ovarian cancer. *Clin Cancer Res, in press.*

#### **Manuscripts with indirect relevance published by the team in 2012/2013:**

1. Sio A, Chehal MK, Tsai K, Fan X, Roberts ME, Nelson BH, Grembecka J, Cierpicki T, Krebs DL, Harder KW. Dysregulated hematopoiesis caused by mammary cancer is associated with epigenetic changes and hox gene expression in hematopoietic cells. *Cancer Res.* 2013 Oct 1;73(19):5892-904. doi:10.1158/0008-5472.CAN-13-0842. Epub 2013 Aug 1. PubMed PMID: 23913828.
2. West NR, Kost SE, Martin SD, Milne K, Deleeuw RJ, Nelson BH, Watson PH. Tumour-infiltrating FOXP3(+) lymphocytes are associated with cytotoxic immune responses and good clinical outcome in oestrogen receptor-negative breast cancer. *Br J Cancer.* 2013 Jan 15;108(1):155-62. doi: 10.1038/bjc.2012.524. Epub 2012 Nov 20. PubMed PMID: 23169287; PubMed Central PMCID: PMC3553524.
3. Cancer Genome Atlas Research Network. The Cancer Genome Atlas Pan-Cancer analysis project. *Nat Genet.* 2013 Sep 26;45(10):1113-20. doi: 10.1038/ng.2764. PubMed PMID: 24071849.
4. Yan Y, Li X, Blanchard A, Bramwell VH, Pritchard KI, Tu D, Shepherd L, Myal Y, Penner C, Watson PH, Leygue E, Murphy LC. Expression of both estrogen receptor-beta 1 (ER- $\beta$ 1) and its co-regulator steroid receptor RNA activator protein (SRAP) are predictive for benefit from tamoxifen therapy in patients with estrogen receptor-alpha (ER- $\alpha$ )-negative early breast cancer (EBC). *Ann Oncol.* 2013 Aug;24(8):1986-93. doi: 10.1093/annonc/mdt132. Epub 2013 Apr 11. PubMed PMID: 23579816.
5. Cancer Genome Atlas Research Network. Comprehensive molecular characterization of clear cell renal cell carcinoma. *Nature.* 2013 Jul 4;499(7456):43-9. doi: 10.1038/nature12222. Epub 2013 Jun 23. PubMed PMID: 23792563; PubMed Central PMCID: PMC3771322.
6. Cancer Genome Atlas Research Network. Genomic and epigenomic landscapes of adult de novo acute myeloid leukemia. *N Engl J Med.* 2013 May 30;368(22):2059-74. doi: 10.1056/NEJMoa1301689. Epub 2013 May 1. Erratum in: *N Engl J Med.* 2013 Jul 4;369(1):98. PubMed PMID: 23634996; PubMed Central PMCID: PMC3767041.
7. Cancer Genome Atlas Research Network. Integrated genomic characterization of endometrial carcinoma. *Nature.* 2013 May 2;497(7447):67-73. doi: 10.1038/nature12113. Erratum in: *Nature.* 2013 Aug 8;500(7461):242. PubMed PMID: 23636398; PubMed Central PMCID: PMC3704730.

8. West NR, Murray JI, Watson PH. Oncostatin-M promotes phenotypic changes associated with mesenchymal and stem cell-like differentiation in breast cancer. *Oncogene*. 2013 Apr 15. doi: 10.1038/onc.2013.105. [Epub ahead of print] PubMed PMID: 23584474.
9. Cancer Genome Atlas Network. Comprehensive molecular portraits of human breast tumours. *Nature*. 2012 Oct 4;490(7418):61-70. doi: 10.1038/nature11412. Epub 2012 Sep 23. PubMed PMID: 23000897; PubMed Central PMCID: PMC3465532.
10. Cancer Genome Atlas Research Network. Comprehensive genomic characterization of squamous cell lung cancers. *Nature*. 2012 Sep 27;489(7417):519-25. doi: 10.1038/nature11404. Epub 2012 Sep 9. Erratum in: *Nature*. 2012 Nov 8;491(7423):288. Rogers, Kristen [corrected to Rodgers, Kristen]. PubMed PMID: 22960745; PubMed Central PMCID: PMC3466113.
11. Spowart JE, Townsend KN, Huwait H, Eshragh S, West NR, Ries JN, Kalloger S, Anglesio M, Gorski SM, Watson PH, Gilks CB, Huntsman DG, Lum JJ. The Autophagy Protein LC3A Correlates with Hypoxia and is a Prognostic Marker of Patient Survival in Clear Cell Ovarian Cancer. *J Pathol*. 2012 Aug 27. doi: 10.1002/path.4090. [Epub ahead of print] PubMed PMID: 22926683.
12. Cancer Genome Atlas Network. Comprehensive molecular characterization of human colon and rectal cancer. *Nature*. 2012 Jul 18;487(7407):330-7. doi: 10.1038/nature11252. PubMed PMID: 22810696; PubMed Central PMCID: PMC3401966.
13. McAlpine JN, Porter H, Köbel M, Nelson BH, Prentice LM, Kalloger SE, Senz J, Milne K, Ding J, Shah SP, Huntsman DG, Gilks CB. BRCA1 and BRCA2 mutations correlate with TP53 abnormalities and presence of immune cell infiltrates in ovarian high-grade serous carcinoma. *Mod Pathol*. 2012 May;25(5):740-50. doi: 10.1038/modpathol.2011.211. Epub 2012 Jan 27. PubMed PMID: 22282309.
14. West NR, Murphy LC, Watson PH. Oncostatin M suppresses oestrogen receptor- $\alpha$  expression and is associated with poor outcome in human breast cancer. *Endocr Relat Cancer*. 2012 Apr 10;19(2):181-95. doi: 10.1530/ERC-11-0326. Print 2012 Apr. PubMed PMID: 22267707.
15. Castellarin M, Warren RL, Freeman JD, Dreolini L, Krzywinski M, Strauss J, Barnes R, Watson P, Allen-Vercoe E, Moore RA, Holt RA. *Fusobacterium nucleatum* infection is prevalent in human colorectal carcinoma. *Genome Res*. 2012 Feb;22(2):299-306. doi: 10.1101/gr.126516.111. Epub 2011 Oct 18. PubMed PMID: 22009989; PubMed Central PMCID: PMC3266037.
16. Madhurantakam C, Duru AD, Sandalova T, Webb JR, Achour A. Inflammation-associated nitrotyrosination affects TCR recognition through reduced stability and alteration of the molecular surface of the MHC complex. *PLoS One*. 2012;7(3):e32805. doi: 10.1371/journal.pone.0032805. Epub 2012 Mar 14. PubMed PMID: 22431983; PubMed Central PMCID: PMC3303804.

**Leveraged funding:**

In 2012, we obtained three new grants that, although not directly relevant to ovarian cancer, are helping us to build our team and infrastructure in the cancer immunotherapy field:

1. The mutated lymphoma genome: a target for therapeutic vaccination

Source: Canadian Cancer Society Research Institute

Dates: 02/2013 – 01/2015

Term: 2 years

PI: Brad Nelson

The major goal of this project is to assess the immunogenicity of the lymphoma genome and develop personalized therapeutic vaccines.

2. Targeting the Breast Cancer Genome with Personalized Therapeutic Vaccines

Source: Canadian Breast Cancer Foundation BC/Yukon

Dates: 08/2012 – 07/2015

Term: 3 years

PI: Brad Nelson

The major goal of this project is to use genome and transcriptome sequencing data to design personalized cancer vaccines that target mutations and destroy spontaneous mammary tumours.

3. Small-molecule inhibitors of the PD1-PDL1 interaction for treating metastatic cancer

Source: Canadian Cancer Society Research Institute

Dates: 02/2013 – 01/2015

Term: 2 years

PI: Jeremy Wulff, Co-applicant: Brad Nelson

The major goal of this project is to develop small molecules that enhance anti-tumor T cell responses by inhibiting the PD1-PDL1 interaction.

**CONCLUSION:**

Overall, this study is progressing on schedule and on budget, with no major deviations from the original proposal. We have developed the necessary methods to complete Tasks 1 and 2, which will enable progress to Tasks 3 and 4 as originally scheduled. We published 10 relevant manuscripts in 2012-2013, and 16 with indirect relevance. Additional funding has been received from several other agencies, enhancing the strength of our cancer immunology research program.

**REFERENCES:**

1. Warren RL, Freeman JD, Zeng T, Choe G, Munro S, Moore R, et al. Exhaustive T-cell repertoire sequencing of human peripheral blood samples reveals signatures of antigen selection and a directly measured repertoire size of at least 1 million clonotypes. *Genome Res.* 2011;21:790-7.
2. Freeman JD, Warren RL, Webb JR, Nelson BH, Holt RA. Profiling the T-cell receptor beta-chain repertoire by massively parallel sequencing. *Genome Res.* 2009;19:1817-24.
3. Tiller T, Meffre E, Yurasov S, Tsuiji M, Nussenzweig MC, Wardemann H. Efficient generation of monoclonal antibodies from single human B cells by single cell RT-PCR and expression vector cloning. *J Immunol Methods.* 2008;329:112-24.
4. Turchaninova MA, Britanova OV, Bolotin DA, Shugay M, Putintseva EV, Staroverov DB, et al. Pairing of T-cell receptor chains via emulsion PCR. *Eur J Immunol.* 2013;43:2507-15.

5. DeKosky BJ, Ippolito GC, Deschner RP, Lavinder JJ, Wine Y, Rawlings BM, et al. High-throughput sequencing of the paired human immunoglobulin heavy and light chain repertoire. *Nat Biotechnol.* 2013;31:166-9.

**APPENDICES:**

- A. Castellarin M, Milne K, Zeng T, Tse K, Mayo M, Zhao Y, Webb JR, Watson PH, Nelson BH, Holt RA. Clonal evolution of high-grade serous ovarian carcinoma from primary to recurrent disease. *J Pathol.* 2013 Mar;229(4):515-24. doi:10.1002/path.4105. Epub 2012 Nov 29. PubMed PMID: 22996961.
- B. Nielsen JS, Sahota RA, Milne K, Kost SE, Nesslinger NJ, Watson PH, Nelson BH. CD20+ tumor-infiltrating lymphocytes have an atypical CD27- memory phenotype and together with CD8+ T cells promote favorable prognosis in ovarian cancer. *Clin Cancer Res.* 2012 Jun 15;18(12):3281-92. doi: 10.1158/1078-0432.CCR-12-0234. Epub 2012 May 2. PubMed PMID: 22553348.
- C. deLeeuw RJ, Kost SE, Kakal JA, Nelson BH. The prognostic value of FoxP3+ tumor-infiltrating lymphocytes in cancer: a critical review of the literature. *Clin Cancer Res.* 2012 Jun 1;18(11):3022-9. doi: 10.1158/1078-0432.CCR-11-3216. Epub 2012 Apr 17. Review. PubMed PMID: 22510350.

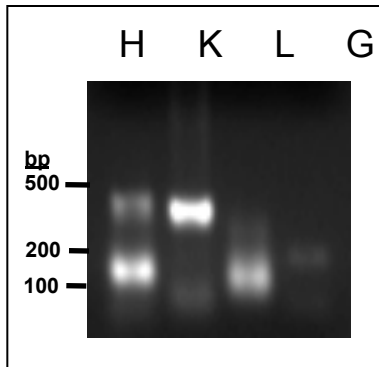
**SUPPORTING DATA:**

None.

**FIGURES:**

See following pages.

**A**



**B**

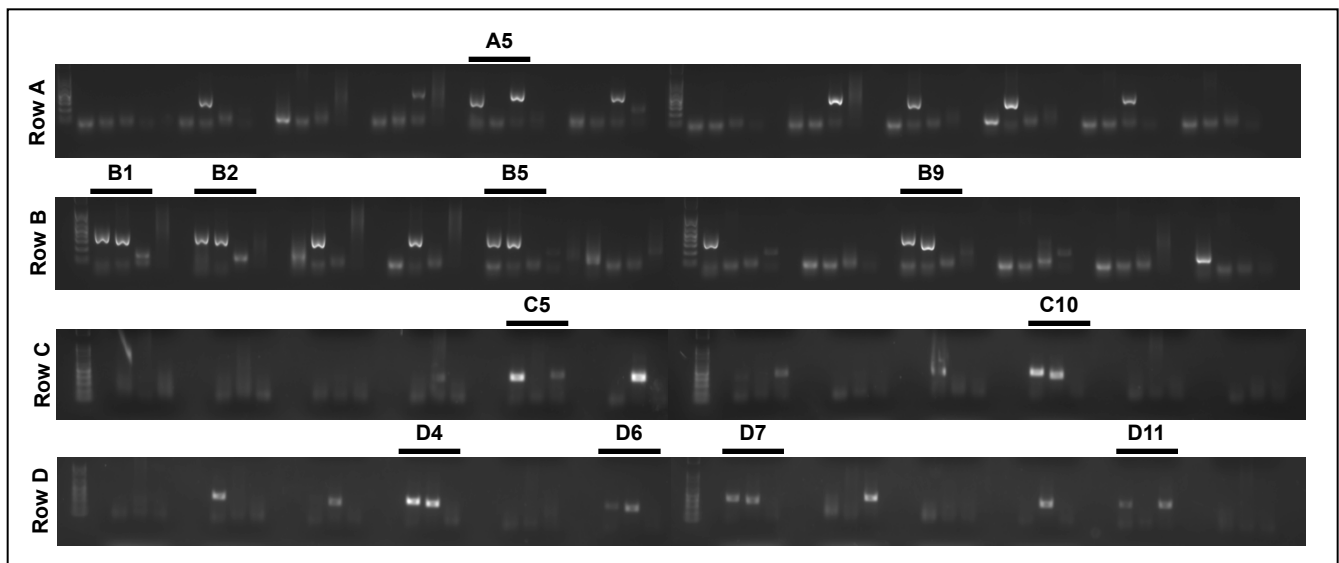


**Figure 1. PCR-based immunoglobulin (Ig) gene amplification from single tumor-infiltrating B cells** **A)** A representative agarose gel electrophoresis of PCR products corresponding to Ig-heavy (H), Ig-kappa (K), Ig-lambda (L) and GAPDH (G). **B)** Amplified matched Ig heavy and light chain variable portions from 44 single B cells (CD19+ CD20+ IgG+) sorted from the disaggregated tumor of an individual high grade serous ovarian cancer patient. Each row contains products derived from 11 single sorted B cells and one control where no B cell was sorted (last set of reactions in each row). As indicated, a total of 11/44 matched heavy and light chain pairs were observed (A5-D11).

rig clone	V region	% identity	J region	% identity	D region	CDR3 aa sequence
IROC070 A5 H IROC070 A5 L	IGHV4-59*02 F IGLV2-14*01 F	83.37 94.79	IGHJ3*01/02 F IGLJ2*01 F	78 92.11	IGHD3-10*01 F	CARSRGLITMPSW CSSYSSALYSSSGTLVF
IROC070 B1 H IROC070 B1 K	IGHV3-15*01 F IGKV2-28*01 F	94.24 96.94	IGHJ4*02 F IGKJ3*01 F	93.75 100	IGHD3-10*01 F	CITDVDYYGSGSSWGPHFDYW CMQALQFTF
IROC070 B2 H IROC070 B2 K	IGHV1-3*01 F IGKV3-15*01 F	97.92 99.64	IGHJ4*02 F IGKJ1*01 F	91.67 91.89	IGHD3-3*01	CARGGDDFWSGYRPFQYW CQQYNNWPGTF
IROC070 B5 H IROC070 B5 K	IGHV3-86*01/04 F IGKV1-39*01	94.44 95.34	IGHJ6*02 F IGKJ2*02 F	88.71 88.89	IGHD7-27*01 F	CARDGENKGYGCAMDVW CQQSYTTPRTF
IROC070 B9 H IROC070 B9 K	IGHV3-49*05 F IGVK2-28*01 F	92.86 96.26	IGHJ6*02 F IGKJ5*01 F	82.26 94.44	IGHD3-10*01 F	CVRHYAYSEKERRAGQPNYGMVW CMQALQTPRTF
IROC070 C5H IROC070 C5L	IGHV4-4*02 F IGLV3-21*02F	93.75 92.83	IGJ4*02 F IGL1*01 F	91.67 100	IGHD2-21*02F	CARGGGDSFDLW CQVWDSQDQNSDQNYVF
IROC070 C10H IROC070 C10K	IGHV3-53 IGKV3-15*01	92.98 96.06	IGJ2*01 F IGKJ4*01 F	92.45 91.67	IGHD2-15*01F	CAKVGSGGACHAGYWFQDLW CQHYDNWLSF
IROC070 D4H IROC070 D4K	IGHV3-15*01 IGKV2-28*01 F	97.28 99.32	IGHJ1*01 F IGKJ1*01F	75 97.22	IGHD6-35*01F	CTTLLMGRIGVATGGW CMQALQTPRTF
IROC070 D6H IROC070 D6K	IGHV3-86*01 F IGKV3-15*01 F	93.33 96.42	IGHJ5*02 IGKJ4*01 F	86.27 97.22	IGHD2-21*01 F	CARRGGDLWWLDLW CQQYNNWPLTF
IROC070 D7H IROC070 D7K	IGHV1-18*01 F IGKV3-11*01F	87.85 95.7	IGHJ4*02 F IGKJ4*01 F	97.92 91.67	IGHD2-8*01	CARLSGPLILYFFDYW CQQRSNWLSF
IROC070 D11H IROC070 D11L	IGHV3-15*01 F IGLV1-47*01	90.82 89.47	IGHJ6*02 F IGLJ3*02F	87.1 91.43	IGHD1-14*01	CTTDGTEPPYQYGMVW CSTRDRLRSPEF

**Figure 2. Molecular cloning, sequencing, and alignment of paired immunoglobulin genes.** Following PCR amplification, pairs of immunoglobulin genes were molecularly cloned into expression vectors. Inserted portions were then sequenced by Sanger sequencing. Following sequencing, the variable portions of cloned immunoglobulin sequences were aligned to the germline elements via the IMGT V-Quest software.

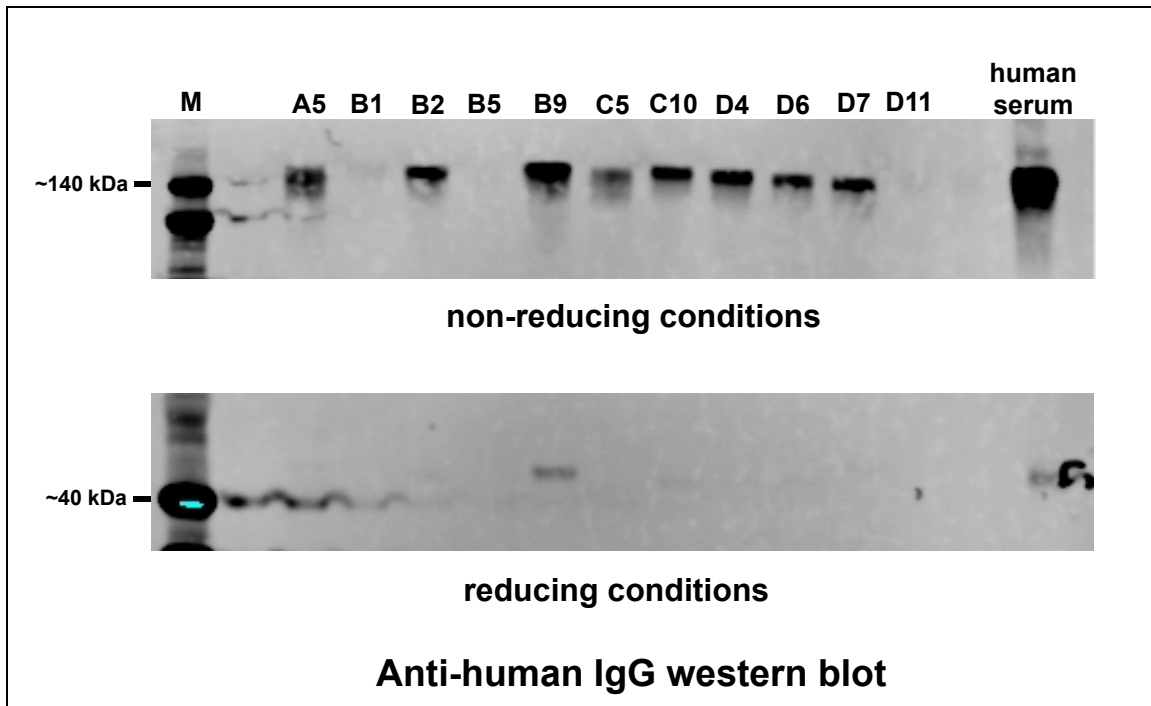
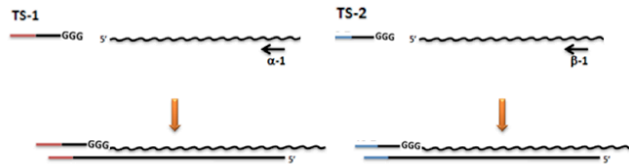


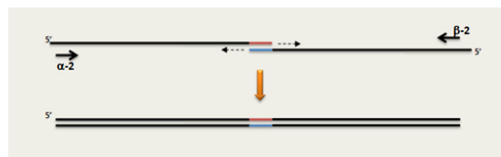
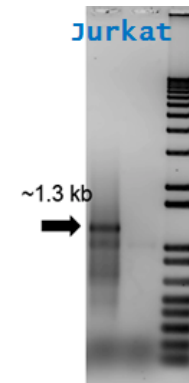
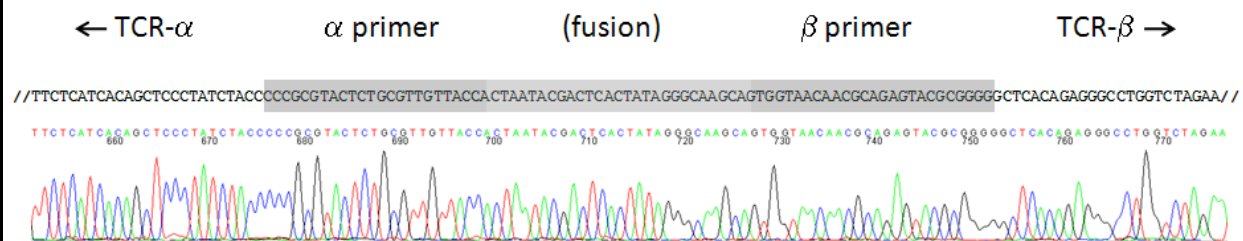
**Figure 3. *In vitro* production of recombinant IgG from immunoglobulin genes derived from tumor-infiltrating B lymphocytes.** After cloning PCR-amplified Ig variable portions into expression vectors containing the constant portion of IgH or IgK/IgL, recombinant antibodies (rIgG) were produced in 293T cells co-transfected with matched heavy and light chain-encoding vectors. The presence of fully assembled IgG antibody in the supernatant was confirmed by western blot under non-reducing conditions as a 150kDa band. The presence of IgG heavy chain (~50kDa) was confirmed under reducing conditions.

**A**

1. RT using 5' TS oligos with complementary tails



2. PCR with alpha and beta C-gene primers

**B****C**

**Figure 4. Pairwise sequencing of TCR  $\alpha$  and  $\beta$  subunits.** **A.** For cDNA synthesis we use a mix of TCR $\alpha$  and TCR $\beta$  gene-specific 3' primers, and the common SMRT template switching method (Clontech) to add 5' cDNA priming sites. In step 1, the gene-specific oligos ( $\alpha$ -1 and  $\beta$ -1) prime reverse transcription, which adds the 5' anchor sequence provided by the template switching oligos TS-1 and TS-2. The tail sequence of TS-1 (pink) is the reverse complement of the TS-2 tail sequence (blue). These complementary tail sequences are thereby incorporated into the reverse transcription products. In step 2, the complementary sequences incorporated into the first strand cDNA prime bidirectional extension to yield a single double stranded DNA fragment comprised of the two TCR subunits in tandem that serve as template for further PCR amplification. By chance, fusions may be both TCR $\alpha$  or both TCR $\beta$ , but these do not amplify due to suppressive self annealing, and paired  $\alpha\beta$  chains are the main PCR product. **B.** Using total RNA from Jurkat cells (a human CD4<sup>+</sup> T cell line that expresses a distinct  $\alpha\beta$ TCR) we can effectively amplify the approximately 1.3 Kb abTCR fusion product. **C.** Verification of the Jurkat  $\alpha\beta$ TCR fusion product by capillary sequencing.

# Clonal evolution of high-grade serous ovarian carcinoma from primary to recurrent disease

Mauro Castellarin,<sup>1,2</sup> Katy Milne,<sup>3</sup> Thomas Zeng,<sup>1</sup> Kane Tse,<sup>1</sup> Michael Mayo,<sup>1</sup> Yongjun Zhao,<sup>1</sup> John R Webb,<sup>3,4</sup> Peter H Watson,<sup>3</sup> Brad H Nelson<sup>3,5,\*†</sup> and Robert A Holt<sup>1,2,5,\*†</sup>

<sup>1</sup> BC Cancer Agency, Michael Smith Genome Sciences Centre, 675 West 10th Avenue, Vancouver, BC, V5Z 1 L3, Canada

<sup>2</sup> Department of Molecular Biology and Biochemistry, Simon Fraser University, Burnaby, British Columbia, Canada

<sup>3</sup> BC Cancer Agency, Deeley Research Centre, 2410 Lee Ave, Victoria, BC, V8R 6 V5, Canada

<sup>4</sup> Department of Biochemistry/Microbiology, University of Victoria, Victoria, BC, Canada

<sup>5</sup> Department of Medical Genetics, University of British Columbia, Vancouver, BC, Canada

\*Correspondence to: Robert A Holt, BC Cancer Agency, Michael Smith Genome Sciences Centre, 675 West 10th Avenue, Vancouver, BC V5Z 1 L3, Canada. e-mail: rholt@bcgsc.ca

Brad H Nelson, BC Cancer Agency, Deeley Research Centre, 2410 Lee Ave, Victoria, BC V8R 6 V5, Canada. e-mail: bnelson@bccancer.bc.ca

†These authors contributed equally to this work.

## Abstract

High-grade serous carcinoma (HGSC) is the most common and fatal form of ovarian cancer. While most tumours are highly sensitive to cytoreductive surgery and platinum- and taxane-based chemotherapy, the majority of patients experience recurrence of treatment-resistant tumours. The clonal origin and mutational adaptations associated with recurrent disease are poorly understood. We performed whole exome sequencing on tumour cells harvested from ascites at three time points (primary, first recurrence, and second recurrence) for three HGSC patients receiving standard treatment. Somatic point mutations and small insertions and deletions were identified by comparison to constitutional DNA. The clonal structure and evolution of tumours were inferred from patterns of mutant allele frequencies. *TP53* mutations were predominant in all patients at all time points, consistent with the known founder role of this gene. Tumours from all three patients also harboured mutations associated with cell cycle checkpoint function and Golgi vesicle trafficking. There was convergence of germline and somatic variants within the DNA repair, ECM, cell cycle control, and Golgi vesicle pathways. The vast majority of somatic variants found in recurrent tumours were present in primary tumours. Our findings highlight both known and novel pathways that are commonly mutated in HGSC. Moreover, they provide the first evidence at single nucleotide resolution that recurrent HGSC arises from multiple clones present in the primary tumour with negligible accumulation of new mutations during standard treatment.

Copyright © 2012 Pathological Society of Great Britain and Ireland. Published by John Wiley & Sons, Ltd.

**Keywords:** tumour genomics; *TP53*; variant detection; *BRCA1*; Golgi apparatus; cancer relapse; COPI; *RG56*; ubiquitin C; chemotherapy

Received 13 June 2012; Revised 17 August 2012; Accepted 11 September 2012

No conflicts of interest were declared.

## Introduction

Each year, over 220 000 women are diagnosed with ovarian cancer and 140 000 die of the disease [1]. Of the four major histological subtypes of epithelial ovarian cancer, high-grade serous carcinoma (HGSC) is the most common and fatal [2,3]. HGSC tumours are thought to arise from the ovarian surface epithelium and the fimbrial region of the Fallopian tubes [4].

Our knowledge of the mutational landscape of HGSC is improving. Approximately 13–15% of HGSC cases are associated with germline mutations in *BRCA1* and *BRCA2* [5,6], and additional susceptibility genes are known to alter the *BRCA1/2* DNA repair pathway (eg *RAD51C*, *RAD51D*, *BRIP1*, *BARD1*, *CHEK2*,

*MRE11A*, *NBN*, *PALB2*, and *RAD50* [7]). Moreover, at least one-third of sporadic HGSC cases show inactivation of the *BRCA1* or *BRCA2* pathways through acquired mutations or gene silencing by DNA methylation [8] such that altogether, homologous recombination-based DNA repair is defective in about half of HGSC cases [9]. In addition, the tumour suppressor gene *TP53* is mutated in over 96% of HGSCs [9,10]. Other commonly mutated genes in HGSC include *FAT3*, *CSMD3*, *NF1*, *RB1*, *GABRA6*, and *CDK12* [9]. Finally, a common gene fusion involving *ESRRA* and *C11orf20* is found in 10–15% of HGSCs [11].

Treatment of HGSC typically comprises platinum-based chemotherapeutic agents including cisplatin, carboplatin, and oxaliplatin. These compounds exert

an anti-tumour effect by inducing intra-strand and inter-strand crosslinks in genomic DNA and are cell cycle-non-specific in action. Ovarian cancer cells with inactivating mutations in the *BRCA1* or *BRCA2* genes are more prone to the DNA-damaging effects of platinum compounds. However, platinum chemoresistance can arise through a variety of mechanisms in HGSC, including acquired mutations that restore the *BRCA1* and *BRCA2* open reading frames [12–16]. Additionally, drug resistance in relapsed tumours can result from genetic alterations that affect drug efflux, drug metabolism, intracellular signalling, membrane receptors, apoptotic signalling, and interference with cell replication [17].

There is increasing appreciation for the genetic heterogeneity of epithelial cancers within individual patients [18–23]. The presence of multiple tumour clones in a patient creates the opportunity for evolutionary selection during treatment. Indeed, a previous study of recurrent HGSC using FISH, SNP arrays, and array CGH concluded that chemotherapy-resistant clones arise from minor clones present in primary tumours [24]. However, the extent to which recurrent tumours further evolve by accumulating additional mutations has yet to be systematically addressed in HGSC. Here, we performed whole exome sequencing of genomic DNA from tumour cells obtained from ascites of three HGSC patients at multiple time points (primary treatment, first recurrence, and second recurrence). We inferred tumour clonality and relapse-associated mutations by analysing trends in mutant allele frequencies. The possible functional consequences of mutations were assessed by pathway analysis. Furthermore, to gain a more comprehensive view of HGSC genetic susceptibility for these patients, we investigated the coincidence of germline and somatic variants within gene interaction networks.

## Materials and methods

### Clinical specimens

Biospecimens and clinical data were collected with informed patient consent through a prospective study entitled BC Cancer Agency's Tumor Tissue Repository/Immune Response to Ovarian Cancer (IROC), which was approved by the Research Ethics Board of the BC Cancer Agency and the University of British Columbia. Inclusion criteria included a diagnosis of HGSC, standard treatment with surgery followed by platinum-based chemotherapy (with or without taxanes), and biospecimen availability. Peripheral blood mononuclear cells (PBMCs) and primary ascites specimens were collected at the time of surgery. Recurrent ascites specimens were collected during palliative paracentesis. Ascites cells were pelleted by centrifugation, cryopreserved immediately, and stored in liquid nitrogen.

### Tumour cell enrichment

Bulk ascites cells were thawed and resuspended in complete RPMI medium (cRPMI; RPMI 1640, 10% FBS, HEPES, L-glutamine,  $\beta$ -mercaptoethanol) at a concentration of  $10^7$  cells per 80  $\mu$ l. To remove haematopoietic cells, 20  $\mu$ l of anti-human CD45 microbeads (Miltenyi, Bergisch Gladbach, Germany) was added per  $10^7$  total cells and the mixture was incubated at 4 °C for 15 min. Cells were washed twice with 10 ml of cRPMI and then passed over an LS column (Miltenyi) that had been pre-wetted with 0.5 ml of cRPMI. CD45<sup>−</sup> cells passing through the column were collected, pelleted, and snap frozen at −80 °C for subsequent DNA preparation.

### Exome library construction and sequencing

Genomic DNA (gDNA) was isolated, acoustically sheared, size-selected by polyacrylamide gel electrophoresis (PAGE), and end-polished. gDNA fragments were ligated with Illumina library adapters and amplified with Illumina sequencing primers (Illumina, San Diego, CA, USA). The library was then enriched for exon sequences using the Agilent Sureselect Human All Exon 50 Mb kit [25] according to the manufacturer's instructions (Agilent Technologies, Santa Clara, CA, USA). The exome fraction was subjected to massively parallel sequencing on the Illumina platform. Between 50 and 90 million paired 100 bp raw reads were obtained from each sample.

### Bioinformatic analysis

The short Illumina sequence reads were aligned to the human genome (hg18) using the Burrows–Wheeler Aligner (BWA) [26]. Single nucleotide variant (SNV) detection was performed using Samtools varfilter [27] and SNVMix1 [28] software to identify high-quality, novel, protein-coding variants between the sample sequence and the human reference sequences. Insertions and deletions were detected using Samtools varfilter and then selected as protein-coding variants as delineated in the Hg18 reference sequence. Somatic mutations were determined by subtracting variants found in matched normal samples. The false-negative rate for SNVs was reduced by selecting those that were found by both Samtools and SNVMix1 and by reducing mapping errors using a targeted *de novo* assembler, TASR [29]. All somatic variants were manually curated using the Integrative Genome Viewer (IGV) [30]. Germline SNVs were identified from the exome data and were considered homozygous if they had a greater than 80% probability of being homozygous as determined by SNVMix1. Genomic coordinates for the germline and somatic variants were converted from the hg18 reference genome to the hg19 reference genome using the UCSC Lift Genome Annotations tool [31].

Biological pathway analysis was performed using both the GeneMania plugin [32] in Cytoscape v2.8.3 [33] and Ingenuity Pathways Analysis

(Ingenuity® Systems, Inc, Redwood City, CA, USA; <http://www.ingenuity.com>) on genes with homozygous germline SNVs that were found to be shared in all sequencing libraries (tumour and matched normal) from all three patients. Gene identifiers that contained shared, homozygous, germline SNVs were mapped to their corresponding objects based on direct interactions and overlaid onto a global molecular network that was developed from the Ingenuity® Knowledge Base or the GeneMania human interaction database version 2012-01-06, which contains 102 821 535 interactions. The functional interaction analysis of a network identified the biological functions and/or diseases that were most significant to the molecules in the network. The network molecules associated with biological functions and/or diseases in the Ingenuity® Knowledge Base or GeneMania database were analysed. The Fisher's exact test, as implemented in the Ingenuity® Knowledge Base, was used to calculate the probability that each biological function and/or disease assigned to that network was due to chance alone. Gene clustering was performed with JMP8 statistical software [34] using a hierarchical Ward clustering algorithm based on somatic SNV allelic frequencies. Gene Ontology (GO) [35] annotated functions of gene clusters were predicted based on physical interactions and pathway data sources using GeneMania [36]. GeneMania estimates the false discovery rate (FDR), the proportion of positives that are expected to be false positives, as  $q$ -values by using the Benjamini–Hochberg procedure, and it is this number that we report. Nodes were partitioned according to network modules using the Reactome FI Cytoscape plugin [37] and network diagrams were depicted using the circular layout in Cytoscape.

### Sequence validation

Sequence validation was performed by PCR amplification of targeted mutant loci followed by Illumina sequencing of indexed products on a single cell lane of 100 bp paired-end reads on an Illumina HiSeq platform. The short Illumina sequence reads were then aligned to the human genome (hg18) using the BWA [26]. Variant detection was performed using Samtools mpileup [27] and validated somatic variants were visually curated using IGV [30].

## Results

### Patient selection and clinical course

We selected three HGSC patients for whom matched ascites tumour specimens were available from the time of primary surgery and two subsequent recurrences. As fluid, ascites had the advantage of providing serial samples unrestricted to any specific tumour region. As shown in Figure 1, patient 1 received adjuvant chemotherapy with five cycles of carboplatin and paclitaxel. In response to recurrence of disease

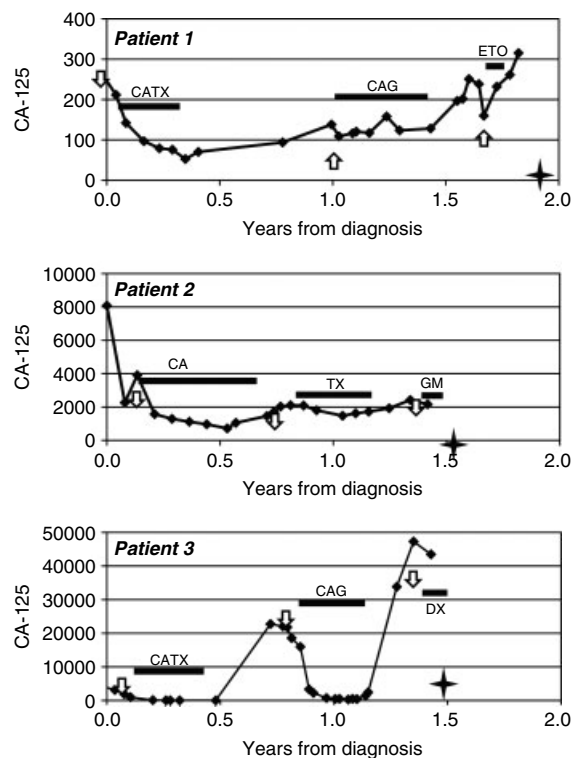


Figure 1. Clinical course for the three HGSC patients from this study. Black squares indicate CA-125 levels (kU/l) over time. Arrows indicate collection of ascites tumour specimens. Black bars indicate chemotherapy. Stars indicate time of death. CATX, carboplatin with paclitaxel; CA, carboplatin; TX, taxol; CAG, carboplatin with gemcitabine; ETO, etoposide; GM, gemcitabine; DX, pegylated liposomal doxorubicin.

8 months after completion of the first round of therapy, she received six cycles of carboplatin with gemcitabine, which slowed tumour progression for several months. Upon further progression, she received two courses of etoposide, to which she failed to respond. Patient 2 received adjuvant chemotherapy with six cycles of carboplatin. In response to progressive disease, she was treated with seven cycles of paclitaxel, which stabilized her disease for about 2 months. Upon further progression, she received one cycle of gemcitabine, to which she failed to respond. Finally, patient 3 received adjuvant chemotherapy with six cycles of carboplatin and paclitaxel, which led to complete remission. Upon disease recurrence at 9 months, she received six cycles of carboplatin with gemcitabine, which led to a second complete remission. Upon disease recurrence, she received three cycles of pegylated liposomal doxorubicin, to which she failed to respond.

### Identification of somatic mutations by whole exome sequencing

Whole exome sequencing was performed to profile somatic mutations in ascites tumour samples. Single nucleotide variants and insertions/deletions (indels) were validated by targeted re-sequencing at a depth of  $\geq 50\,000$  reads using germline DNA for comparison. We identified a total of 22–40 somatic variants (somatic point mutations plus somatic indels) per

patient (Tables 1 and 2). Table 1 lists all somatic point mutations, their allelic frequencies, and their predicted effects on protein function according to the SIFT program [38]. Of the 88 somatic point mutations that we found, only two have been previously reported, one in *BRCA1* and the other in *CSMD3* [39]. Of the remaining 86 somatic point mutations, 69 were within genes previously found to be mutated in ovarian serous carcinoma according to the Catalogue of Somatic Mutations in Cancer (COSMIC) database [40]. By SIFT analysis, 28% of somatic point mutations were predicted at high confidence to impair protein function. In addition to somatic point mutations, we found five somatic indels, which involved the genes *TP53* (patient 1), *MACF1* (patient 2), and *CAPN7*, *DMD*, and *OR5A1* (patient 3) (Table 2). The only gene found to contain a somatic point mutation or indel in all three patients was *TP53*.

### Clonal structure and evolution of tumours

Somatic variants were subjected to high-depth targeted re-sequencing using tumour samples from all three time points. This allowed quantification of allele frequencies over time, even for mutations that fell below the limit of detection in the original exome sequencing libraries. We found that the vast majority of mutations that were present in relapse samples were present in primary samples (Table 1). Likewise, the majority of mutations that were present in primary samples persisted in relapse samples (Table 1).

We used a hierarchical clustering model to infer tumour clonality based on concordant changes in mutant allele frequencies (Figure 2). Mutations from patient 1 formed three distinct clusters, which may reflect three distinct clonal populations. Cluster 1 was markedly more abundant than the other two clusters and contained a heterozygous *TP53* mutation. The relapse tumours from patient 1 showed a doubling in allelic frequency of the *TP53* mutation, suggesting a loss of heterozygosity at the *TP53* locus (Table 1). The relative proportions of the three clusters did not change significantly across the three time points. One exception was the *PLXB2* mutation in cluster 1, which occurred at a frequency of 25% in the primary tumour sample but close to 100% in relapse samples. This suggests that the *PLXB2* mutation occurred after the other cluster 1 mutations and that a subclone expressing this mutation increased in frequency at relapse compared with primary tissue. Patient 2 showed four major clusters of mutations. As with patient 1, the cluster containing mutant *TP53* was dominant at all time points. Patient 3 showed five clusters of mutations and much more complex dynamics, possibly reflecting the dramatic changes in tumour burden seen with this patient during chemotherapy (Figure 1). Again, the cluster containing mutant *TP53* (cluster 1) was dominant at all time points. Cluster 3 increased in prevalence at first relapse and remained prominent at second relapse. Cluster 5 showed the opposite pattern, being prevalent in the primary tumour but absent at relapse.

### Functional annotation of mutant genes

Mutant genes from each cluster were functionally annotated using the Gene Ontology (GO) [35]. Despite the lack of shared mutations among patients, the mutations fell into several shared functional categories. The predominant cluster from all three patients had cell cycle checkpoint function. In addition, statistically significant functional annotations that involved Golgi vesicles were found in cluster 3 from patient 1 ( $\text{FDR} = 9.3 \times 10^{-14}$ ), cluster 4 from patient 2 ( $\text{FDR} = 1.47 \times 10^{-2}$ ), and cluster 2 from patient 3 ( $\text{FDR} = 1.38 \times 10^{-8}$ ).

### Analysis of shared pathways among somatic mutations and germline variants

Germline mutations can increase the risk of developing cancer but further somatic mutations are needed to cause the actual onset of the disease. In HGSC, the *BRCA1*, *BRCA2*, and *TP53* genes frequently harbour somatic mutations, and germline mutations can contribute to a familial predisposition. In general, tumourigenesis and disease progression require multiple, parallel pathways that can be altered by either germline or somatic genetic lesions [41]. SNPs that are shared among these patients may constitute a common predisposition to perturbed pathways that can become altered further by somatic mutations. We asked whether in these patients, somatically mutated genes were related to genes carrying germline coding variation. We identified 972 high-confidence homozygous, non-synonymous SNPs that were common to all three patients. These SNPs were contained within 804 distinct genes (Supplementary Table 1). Of the germline SNPs that resulted in SIFT scores, 3% were predicted at high confidence to impair protein function. Using the Cytoscape GeneMania plugin [32] and the Reactome FI plugin [37], we performed network analysis on both the shared homozygous germline variants and the somatic variants (Figure 3). The network revealed connectivity among somatic and germline variants that defined highly connected modules. The top two interacting nodes that were represented as network hubs were *TP53* and fibronectin 1. The sets of mutated genes within each module were then assessed for functional annotation based on GO terms. The module with the largest number of nodes (57) had a GO annotation of 'DNA repair' with a  $q$ -value of  $2.8 \times 10^{-8}$ . The other functionally categorized modules were 'extracellular matrix' (40 nodes,  $q$ -value =  $1.0 \times 10^{-20}$ ), 'G2/M transition of mitotic cell cycle' (22 nodes,  $q$ -value =  $3.3 \times 10^{-7}$ ), 'trans-Golgi network' (13 nodes,  $q$ -value =  $5.6 \times 10^{-3}$ ), and 'Golgi vesicle targeting/membrane budding' (12 nodes,  $q$ -value =  $1.1 \times 10^{-7}$ ). Within the modules characterized as 'DNA repair' and 'Golgi vesicle targeting/membrane budding', there was enrichment of somatic mutations relative to germline variants [11/57 (19.3%) and 2/7 (28.6%), respectively] when compared

Table 1. Validated non-synonymous somatic mutations ranked by allelic frequencies for each of the three HGSC patients

	Mutant allele frequency by tissue												
	Hg18 genomic position	Gene ID	Type of mutation <sup>†</sup>	Allele change	Amino acid change	Normal PBMC	Primary ascites	1st relapse ascites	2nd relapse ascites	SIFT score	SIFT prediction <sup>‡</sup>	dbSNP ID	COSMIC
Patient 1	Chr17:38497955	BRCA1	NS	C>T	S744N	52.9	65.1	97.5	96.7	0.08	T	rs4986852:T	Yes
	Chr17:35808624	TOP2A	NS	T>C	Y1163C	0.1	50.2	97.1	95.4	0	D	Novel	Yes
	Chr8:113310264	CSMD3	NS	T>G	N3621H	49.7	59.2	93.0	94.3	0.56	T	rs1592624:G	Yes
	Chr22:49070711	PLXNB2	NS	C>T	V144M	0.3	27.8	92.8	85.2	0.01	D	Novel	Yes
	Chr15:46367984	SLC12A1	NS	G>A	R951H	0.1	25.4	56.3	64.1	N/A	NS	Novel	Yes
	Chr2:136589859	CXCR4	US	T>A	N41Y	0.1	15.2	47.9	56.2	N/A	NS	Novel	No
	Chr10:92972714	PCGF5	NS	C>A	H36N	0.1	23.8	40.4	53.2	0	D	Novel	No
	Chr19:61061829	NLRP4	NS	C>T	R420W	0.2	25.9	57.7	47.2	0	D	Novel	Yes
	Chr8:141637781	EIF2C2	NS	G>T	P288H	0.1	29.7	37.1	44.7	0	D	Novel	No
	Chr15:31659551	RYS3	NS	C>T	Q451*	0.2	18.4	25.1	35.4	N/A	N/A	Novel	Yes
	Chr19:6616095	TNFSF14	NS	G>A	R189W	0.1	17.7	30.1	30.5	0	DLC	Novel	Yes
	Chr14:19834390	TTC5	NS	G>A	T232M	0.4	12.9	40.5	29.7	0.14	T	Novel	Yes
	Chr8:69119340	PREX2	NS	A>C	T302P	0.0	0.0	19.1	28.6	0	DLC	Novel	Yes
	Chr14:41430594	LRFN5	NS	G>T	A593S	0.1	15.8	16.5	28.2	0.23	T	Novel	Yes
	Chr20:4798604	SLC23A2	NS	C>T	A400T	0.1	22.3	41.6	27.7	0.24	T	Novel	Yes
	Chr17:5374631	NLRP1	NS	C>G	E1142D	0.2	15.7	17.6	26.7	0.3	T	Novel	Yes
	Chr3:123608886	FAM162A	NS	C>T	T111M	0.1	9.1	20.3	26.2	0	D	Novel	Yes
	Chr3:174157167	SPATA16	NS	A>G	Y359H	0.1	4.8	28.8	23.1	0	DLC	Novel	Yes
	Chr9:140135932	CACNA1B	NS	G>A	G2165S	0.1	20.4	28.1	22.6	0.76	T	Novel	Yes
	Chr14:94023488	SERPINA12	NS	C>T	V384I	0.0	9.7	12.4	21.8	0.95	T	Novel	Yes
	Chr3:140576092	COPB2	NS	C>T	G227E	0.0	12.3	27.3	17.9	0	D	Novel	Yes
Patient 2	Chr8:94815372	RBM12B	US	G>A	P815S	50.0	68.0	97.9	99.9	N/A	NS	Novel	Yes
	Chr17:7518901	TP53	PSS	C>T	N/A	0.4	99.7	99.1	99.8	N/A	N/A	Novel	Yes
	Chr19:3498535	C19orf28	NS	A>C	L283R	47.4	99.8	99.8	99.8	0	DLC	Novel	No
	ChrX:125513552	DCAF12L1	NS	C>G	V241L	0.2	99.1	91.7	98.9	0.15	T	Novel	Yes
	Chr21:46811715	DIP2A	US	G>T	V1447L	0.7	66.4	66.4	78.1	N/A	NS	Novel	Yes
	Chr10:120791840	EIF3A	NS	C>T	R1061H	0.4	39.5	62.6	62.2	0.02	DLC	Novel	No
	Chr19:47483139	CIC	NS	G>C	G120A	0.5	51.3	59.5	55.4	0.65	T	Novel	Yes
	Chr11:14810942	PDE3B	NS	T>A	Y731*	0.6	52.4	45	53.8	N/A	N/A	Novel	No
	Chr2:235069395	ARL4C	NS	C>G	R192P	0.2	38.2	36.0	53.3	0	DLC	Novel	Yes
	Chr9:130385899	SPTAN1	NS	C>T	R675C	0.2	41.7	56.7	51.6	0.01	DLC	Novel	Yes
	Chr4:187779522	FAT1	US	G>A	Q1741*	0.3	29.8	47	51.1	N/A	NS	Novel	Yes
	Chr9:130061400	GOLGA2	NS	T>C	Q616R	0.5	46.7	42.6	50.5	0.4	T	Novel	Yes
	Chr5:71775527	ZNF366	NS	G>T	L683I	0.9	45.1	54.2	49.3	0.32	T	Novel	No
	Chr9:91198306	SEMA4D	NS	C>T	V167I	0.3	64.6	57.6	47.7	0.23	T	Novel	Yes
	Chr11:51268538	OR4A5	NS	A>G	V145A	0.1	30.7	41.1	40.2	0.33	T	Novel	Yes
	Chr17:33738996	GPR179	US	G>C	R1328G	0.5	21.4	48.1	37.5	N/A	NS	Novel	Yes
	Chr7:147545382	CNTNAP2	NS	G>A	R1027K	0.1	15.9	34.5	37.3	1	T	Novel	Yes
	ChrX:22005541	PHEX	NS	C>G	P155A	0.0	0.0	0.1	35.5	0	D	Novel	Yes
	Chr1:31923029	COL16A1	NS	G>A	R677C	0.3	47.9	35.3	34.2	0.01	D	Novel	Yes
	Chr10:104818466	CNNM2	NS	C>A	P723T	0.4	27.2	31.5	34.1	0.52	T	Novel	Yes
	Chr2:21085858	APOB	NS	C>A	A2463S	0.6	56.9	31.1	27.6	0.09	T	Novel	Yes
	Chr16:20556245	ACSM1	NS	C>T	M1I	0.1	0.1	0.1	21.5	0.02	DLC	Novel	No
	Chr1:32034882	SPOCD1	NS	G>A	Q216*	0.1	0.1	0.0	19.7	N/A	N/A	Novel	Yes
	Chr22:28075220	AP1B1	NS	T>C	D475G	0.0	0.0	0.0	19.3	0.02	D	Novel	Yes
	Chr1:148124765	HIST2H2BE	NS	T>C	K17R	0.3	22.3	21.3	18.3	0.05	DLC	Novel	Yes
	Chr20:32934365	ACSS2	NS	A>T	M96L	0.4	16.6	24.6	11.0	0	D	Novel	No
	Chr3:13345395	NUP210	NS	G>C	Q1388E	0.1	39.8	39.2	9.3	N/A	NS	Novel	Yes
Chr10:95921058	PLCE1	NS	C>T	Q542*	0.0	0.0	0.1	8.4	N/A	N/A	Novel	Yes	
Chr16:28816828	ATP2A1	NS	C>A	R476S	0.1	4.5	19.9	1.4	0.4	T	Novel	Yes	
Chr8:88954771	DCAF4L2	NS	A>G	I182T	0.3	24.1	0.1	0.0	0.01	DLC	Novel	Yes	
Patient 3	Chr6:146761919	GRM1	NS	G>T	R684L	0.1	83.9	65.3	96.7	0	D	Novel	Yes
	Chr18:75996662	ADNP2	NS	G>C	R792T	0.0	86.2	43.6	96.1	0.48	T	Novel	Yes
	Chr14:73894317	C14orf115	NS	T>A	C360S	0.0	93.9	65.6	94.2	0.95	T	Novel	No
	Chr17:7519015	TP53	PSS	C>T	N/A	0.0	92.5	74.6	93.5	N/A	N/A	Novel	Yes
	ChrX:47200359	ZNF41	NS	C>T	G67E	0.1	56.4	54.1	69.6	0	D	Novel	Yes
	ChrX:135254619	GPR112	NS	A>G	E300G	0.1	46.9	54.6	67.0	0	DLC	Novel	Yes
	Chr16:11839419	RSL1D1	US	C>G	S400T	0.0	58.0	46.5	64.8	N/A	NS	Novel	No
	Chr4:120170760	SYNPO2	NS	A>C	N461T	0.0	45.7	52.8	62.9	0.31	T	Novel	Yes
	Chr16:82722355	HSDL1	NS	G>C	L25V	0.0	3.5	55.0	60.2	0	D	Novel	No
	Chr17:16553073	CCDC144A	NS	G>C	R326T	0.0	0.0	35.2	60.0	0	DLC	Novel	No
	Chr11:88794758	NOX4	NS	A>T	F197I	0.0	20.5	45.0	56.5	0	D	Novel	Yes

Table 1. (Continued)

		Mutant allele frequency by tissue										
Hg18 genomic position	Gene ID	Type of mutation <sup>†</sup>	Allele change	Amino acid change	Normal PBMC	Primary ascites	1st relapse ascites	2nd relapse ascites	SIFT score	SIFT prediction <sup>*</sup>	dbSNP ID	COSMIC
Chr3:130452227	<i>COPG</i>	NS	A>G	N17S	0.0	50.1	38.3	55.0	0.32	T	Novel	Yes
Chr12:48141063	<i>SPATS2</i>	NS	A>G	M1V	0.0	51.3	51.2	52.9	0.29	T	Novel	No
Chr9:108728098	<i>ZNF462</i>	NS	G>A	R695K	0.0	44.1	37.6	52.2	0	DLC	Novel	Yes
Chr12:103804310	<i>SLC41A2</i>	NS	C>G	K223N	0.1	22.8	23.1	45.8	0.06	T	Novel	Yes
Chr9:73549906	<i>TMEM2</i>	NS	G>T	S294R	0.0	31.3	24.1	40.1	0	D	Novel	Yes
Chr19:45234235	<i>ZNF780B</i>	US	T>C	Y168C	0.0	2.1	26.1	40.0	N/A	NS	Novel	Yes
Chr11:55127965	<i>OR4C11</i>	NS	G>T	S154Y	0.0	0.5	26.2	35.5	0	D	Novel	Yes
Chr10:125629803	<i>CPXM2</i>	NS	T>C	N106S	0.1	47.1	28.8	33.2	0.14	T	Novel	Yes
Chr2:197302318	<i>CCDC150</i>	NS	G>C	A392P	0.0	27.2	31.3	32.9	0.16	T	Novel	No
Chr12:69256442	<i>PTPRB</i>	US	G>C	S725R	0.1	2	26.2	31.9	N/A	NS	Novel	No
Chr10:102673818	<i>FAM178A</i>	NS	G>T	R357I	0.0	23.6	32.9	30.0	0.01	DLC	Novel	No
Chr1:152190704	<i>CRTC2</i>	NS	C>A	A34S	0.0	34.3	23.9	29.7	0	DLC	Novel	Yes
Chr1:165933526	<i>RCSD1</i>	NS	G>C	E347D	0.0	24.8	19	23.4	0	DLC	Novel	Yes
Chr12:64990591	<i>HELB</i>	NS	C>G	P539R	0.0	0.1	25.9	22.0	0	D	Novel	No
Chr3:9966618	<i>PRRT3</i>	NS	A>T	F61Y	0.1	39.9	19	20.9	0	DLC	Novel	No
Chr6:57120371	<i>ZNF451</i>	NS	C>G	S510*	0.0	0.6	19.6	20.8	N/A	N/A	Novel	Yes
Chr1:6627704	<i>DNAJC11</i>	NS	C>G	V322L	0.0	2.6	24	20.1	1	T	Novel	Yes
Chr1:184381645	<i>HMCN1</i>	NS	C>G	Q4859E	0.0	19.8	18.1	16.8	0	DLC	Novel	Yes
Chr15:19884381	<i>OR4N4</i>	NS	G>A	R182Q	0.1	1.8	12.9	16	0.28	T	Novel	Yes
Chr12:877064	<i>WNK1</i>	NS	C>G	S1889C	0.0	9.4	0.0	0.0	0	DLC	Novel	Yes
Chr5:124010504	<i>ZNF608</i>	NS	A>T	S1158T	0.1	18.1	0.1	0.0	0.16	T	Novel	Yes
Chr12:13099988	<i>KIAA1467</i>	NS	C>G	Q92E	0.0	27.2	0.0	0.0	1	T	Novel	Yes
Chr11:63419288	<i>MARK2</i>	NS	G>A	E13K	0.0	28.9	0.0	0.0	0.08	T	Novel	Yes
Chr14:72072653	<i>RGS6</i>	NS	A>C	I429L	0.0	44.4	0.0	0.0	0	D	Novel	No
Chr17:57022774	<i>NACA2</i>	NS	C>G	V184L	0.1	26.6	0.1	0.0	0	D	Novel	Yes
Chr12:38234148	<i>ABCD2</i>	NS	C>G	E686Q	0.0	16.9	0.0	0.0	0.44	T	Novel	Yes

\*Stop codon.

<sup>†</sup>NS = non-synonymous substitution; US = unknown substitution; PSS = possible splice site.<sup>\*</sup>D = damaging; DLC = damaging (low confidence); T = tolerated; NS = not scored; N/A = not available.

Table 2. Validated indels identified in the three HGSC patients

Hg18 genomic position	Gene ID	Type of mutation	Allele change	COSMIC mutation	dbSNP ID	Origin of indel by patient		
						Patient 1	Patient 2	Patient 3
Chr14:22618623	<i>ACIN1</i>	Insertion	AGAACGTGAACGTGA> AGAACGTGAACGT- GAACGTGA	Yes	rs14803158		Germline	Germline
Chr7:150344835	<i>ATG9B</i>	Insertion	GC>GCC	Yes	novel	Germline		Germline
Chr11:76429189	<i>B3GNT6</i>	Deletion	CTT>CT	No	novel	Germline	Germline	Germline
Chr19:40950777	<i>C19orf55</i>	Deletion	AGGG>AGG	No	rs66706567	Germline	Germline	Germline
Chr3:15263894	<i>CAPN7</i>	Deletion	TCACAAAATAACCCCA>TCA	Yes	novel			Somatic
ChrX:31435324	<i>DMD</i>	Deletion	GTTGAGAGACTTTT>GTTT	Yes	novel			Somatic
Chr2:176696536	<i>HOXD9</i>	Insertion	CGCAGCAGCAGCA> CGCAGCAGCAGCAGCA	No	rs66706567	Germline		Germline
Chr14:93651883	<i>IFI27</i>	Insertion	TGCC>TGGCCATGGCGGC	No	novel	Germline	Germline	Germline
Chr1:39553852	<i>MACF1</i>	Deletion	AGTCTCCATCTAGTTCAAGTGTC> AGTCTAGTGTC	Yes	novel		Somatic	
Chr11:58967477	<i>OR5A1</i>	Deletion	ACTTCTTCT>ACTTCT	Yes	novel			Somatic
Chr17:3541025	<i>P2RX5/TAX1BP3</i>	Deletion	TGGGGG>TGGGG	Yes	rs150260459	Germline		Germline
Chr2:113710767	<i>Pax8</i>	Insertion	GCC>GCC	No	rs5826760	Germline	Germline	Germline
Chr19:2291154	<i>SPPL2B</i>	Insertion	GCC>GCCC	No	novel	Germline	Germline	Germline
Chr7:149107599	<i>SSPO</i>	Insertion	GCCCC>GCCCCC	No	novel	Germline	Germline	Germline
Chr20:42127972	<i>TOX2</i>	Deletion	CCCGCCGCCGCC> CCCGCCGCCGCC	Yes	novel		Germline	
Chr17:7520114	<i>TP53</i>	Deletion	GGGAAGG>GGG	Yes	novel	Somatic		
Chr4:75995	<i>ZNF595</i>	Insertion	CA>CAA	No	rs139953554	Germline	Germline	Germline

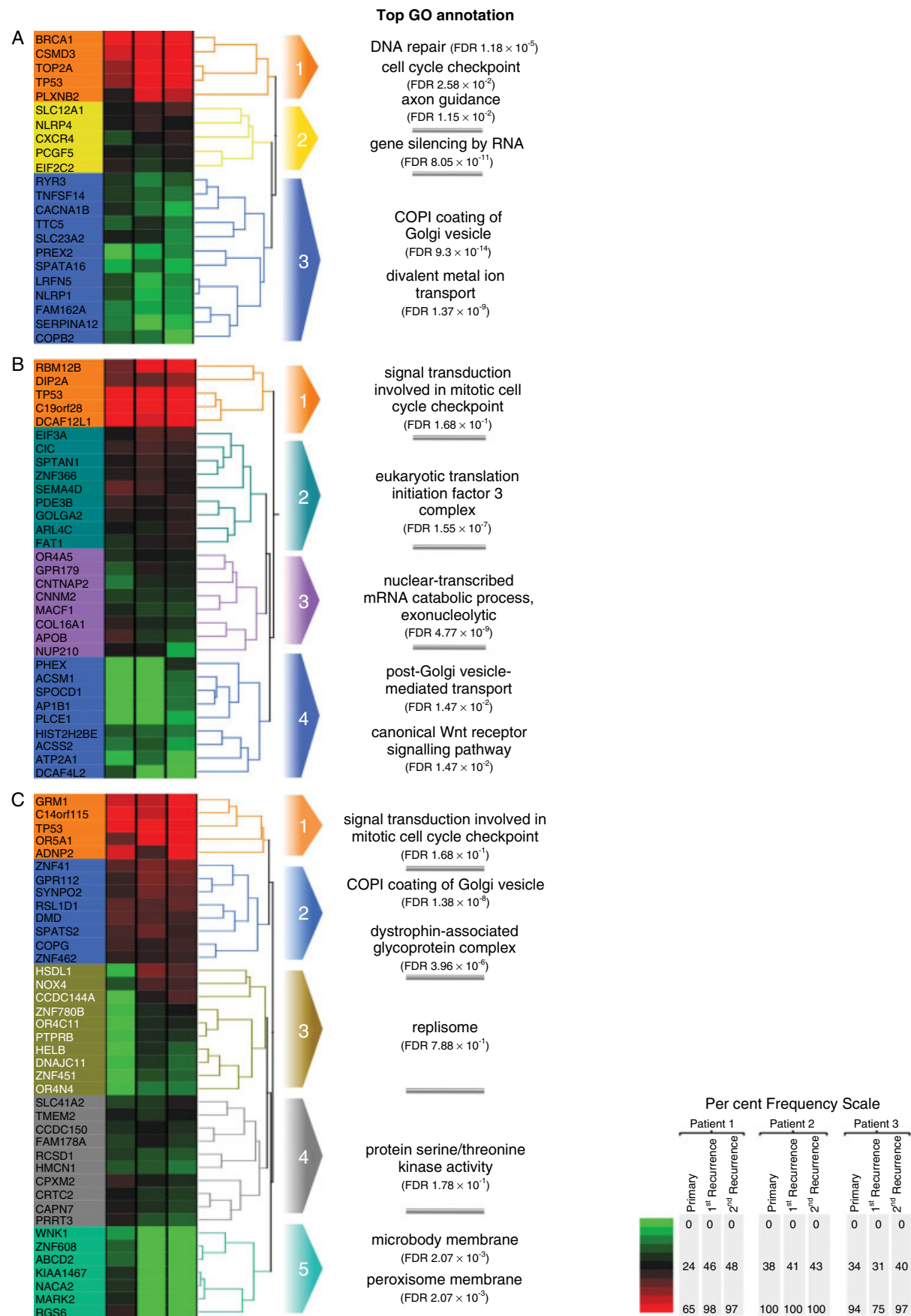
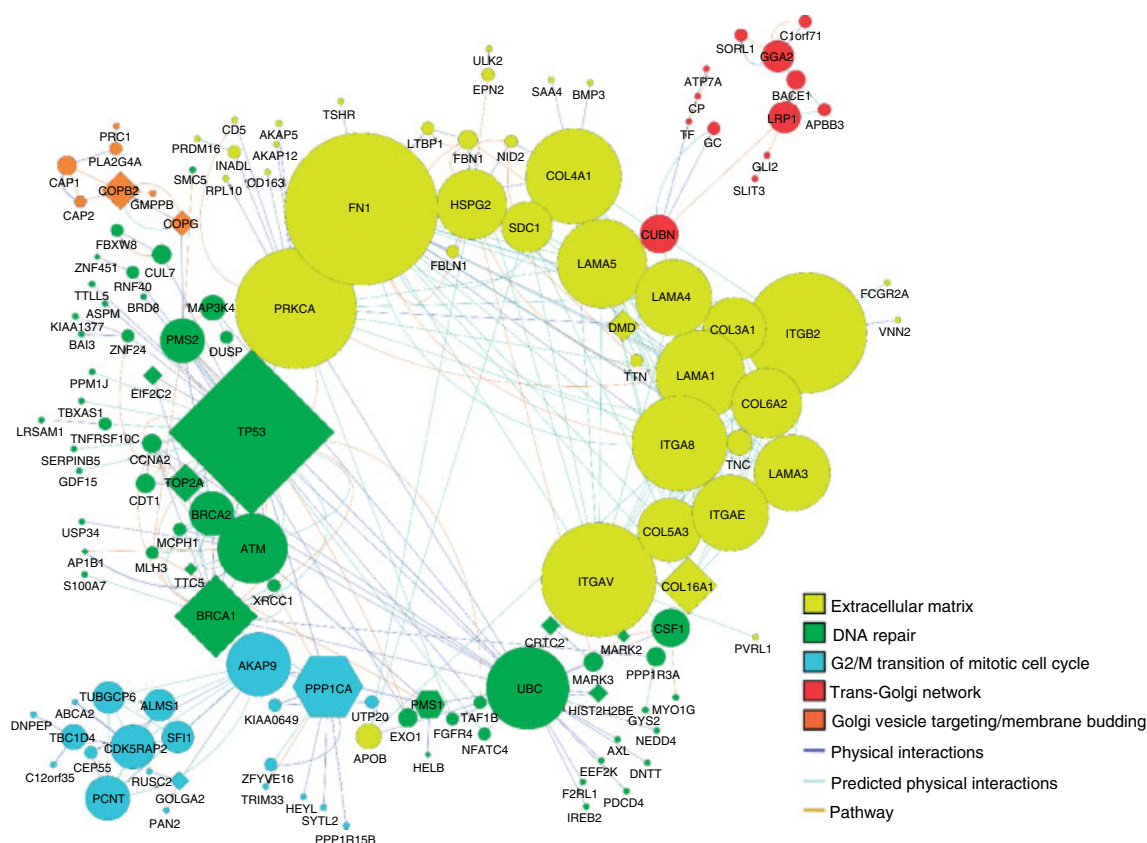


Figure 2. Mutant allele frequency trend and inference of tumour clonality. Mutant allele frequencies (0–100%) are represented by the green–red heat map, according to the indicated scale. Clonality was inferred using a hierarchical Ward clustering algorithm based on temporal changes in non-synonymous mutant allele frequencies. Gene Ontology (GO) annotation of function was performed on the genes specified by each cluster using the Cytoscape Genemania plugin. (A) Patient 1; (B) patient 2; (C) patient 3.



**Figure 3.** Functional interactions network analysis of germline and somatic non-synonymous coding variants. Direct interactions are illustrated by connecting edges and node size is relative to the number of interactions. Genes that contained shared, homozygous, germline variants (circular nodes) in all three patients and somatic mutations (diamond nodes) were analysed by the network analysis tool Cytoscape Genemania plugin. Genes predicted by GeneMania are shown as hexagonally shaped nodes. Data sources used for the predictions included 'pathway' data, which describe two genes that share a reaction, or 'physical' data, which describe protein–protein interactions. Node colours denote genes that belong to network modules with annotated GO terms.

with the total number of somatic versus germline variants, 93/804 (11.6%). The modules for 'extracellular matrix' and 'G2/M transition of mitotic cell cycle' also contained both somatic mutations and germline variants. These results suggest possible interplay between SNPs that may impart a hereditary predisposition to HGSC and subsequently acquired somatic mutations.

## Discussion

Epithelial ovarian cancer is highly responsive to front-line treatment, but relapse with chemotherapy-resistant disease occurs in the majority of cases. To assess disease progression, we used CD45<sup>+</sup> sorted ascites cells as a surrogate for solid tumour biopsies since recurrent samples are not surgically resected and ascites is the only available source of tumour in most cases. We sequenced the exomes of primary, first, and second relapse tumours and discovered mutations affecting multiple cellular processes and structures, including cell cycle control, Golgi vesicles, DNA repair, and extracellular matrix. Remarkably, 89% of mutations found in relapse tumours were present in matched primary tumours, indicating that recurrent

HGSC arises from the selective persistence or out-growth of pre-existing tumour clones, with relatively little accumulation of new mutations. Our results raise the encouraging possibility that improved targeting of mutated pathways in primary tumours could potentially prevent the development of recurrent disease.

Our finding that the majority of mutations in recurrent disease were present in the primary tumour sample is consistent with a prior study of HGSC that used FISH, SNP arrays, and array CGH [24]. Given the genotoxic effects of platinum-based chemotherapy, it is surprising that so few new mutations were found in relapse tumours. Rather, our data indicate that chemotherapy failed to destroy the major clones present in the primary tumour, as indicated by the fact that fewer than 10% of mutations were lost after treatment. An exception was patient 3, who responded dramatically to her first round of treatment based on decreased CA-125 levels (Figure 1) and complete disappearance of a mutational cluster (cluster 5 in Figure 2). Patient 3 also showed the greatest number of new mutations in relapse samples. Relapse-specific mutations observed in patients 1 and 2 included *PREX2*, which has recently been reported in metastatic melanomas [42], and *AP1b1*, which is associated with vesicle formation in the trans-Golgi network [43]. It

is unknown whether these mutations were due to the DNA-damaging effects of chemotherapy or the expansion of a minor tumour clone from the primary tumour.

In all three patients, GO annotated somatic mutation clusters were seen that involved either the Golgi vesicle or Golgi transport (Figure 2). Similarly, network analysis of somatic mutations and germline SNPs revealed two modules that were annotated for the trans-Golgi network and Golgi vesicle targeting (Figure 3). The Golgi apparatus has been previously implicated in cancer processes such as drug efflux, apoptosis, and proliferation. Cisplatin is sequestered by the Golgi in ovarian carcinoma cells, which may be necessary for platinum efflux [44]. The Golgi has also been implicated in apoptosis by such means as compartmentalizing caspase 2, triggering mitochondrial membrane permeability, releasing death receptors to the cell surface, and sensing misfolded proteins [45]. Additionally, anti-cancer drugs such as 2-phenyl benzimidazole (2-PB) disrupt the Golgi apparatus, which leads to reduced cell proliferation and tumour growth [46].

Germline SNPs and somatic mutations were also found in the extracellular matrix (ECM) pathway, including collagens, laminins, integrins, syndecan 1, and fibronectin 1. These proteins are involved in cell adhesion, cell signalling, and cytoskeletal organization, and alterations to ECM pathways have been found during the evolution of other cancers [20,47] but not previously in HGSC.

Germline and somatic variants were found in pathways such as p53, cell cycle progression, and DNA repair (Figure 3), which are known HGSC susceptibility pathways [7]. *TP53* was the only gene found to harbour a somatic mutation in all three patients, while *BRCA1* was somatically mutated in patient 1 and all three patients shared the same germline SNPs in *BRCA2* and *ATM* (Table 1, Supplementary Table 1 and Supplementary Table 2). An apparent chemotherapy-susceptible clone, cluster 5 from patient 3, contained a highly abundant *RGS6* mutation, which is a gene that has been shown to be associated with cancer risk [48]. More recently, *RGS6* has been reported to activate the intrinsic pathway of apoptosis in a p53-independent manner and affected doxorubicin susceptibility in breast cancer cells [49].

Cancer pathogenesis can occur through the loss of both alleles in a tumour suppressor gene in the classical 'two-hit' hypothesis of tumour suppression or through a more subtle, titrated loss of tumour suppressor gene function as described by a continuum model of tumour suppression [50]. Consistent with the continuum model, tumourigenesis can be initiated by p53 haploinsufficiency, as seen in patients with Li–Fraumeni syndrome and, it appears, patient 1 (Table 1). The continuum model of disease progression may extend beyond tumour suppressor genes, since we observed several examples of pathways that were altered by germline variants and became further perturbed by somatic mutations (Figure 3).

We have shown here that HGSC tumours are heterogeneous, with multiple, genetically distinct clones present prior to treatment. Most of the mutations in primary tumours persist despite treatment, suggesting that most clones are able to evade current chemotherapy treatments. Furthermore, there is little accumulation of new mutations in recurrent tumours, even after two rounds of chemotherapy. Encouragingly, we found novel mutations in the Golgi and ECM pathways, which may offer new therapeutic targets for HGSC. Moreover, the relatively stable nature of the HGSC genome over time provides hope that improved therapeutic targeting of the genetic lesions present in primary tumours will ultimately be effective for preventing tumour recurrence.

## Acknowledgments

This work was supported by the US Department of Defense, the Ovarian Cancer Research Program (OC080380), and the British Columbia Cancer Foundation. We thank Ryan Morin, Rodrigo Goya, Rod Docking, and Rene Warren for their technical help with the bioinformatic programs. We thank Scott Brown for his help compiling data and also Dr Joanne Johnson for project management assistance.

## Author contribution statement

MC, BHN, RAH, JRW, and PHW conceived experiments. MC, TZ, KT, MM, and YZ carried out experiments. MC analysed data and MC, KM, and BHN created figures. MC, RAH, and BHN were involved in writing the paper and all authors had final approval of the submitted and published versions.

## References

1. GLOBOCAN 2008 v1.2, Cancer Incidence and Mortality Worldwide: IARC CancerBase no. 10 [Internet]. Lyon, France: International Agency for Research on Cancer, 2010. [Accessed 4 May 2012]; Available from: <http://globocan.iarc.fr>
2. Cho K, Shih I. Ovarian cancer. *Annu Rev Pathol* 2009; **4**: 287–313.
3. Bowtell D. The genesis and evolution of high-grade serous ovarian cancer. *Nature Rev Cancer* 2010; **10**: 803–808.
4. Levanon K, Drapkin R. New insights into the pathogenesis of serous ovarian cancer and its clinical impact. *J Clin Oncol* 2008; **26**: 5284–5293.
5. Bristow RE, Armstrong DK. *Early Diagnosis and Treatment of Cancer Series: Ovarian Cancer*. Saunders/Elsevier: Philadelphia, 2010.
6. Pal T, Permuth-Wey J, Betts JA, *et al.* *BRCA1* and *BRCA2* mutations account for a large proportion of ovarian carcinoma cases. *Cancer* 2005; **104**: 2807–2816.
7. Pennington KP, Swisher EM. Hereditary ovarian cancer: beyond the usual suspects. *Gynecol Oncol* 2012; **124**: 347–353.
8. Weberpals JI, Koti M, Squire JA. Targeting genetic and epigenetic alterations in the treatment of serous ovarian cancer. *Cancer Genet* 2011; **204**: 525–535.

9. Bell D, Cramer DW. Integrated genomic analyses of ovarian carcinoma. *Nature* 2011; **474**: 609–615.
10. Ahmed A, Sharma R. Driver mutations in TP53 are ubiquitous in high grade serous carcinoma of the ovary. *J Pathol* 2010; **221**: 49–56.
11. Salzman J, Marinelli RJ, Wang PL, et al. ESRRA–C11orf20 is a recurrent gene fusion in serous ovarian carcinoma. *PLoS Biol* 2011; **9**: e1001156.
12. Edwards S, Levine D. Resistance to therapy caused by intragenic deletion in *BRCA2*. *Nature* 2008; **451**: 1111–1115.
13. Sakai W, Friedman C. Secondary mutations as a mechanism of cisplatin resistance in *BRCA2*-mutated cancers. *Nature* 2008; **451**: 1116–1120.
14. Swisher EM, Sakai W, Karlan BY, et al. Secondary *BRCA1* mutations in *BRCA1*-mutated ovarian carcinomas with platinum resistance. *Cancer Res* 2008; **68**: 2581–2586.
15. Norquist B, Wurz KA, Pennil CC, et al. Secondary somatic mutations restoring *BRCA1/2* predict chemotherapy resistance in hereditary ovarian carcinomas. *J Clin Oncol* 2011; **29**: 3008–3015.
16. Dhillon KK, Swisher EM, Taniguchi T. Secondary mutations of *BRCA1/2* and drug resistance. *Cancer Sci* 2011; **102**: 663–669.
17. Fodale V, Petricoin E. Mechanism of cell adaptation: when and how do cancer cells develop chemoresistance? *Cancer J* 2011; **17**: 89–95.
18. Gerlinger M, Rowan AJ, Horswell S, et al. Intratumor heterogeneity and branched evolution revealed by multiregion sequencing. *N Engl J Med* 2012; **366**: 883–892.
19. Ley TJ, McLellan MD. DNA sequencing of a cytogenetically normal acute myeloid leukaemia genome. *Nature* 2008; **456**: 66–72.
20. Shah SP, Roth A, Goya R, et al. The clonal and mutational evolution spectrum of primary triple-negative breast cancers. *Nature* 2012; **486**: 395–399.
21. Navin N, Kendall J, Troge J, et al. Tumour evolution inferred by single-cell sequencing. *Nature* 2011; **472**: 90–94.
22. Yachida S, Jones S, Bozic I, et al. Distant metastasis occurs late during the genetic evolution of pancreatic cancer. *Nature* 2010; **467**: 1114–1117.
23. Campbell PJ, Yachida S, Mudie LJ, et al. The patterns and dynamics of genomic instability in metastatic pancreatic cancer. *Nature* 2010; **467**: 1109–1113.
24. Cooke S, Ng C, Melnyk N, et al. Genomic analysis of genetic heterogeneity and evolution in high-grade serous ovarian carcinoma. *Oncogene* 2010; **29**: 4905–4913.
25. Tewhey R, Nakano M, Wang X, et al. Enrichment of sequencing targets from the human genome by solution hybridization. *Genome Biol* 2009; **10**: R116.
26. Li H, Durbin R. Fast and accurate long-read alignment with Burrows–Wheeler transform. *Bioinformatics* 2010; **26**: 589–595.
27. Li H, Handsaker B, Wysoker A, et al. The Sequence Alignment/Map format and SAMtools. *Bioinformatics* 2009; **25**: 2078–2079.
28. Goya R, Sun M, Morin R, et al. SNVMix: predicting single nucleotide variants from next-generation sequencing of tumors. *Bioinformatics* 2010; **26**: 730–736.
29. Warren R, Holt R. Targeted assembly of short sequence reads. *PLoS One* 2011; **6**: e19816.
30. Robinson JT, Thorvaldsdottir H, Winckler W, et al. Integrative genomics viewer. *Nature Biotechnol* 2011; **29**: 24–26.
31. Fujita PA, Rhead B, Zweig AS, et al. The UCSC Genome Browser database: update 2011. *Nucleic Acids Res* 2011; **39**: D876–D882.
32. Montojo J, Zuberi K, Rodriguez H, et al. GeneMANIA Cytoscape plugin: fast gene function predictions on the desktop. *Bioinformatics* 2010; **26**: 2927–2928.
33. Smoot ME, Ono K, Ruscheinski J, et al. Cytoscape 2.8: new features for data integration and network visualization. *Bioinformatics* 2011; **27**: 431–432.
34. JMP, Version 8. SAS Institute Inc, Cary, NC, 1989–2012.
35. Ashburner M, Ball CA, Blake JA, et al. Gene ontology: tool for the unification of biology. *The Gene Ontology Consortium. Nature Genet* 2000; **25**: 25–29.
36. Warde-Farley D, Donaldson SL, Comes O, et al. The GeneMANIA prediction server: biological network integration for gene prioritization and predicting gene function. *Nucleic Acids Res* 2010; **38**: W214–20.
37. Wu G, Stein L. A human functional protein interaction network and its application to cancer data analysis. *Genome Biol* 2010; **11**: R53.
38. Kumar P, Henikoff S, Ng PC. Predicting the effects of coding non-synonymous variants on protein function using the SIFT algorithm. *Nature Protoc* 2009; **4**: 1073–1081.
39. Database of Single Nucleotide Polymorphisms (dbSNP) [Internet]. Bethesda (MD): National Center for Biotechnology Information, National Library of Medicine. dbSNP Accession: Rs4986852:T, rs1592624:G (dbSNP Build ID: 135). [Accessed 1 May, 2012]: Available from: <http://www.Ncbi.Nlm.Nih.gov/SNP/>
40. Forbes SA, Bindal N, Bamford S, et al. COSMIC: mining complete cancer genomes in the Catalogue of Somatic Mutations in Cancer. *Nucleic Acids Res* 2011; **39**: D945–D950.
41. Hanahan D, Weinberg RA. Hallmarks of cancer: the next generation. *Cell* 2011; **144**: 646–674.
42. Berger MF, Lawrence MS. Melanoma genome sequencing reveals frequent *PREX2* mutations. *Nature* 2012; **485**: 502–506.
43. Kirchhausen T. Three ways to make a vesicle. *Nature Rev Mol Cell Biol* 2000; **1**: 187–198.
44. Safaei R, Holzer AK. Intracellular localization and trafficking of fluorescein-labeled cisplatin in human ovarian carcinoma cells. *Clin Cancer Res* 2005; **11**: 756–767.
45. Wlodkowic D, Darzynkiewicz Z. ER–Golgi network – a future target for anti-cancer therapy. *Leuk Res* 2009; **33**: 1440–1447.
46. Lio SC, Millis D. Disruption of Golgi processing by 2-phenyl benzimidazole analogs blocks cell proliferation and slows tumor growth. *Cancer Chemother Pharmacol* 2008; **61**: 1045–1058.
47. Walter MJ, Shen D, Ding L, et al. Clonal architecture of secondary acute myeloid leukemia. *N Engl J Med* 2012; **366**: 1090–1098.
48. Berman DM, Wang Y, Liu Z, et al. A functional polymorphism in *RGS6* modulates the risk of bladder cancer. *Cancer Res* 2004; **64**: 6820–6826.
49. Maity B, Bera S. Regulator of G Protein Signaling 6 (*RGS6*) induces apoptosis via a mitochondrial-dependent pathway not involving its GTPase-activating protein activity. *J Biol Chem* 2011; **286**: 1409–1419.
50. Berger AH, Knudson AG, Pandolfi PP. A continuum model for tumour suppression. *Nature* 2011; **476**: 163–169.

## SUPPORTING INFORMATION ON THE INTERNET

The following supporting information may be found in the online version of this article.

**Table S1** Homozygous SNPs shared by the three HGSC patients.

**Table S2** Conversion of variant genomic positions from the Hg18 to the Hg19 reference genomes.

# CD20<sup>+</sup> Tumor-Infiltrating Lymphocytes Have an Atypical CD27<sup>-</sup> Memory Phenotype and Together with CD8<sup>+</sup> T cells Promote Favorable Prognosis in Ovarian Cancer

Julie S. Nielsen<sup>1,3</sup>, Rob A. Sahota<sup>1</sup>, Katy Milne<sup>1</sup>, Sara E. Kost<sup>1,2</sup>, Nancy J. Nesslinger<sup>1</sup>, Peter H. Watson<sup>1,2,4</sup>, and Brad H. Nelson<sup>1,2,3</sup>

## Abstract

**Purpose:** Tumor-infiltrating lymphocytes (TIL), in particular CD8<sup>+</sup> T cells and CD20<sup>+</sup> B cells, are strongly associated with survival in ovarian cancer and other carcinomas. Although CD8<sup>+</sup> TIL can mediate direct cytolytic activity against tumors, the role of CD20<sup>+</sup> TIL is poorly understood. Here, we investigate the possible contributions of CD20<sup>+</sup> TIL to humoral and cellular tumor immunity.

**Experimental Design:** Tumor and serum specimens were obtained from patients with high-grade serous ovarian cancer. CD8<sup>+</sup> and CD20<sup>+</sup> TIL were analyzed by immunohistochemistry and flow cytometry. Immunoglobulin molecules were evaluated by DNA sequencing. Serum autoantibody responses to the tumor antigens p53 and NY-ESO-1 were measured by ELISA.

**Results:** The vast majority of CD20<sup>+</sup> TIL were antigen experienced, as evidenced by class-switching, somatic hypermutation, and oligoclonality, yet they failed to express the canonical memory marker CD27. CD20<sup>+</sup> TIL showed no correlation with serum autoantibodies to p53 or NY-ESO-1. Instead, they colocalized with activated CD8<sup>+</sup> TIL and expressed markers of antigen presentation, including MHC class I, MHC class II, CD40, CD80, and CD86. The presence of both CD20<sup>+</sup> and CD8<sup>+</sup> TIL correlated with increased patient survival compared with CD8<sup>+</sup> TIL alone.

**Conclusions:** In high-grade serous ovarian tumors, CD20<sup>+</sup> TIL have an antigen-experienced but atypical CD27<sup>-</sup> memory B-cell phenotype. They are uncoupled from serum autoantibodies, express markers of antigen-presenting cells, and colocalize with CD8<sup>+</sup> T cells. We propose that the association between CD20<sup>+</sup> TIL and patient survival may reflect a supportive role in cytolytic immune responses. *Clin Cancer Res*; 1–12. ©2012 AACR.

## Introduction

High-grade serous ovarian cancer (hereafter abbreviated HGSC) is the most common and lethal subtype of ovarian cancer, with a 5-year survival rate of only 30% (1). Although most patients are highly responsive to primary surgery and chemotherapy, the majority experience recurrence within 1 to 3 years and ultimately succumb to their disease (2). Despite these unfortunate statistics, a subset of patients experience prolonged disease-free survival. Favorable prog-

nostic indicators for HGSC include early stage and optimal surgical debulking (2). Furthermore, studies over the past 2 decades have revealed strong links between host immunity and survival. In particular, multiple studies have shown that the presence of CD3<sup>+</sup> and CD8<sup>+</sup> tumor-infiltrating lymphocytes (TIL) is associated with markedly prolonged survival (3–8).

In addition to CD8<sup>+</sup> T cells, we have shown that tumor-infiltrating CD20<sup>+</sup> B cells (CD20<sup>+</sup> TIL) are strongly associated with patient survival in HGSC (6). Tumor-infiltrating B cells are also correlated with favorable outcomes in breast, cervical, and non-small cell lung cancer (9–11). In breast cancer and germ cell tumors, tumor-infiltrating B cells have been shown to consist of activated, antigen-experienced, oligoclonal subpopulations (12–18). Beyond this information, the mechanistic role of CD20<sup>+</sup> TIL in tumor immunity remains poorly defined. *A priori*, tumor-infiltrating B cells could mediate their effects through the production of tumor-specific antibodies. Indeed, more than 40% of HGSC patients show autoantibody responses to tumor antigens such as p53 and NY-ESO-1 (19, 20). In theory, tumor-specific autoantibodies could mediate antitumor responses by direct inhibition of target proteins, activation of

**Authors' Affiliations:** <sup>1</sup>Trev and Joyce Deeley Research Centre, British Columbia Cancer Agency; <sup>2</sup>Department of Biochemistry and Microbiology, University of Victoria, Victoria; <sup>3</sup>Department of Medical Genetics, University of British Columbia; and <sup>4</sup>Department of Pathology and Laboratory Medicine, University of British Columbia, Vancouver, British Columbia, Canada

**Note:** Supplementary data for this article are available at Clinical Cancer Research Online (<http://clincancerres.aacrjournals.org/>).

**Corresponding Author:** Julie S. Nielsen, Trev and Joyce Deeley Research Centre, British Columbia Cancer Agency, 2410 Lee Avenue, Victoria, British Columbia, V8R 6V5, Canada. Phone: 250-519-5700; Fax: 250-519-5714; E-mail: [jnielsen@bccancer.bc.ca](mailto:jnielsen@bccancer.bc.ca)

doi: 10.1158/1078-0432.CCR-12-0234

©2012 American Association for Cancer Research.

### Translational Relevance

High-grade serous ovarian cancer has a 5-year survival rate of only 30%, so there is an urgent need for improved treatments. Recent studies have provided unequivocal evidence that patients who mount strong immune responses against their tumor experience markedly prolonged survival. Although tumor-infiltrating T cells are clearly important for tumor immunity, we have recently shown an equally prominent role for B cells. Here, we investigate the underlying mechanisms. Unexpectedly, we found that tumor-infiltrating B cells were uncoupled from antibody responses to common tumor antigens. Instead, they colocalized with T cells and showed characteristics of antigen-presenting cells. The presence of both B cells and T cells in tumors was associated with better prognosis than T cells alone. Thus, tumor-infiltrating B cells seem to support T-cell responses to cancer. Immunotherapeutic strategies that engage both lymphocyte subsets may have more potent and sustained anti-tumor effects.

complement, opsonization of tumor antigens, or triggering of antibody-dependent cellular cytotoxicity. In addition to secreting antibodies, B cells could enhance tumor immunity through cellular mechanisms. For example, B cells can serve as antigen-presenting cells (APC) to T cells (reviewed in ref. 21). In this capacity, B cells have an advantage over dendritic cells in that they can concentrate their cognate antigen through surface Ig molecules, thereby allowing presentation of even low abundance antigens (21).

Additional insights into the possible role(s) of CD20<sup>+</sup>TIL in tumor immunity can be gained from studies of B cell infiltrates in autoimmunity and solid organ transplantation (21–29). In renal allografts, the presence of graft-infiltrating B cells is a sign of impending rejection (25). Intriguingly, in this setting, infiltrating B cells are uncoupled from donor-specific serologic responses (29) and instead are thought to facilitate T-cell responses by serving as APC and by releasing cytokines and chemokines that recruit T cells to affected tissues. Indeed, treatment of renal allograft recipients with anti-CD20 antibody (rituximab) not only depletes B cells but also results in reduced expression of T-cell-associated genes (24). Similar mechanisms are thought to operate in autoimmunity. In a murine xenograft model of rheumatoid arthritis, depletion of B cells with anti-CD20 antibody lead to the disappearance of not only infiltrating B cells but also reduced activation and infiltration of T cells (27). These findings raise the intriguing possibility that CD20<sup>+</sup>TIL may engage in similar cooperative interactions with T cells in cancer.

In this study, we investigated the possible functional roles of CD20<sup>+</sup>TIL in HGSC. Using matched tumor and serum samples from HGSC patients, we examined the relationship between CD20<sup>+</sup>TIL and tumor-specific autoantibody responses. Using multiparameter immunohistochemistry

(IHC) and flow cytometry, we assessed potential contributions of CD20<sup>+</sup>TIL to cellular tumor immunity. Our results provide evidence that CD20<sup>+</sup> and CD8<sup>+</sup>TIL work cooperatively to mediate antitumor immunity in HGSC, leading to markedly prolonged patient survival.

### Materials and Methods

#### Study subjects and sample processing

Studies were carried out with 3 HGSC patient cohorts. Cohort A ( $n = 40$ ), assembled through a prospective study entitled Immune Response to Ovarian Cancer (IROC), included serial serum samples, cryopreserved cells, frozen tissue, and formalin-fixed paraffin-embedded (FFPE) tissue blocks. Clinical characteristics are described in Supplementary Table S1. Cohort B was a small retrospective cohort ( $n = 30$ ) with matched serum samples and FFPE tissue blocks. The clinical characteristics were similar to those of cohort A. Cohort C ( $n = 194$ ) was from a large previously published retrospective cohort, which included only FFPE tissue blocks (6, 30). The clinical characteristics were similar to those of cohort A, with the exception that all patients were optimally debulked during primary surgery. For ELISA experiments, the control group consisted of age-matched women with both ovaries intact and no personal history of cancer. All specimens and clinical data were collected with informed patient consent through the BC Cancer Agency's Tumour Tissue Repository (cohort A) or OvCaRe (cohorts B and C) under protocols approved by the Research Ethics Board of the BC Cancer Agency and the University of British Columbia.

Tumor tissue was obtained at the time of primary cytoreductive surgery before any other treatment. Samples were either preserved in formalin and processed in paraffin for preparation of tissue microarrays, frozen in OCT medium for sectioning and DNA extraction, or processed into single-cell suspensions as previously described (31). Serum was processed using serum separator tubes, aliquoted, and stored at  $-80^{\circ}\text{C}$ . Pretreatment serum was collected before primary surgery (except for patient IROC037, which was collected 1 month postsurgery), and subsequent samples were collected approximately 3, 6, 12, and 24 months following surgery. Peripheral blood mononuclear cells (PBMC) from patients and healthy controls were collected in heparinized Vacutainer tubes, isolated by Ficoll density centrifugation and cryopreserved.

#### Immunohistochemistry

For cohort A, a tissue microarray (TMA) was constructed using a manual tissue arrayer from Beecher Instruments. The TMA consisted of duplicate 1-mm cores taken from representative central regions of nonnecrotic tumor epithelium with some stromal regions, as defined upon review of hematoxylin and eosin-stained sections by a pathologist (PHW). For cohorts B and C, TMAs were constructed in a similar manner but consisted of 0.6-mm duplicate cores and were constructed using a Pathology Devices tissue arrayer. TMAs from cohorts A and B were prepared and

stained as previously described (31) using an anti-CD20 rabbit polyclonal primary antibody (catalog #RB-9013; Lab Vision). The cohort C TMA was prepared and stained as previously described (30).

Scoring of TMAs for cohorts A and B was carried out in a blinded fashion by a pathologist (PHW). Tumor cores were initially scored by assessing at low magnification the proportion of each core that comprised tumor or stroma and then scoring at 20 $\times$  magnification the number of positively stained TIL within the core area (through direct counting up to 20 or by estimation in 10s when in excess of this number), as well as the proportion of TIL present in tumor epithelium versus stroma. For cohort C, cores were scored either 0 (no cells present), 1 (1–5 cells), 2 (6–19 cells), or 3 (20+ cells) and then binarized to negative versus positive (score 0 vs. scores 1, 2, and 3). This binarization was used to generate the survival data in Fig. 6E. Survival curves were not determined for cohorts A and B due to small sample size and insufficient follow-up time.

Two-color IHC was carried out on FFPE sections following deparaffinization in a decloaking chamber (Biocare Medical) with Diva Decloaker. Samples were blocked with Peroxidase-1 and Background Sniper and then labeled with a cocktail of antibodies to CD8 (mouse monoclonal C8/144B; Cell Marque) and CD20 (rabbit polyclonal catalog # E2560; Spring Bio) for 30 minutes at room temperature. The two-color polymer kit Mach-2 DS2 was used to amplify the primary signal, and Betazoid DAB and Warp Red chromogens were used for detection. Slides were counterstained with hematoxylin. All staining reagents were from Biocare Medical. Images were captured using an Olympus BX53 microscope and Nuance multispectral imaging system (CRI).

### Flow cytometry

Cryopreserved cells were labeled with antibodies listed in Supplementary Table S2. Data were acquired using a BD Influx cell sorter (BD Biosciences) and analyzed using FlowJo software (Tree Star). All samples are gated on lymphocytes based on forward and side scatter plots. Antibody specificity was tested using matched isotypes and fluorescence-minus-one controls.

### Idiotypic sequencing

Six independent PCRs were carried out using primer pairs designed to amplify VH1, VH2, VH3, VH4, VH5, and VH6 sequences. After amplification, PCRs were combined in pools of two and cloned into the pENTR/D-TOPO plasmid vector (Invitrogen). At the BC Cancer Agency's Genome Sciences Centre (Vancouver, Canada), plasmids were electroporated into DH10B T1 phage-resistant cells, plated onto selective growth media, and robotically arrayed in 384-well plates. Plasmid DNAs were then extracted and BigDye Terminator (ABI) cycle sequenced on ABI 3730 sequencers using conventional procedures.

DNA sequences were analyzed using the IMGT/V-QUEST tool (32) of IMGT, the international ImmunoGeneTics information system (33). Up to 96 sequences were analyzed

from each tumor sample. Sequences were compared with germline sequences to identify somatic hypermutations, and V-D-J junctions were compared to identify clonal sequences.

### ELISA to detect serum antibodies to NY-ESO-1 and p53

cDNAs encoding the autoantigens NY-ESO-1 and p53 were amplified by reverse transcriptase PCR (RT-PCR) from the ovarian cancer cell line OVCAR3, cloned into the pDEST17 vector, and used for recombinant protein production, as previously described (NY-ESO-1; ref. 31) or using the primer pair: 5'-CACCATGGAGGAGCCGAGTCA and 5'-TTAGTCTGAGTCAGGCCCTTCTGT (p53). Serum was assayed in triplicate for IgG antibodies to recombinant NY-ESO-1 and p53 by ELISA as previously described (31). Triplicate measurements of control sera were used to establish the mean and SD of autoantibody responses to each antigen. For cancer patients, autoantibody responses were scored as positive if they were significantly greater than the mean of the controls. Specifically, the mean of the controls was subtracted from individual patient responses, which were then divided by the SD of all controls. Responses greater than 3.0 SDs from the control mean were considered positive (34). Association between CD20 status and autoantibody responses was assessed using the Fisher exact test with a 2-tailed *P* value (GraphPad Prism). To assess quantitative changes over time, autoantibody titers were determined using a method similar to Gnjatich and colleagues (19). Each serum sample was subjected to 4-fold serial dilutions from 1:100 to 1:6,553,600. Reciprocal titers were determined based on the highest dilution that gave a positive response against NY-ESO-1. The cutoff for positive responses was based on optical density values greater than twice the value of the average optical density of the 4 lowest dilutions of a pool of 5 healthy donor serum samples.

## Results

### CD20<sup>+</sup> TIL are mature, antigen-experienced B cells

We previously reported that CD20<sup>+</sup> TIL are strongly associated with prolonged survival in HGSC (6). To investigate potential immunologic mechanisms underlying this association, we first assessed whether CD20<sup>+</sup> TIL exhibit characteristics of antigen-experienced B cells. We selected 9 HGSC tumors containing CD20<sup>+</sup> TIL, as determined by IHC (Fig. 1A) and used multiparameter flow cytometry to assess surface immunoglobulin expression on CD20<sup>+</sup> B cells from tumor tissue and matched blood samples. In peripheral blood, HGSC patients showed a normal distribution of naive (IgD<sup>+</sup>IgM<sup>+</sup>IgG<sup>-</sup>) and activated (IgD<sup>-</sup>IgM<sup>-</sup>IgG<sup>+</sup>) CD20<sup>+</sup> B cells, which was similar to cancer-free controls (Fig. 1B). In contrast, the vast majority of CD20<sup>+</sup> TIL showed an activated phenotype (IgD<sup>-</sup>IgM<sup>-</sup>IgG<sup>+</sup>), indicating they had undergone Ig class switching in response to antigen exposure (Fig. 1B).

To further investigate whether CD20<sup>+</sup> TIL were antigen experienced, we sequenced up to 96 IgG heavy chain variable regions (including V, D, and J gene segments) from

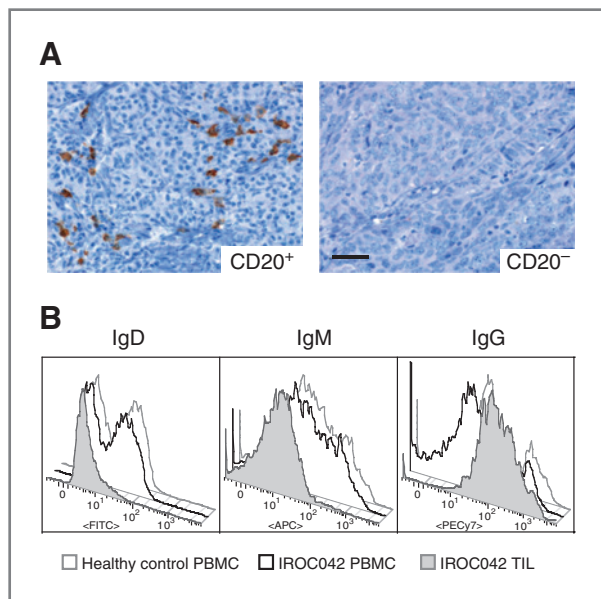


**Figure 1.** Surface immunoglobulin expression by CD20<sup>+</sup> TIL. **A**, immunohistochemical analysis of CD20<sup>+</sup> TIL in representative positive (left) and negative (right) HGSC tumors. Scale bar: 50 μm. **B**, flow cytometry data from a representative patient showing that the majority of CD20<sup>+</sup> TIL express surface IgG, whereas CD20<sup>+</sup> B cells from peripheral blood (PBMC) of patients and healthy controls predominantly express IgD and IgM. Samples were gated on CD20<sup>+</sup> lymphocytes ( $n = 9$ ).

tumor-infiltrating B cells isolated from 3 HGSC patients. We observed a diverse cross-section of sequences from all major VH families (Supplementary Fig. S1). Moreover, tumor-infiltrating B cells exhibited a high level of somatic hypermutation: on average 20 nucleotides were mutated in each approximately 400 nucleotide variable region, resulting in an average of 13 amino acid (aa) substitutions (Fig. 2A). This is consistent with reference values for antigen-experienced B cells (~18 nucleotide and 10 aa substitutions; ref. 18). Moreover, in all 3 tumors, there was evidence of B cells actively undergoing somatic hypermutation, as numerous sequences were identified with identical V-D-J junctions but distinct mutation patterns. An example of a clone with multiple mutated sequences is depicted in Fig. 2B.

Finally, the clonality of CD20<sup>+</sup> TIL was estimated by calculating the prevalence of each variable gene sequence in the dataset. Sequences were defined as clonal if at least 2 independent sequences contained identical V-D-J junctions but differing mutational patterns. Using these criteria, we found evidence for at least 11 to 14 B cell clones in each tumor, some of which were highly represented. For example, in IROC015, 16% of sequences were derived from a single B cell clone, an additional 17% of sequences were derived from 2 other predominant clones, a further 33% of sequences were derived from 8 minor clones, and the remaining 34% of sequences were unrelated (Fig. 2C). These trends were very similar across all 3 patients (Fig. 2C), indicating that CD20<sup>+</sup> TIL represent oligoclonal populations. Note that these are conservative estimates of clonal

abundance, as we disregarded any identical sequences (i.e., sequences that had the same mutational profiles), reasoning that these could result from RT-PCR amplification of mRNA molecules derived from the same B cell. When the analysis was repeated with the inclusion of duplicate sequences, the predominant B-cell clones in each patient represented 22% to 24% of all sequences (compared with 8%–16% of sequences in the initial analysis). We saw no evidence of shared clonotypes between patients (Supplementary Fig. S1). Collectively, these results indicated that CD20<sup>+</sup> TIL have undergone activation, Ig class switching, somatic hypermutation, and clonal expansion, all of which are hallmarks of antigen exposure.

### CD20<sup>+</sup> TIL have an atypical CD27-negative memory phenotype

Given the above results, we further characterized the phenotype of antigen-experienced CD20<sup>+</sup> TIL by flow cytometry to determine whether they exhibit features of germinal center or memory B cells. Triple staining with antibodies against CD20, CD38, and IgD revealed that CD20<sup>+</sup> PBMC from HGSC patients and healthy controls consisted of 2 populations: 50% to 65% of CD20<sup>+</sup> PBMC were IgD<sup>+</sup>CD38<sup>low</sup>, indicative of naive B cells, whereas 35% to 50% were IgD<sup>+</sup>CD38<sup>low</sup>, indicative of memory B cells (Fig. 3A, top panels). The results for CD20<sup>+</sup> TIL were strikingly different. Naive CD20<sup>+</sup> B cells were not seen. In 3 of 9 TIL samples, a small population of IgD<sup>+</sup>CD38<sup>+</sup> cells was observed, consistent with germinal center B cells (Fig. 3A, rightmost CD20<sup>+</sup> TIL panel). Most notably, in all 9 patients the vast majority of CD20<sup>+</sup> TIL were IgD<sup>+</sup>CD38<sup>low</sup>, indicative of a memory B-cell phenotype (Fig. 3A).

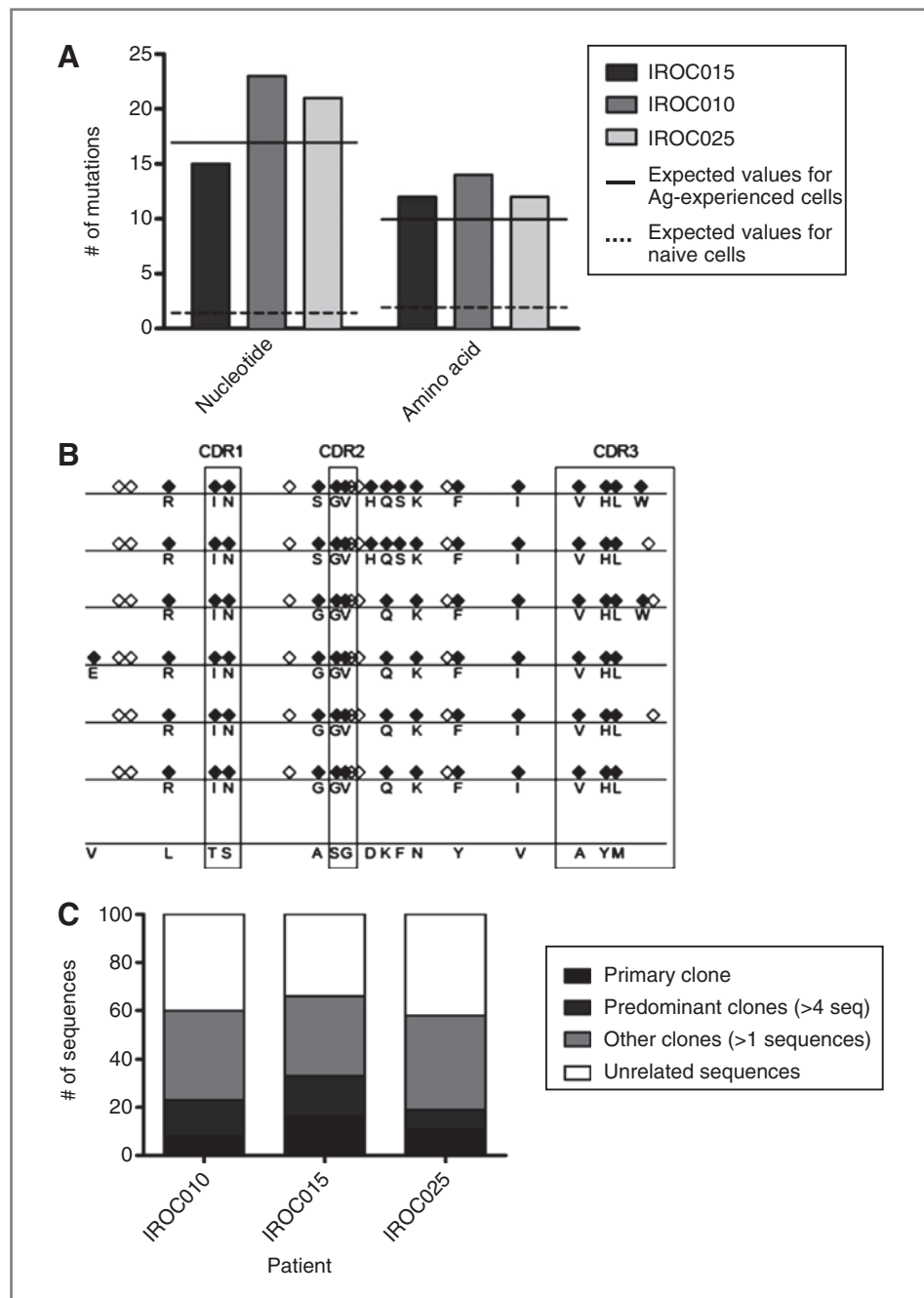
CD27 is a cell-surface protein that is expressed under normal physiologic conditions (35–37). As expected, the vast majority of peripheral blood IgG<sup>+</sup> B cells from HGSC patients and healthy controls expressed CD27 (Fig. 3B), consistent with a memory phenotype, whereas IgD<sup>+</sup> (naive) B cells lacked CD27 expression (data not shown). In sharp contrast, in 8 of 9 tumor samples, virtually all IgG<sup>+</sup>CD20<sup>+</sup> TIL failed to express CD27 (Fig. 3B), suggesting that they represent atypical CD27<sup>+</sup> memory B cells, as described in other physiologic settings (38–41).

In addition to CD20<sup>+</sup> B cells, we analyzed tumor and blood samples for the presence of plasma cells and plasmablasts. There was a complete absence of CD20<sup>+</sup>CD38<sup>+</sup>CD138<sup>+</sup> plasma cells in all analyzed tumors, whereas the majority of analyzed tumors (80%) contained small numbers of cells with a plasmablast phenotype (CD20<sup>+</sup>CD38<sup>+</sup>CD138<sup>+</sup>CD3<sup>+</sup>CD56<sup>+</sup>; Fig. 3C). In summary, B-cell lineage TIL in HGSC are composed predominantly of CD27<sup>+</sup> memory B cells, with small numbers of germinal center B cells and plasmablasts.

### CD20<sup>+</sup> TIL are uncoupled from tumor-specific serum autoantibody responses

The low abundance of plasmablasts and plasma cells in tumors suggested that CD20<sup>+</sup> TIL, though antigen-

**Figure 2.** CD20<sup>+</sup> TIL are oligoclonal and have undergone somatic hypermutation. A, by DNA sequence analysis IgG heavy chain genes from 3 HGSC tumors displayed extensive somatic hypermutation. Solid lines: expected values for antigen-experienced B cells, dotted lines: expected values for naive B cells (18). B, a representative IgG clonal group showing clonal evolution within the tumor. The germline sequence is displayed on the bottom row, whereas all other rows represent unique sequences present in IgG molecules derived from tumor tissue. Black diamonds: nonsynonymous mutations, white diamonds: synonymous mutations, letters: amino acid substitutions. C, IgG sequences from 3 HGSC tumors reveal the oligoclonal composition of CD20<sup>+</sup> TIL. Eight to 16 percent of sequences were derived from a single "primary" clone in each tumor, whereas a large percentage of the remaining sequences were derived from other predominant or minor clones.



experienced, might not contribute significantly to systemic humoral immunity. To further explore this possibility, we evaluated whether CD20<sup>+</sup> TIL were correlated with tumor-specific serum autoantibody responses. We and others have shown that at least 40% of HGSC patients have serum autoantibody responses to one or more tumor antigens (19, 20). Of the target antigens identified to date, NY-ESO-1 and p53 are among the most frequently recognized in ovarian cancer (19, 20), so these 2 antigens were selected for further analysis. By ELISA, 8 of 40 (20%) HGSC patients in cohort A showed a serum autoantibody response to NY-

ESO-1 or p53 (Fig. 4A and B). Notably, these responses were equally prevalent in patients with or without CD20<sup>+</sup> TIL (19% vs. 20%, respectively;  $P = 1.00$ ; Fig. 4A and B). Similar results were seen in an independent cohort of HGSC patients ( $n = 30$ ; cohort B), in which autoantibody responses were equally prevalent in patients with or without CD20<sup>+</sup> TIL (30% vs. 29%, respectively;  $P = 1.00$ ; data not shown).

To further address this issue, we assessed whether removal of CD20<sup>+</sup> TIL, which occurs during primary surgery and chemotherapy, abrogated tumor-specific serum

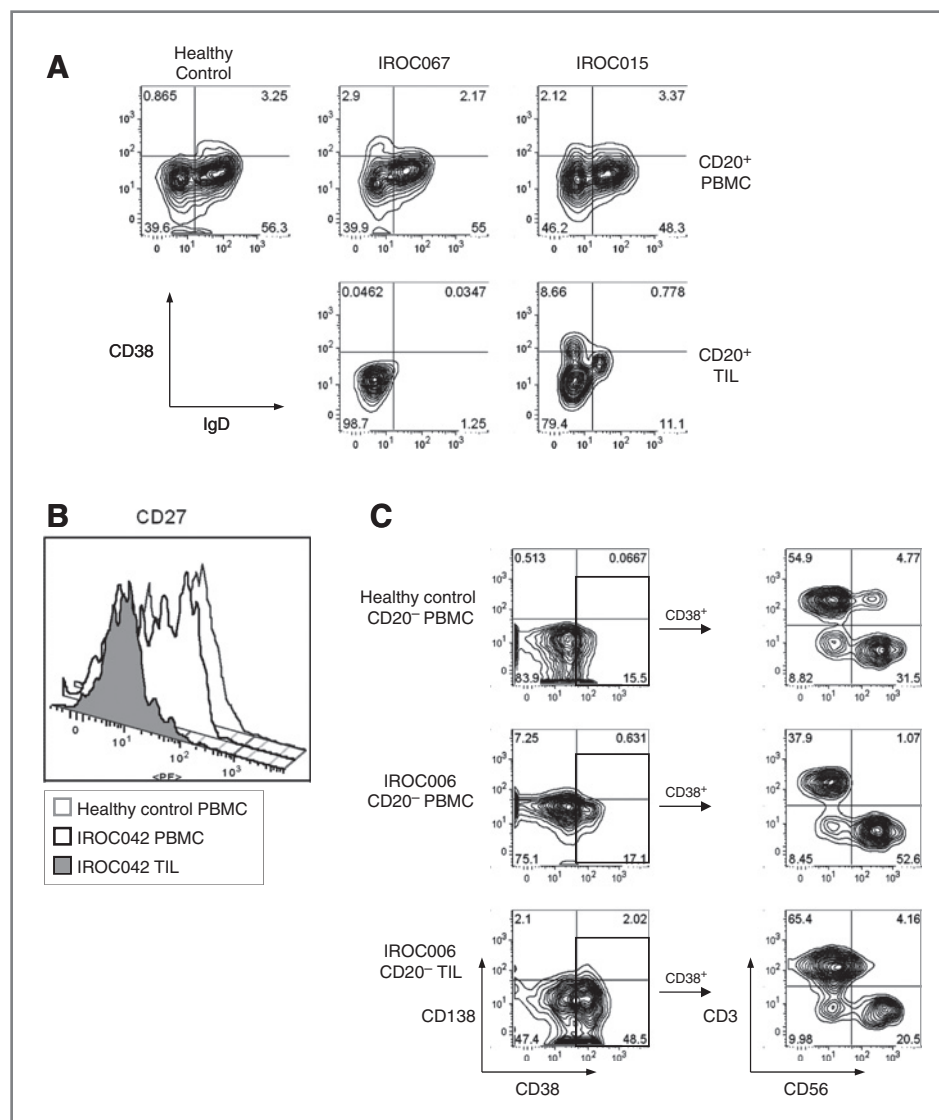


**Figure 3.** Flow cytometric characterization of B cells, plasma cells, and plasmablasts in HGSC. **A**, naive versus memory B cells: Flow cytometric analysis of PBMC and TIL samples stained with antibodies to CD20, IgD, and CD38. As expected, CD20<sup>+</sup> PBMC from healthy controls and HGSC patients consist primarily of naive (IgD<sup>+</sup>CD38<sup>-</sup>) and memory (IgD<sup>-</sup>CD38<sup>+</sup>) B cells (top). In contrast, the vast majority of CD20<sup>+</sup> TIL show a memory phenotype (IgD<sup>-</sup>CD38<sup>+</sup>; bottom). Data are representative of 9 HGSC patients. In 3 of 9 patients (as shown for IROC015), a small population of germinal center CD20<sup>+</sup> B cells (IgD<sup>-</sup>CD38<sup>+</sup>) is also seen. **B**, CD27 expression: Flow cytometric analysis of CD27 expression by PBMC and TIL from a representative healthy donor and HGSC patient. Samples are gated on CD20<sup>+</sup>IgG<sup>+</sup> lymphocytes. As expected, the majority of CD20<sup>+</sup>IgG<sup>+</sup> B cells in PBMC express CD27. In contrast, the vast majority of CD20<sup>+</sup>IgG<sup>+</sup> TIL fail to express CD27. Data are representative of 9 HGSC patients. **C**, Plasmablasts and plasma cells: Flow cytometric analysis of CD38 and CD138 expression by PBMC and TIL from a representative healthy donor and a HGSC patient positive for CD20<sup>+</sup> TIL. Samples were gated on CD45<sup>+</sup>CD20<sup>+</sup> lymphocytes. Left, PBMC and TIL samples generally lack CD20<sup>+</sup>CD38<sup>+</sup> plasma cells (expected to be in top right quadrant). Right, further gating of CD38<sup>+</sup> cells from the left panels reveals the presence of low numbers of cells with a plasmablast phenotype (CD20<sup>+</sup>CD38<sup>+</sup>CD3<sup>-</sup>CD56<sup>-</sup>, bottom left quadrants) in PBMC and TIL samples. Data are representative of 4 of 5 tumor samples.

autoantibody responses. We quantified autoantibody titers to NY-ESO-1 in 6 HGSC patients using serum samples collected before and 2 to 6 months after primary surgery. We selected serum samples that were collected as near as possible to the time of lowest tumor burden according to CA125 levels (Supplementary Table S3). Five of 6 patients showed an objective response to surgery and chemotherapy, as manifested by CA125 levels, CT scan, or physical examination. In most patients, autoantibody levels

decreased after treatment, although one patient (IROC065) showed a reproducible increase (Fig. 4C). Irrespective of these changes, all patients maintained high-titer NY-ESO-1-specific autoantibody responses (range: 1:3,200 to 1:204,800; Supplementary Table S3) after cytoreductive treatment. This indicated that the majority of anti-NY-ESO-1 autoantibody production occurs outside of tumor tissue. Thus, by multiple lines of evidence, CD20<sup>+</sup> TIL are uncoupled from humoral immune responses in HGSC.

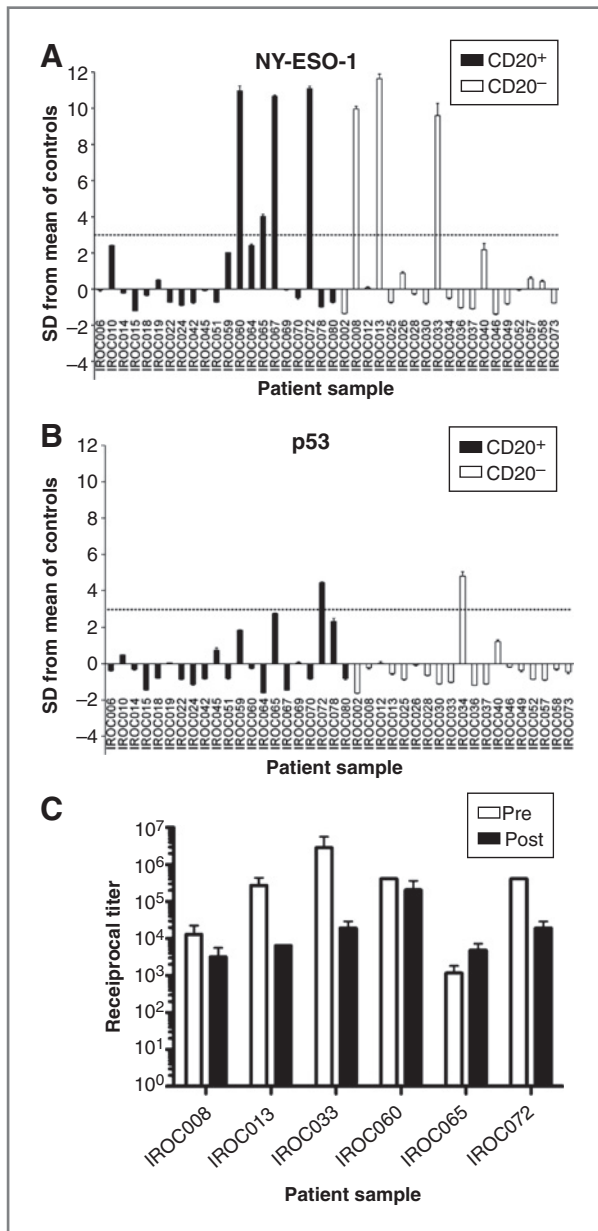


**Figure 4.** CD20<sup>+</sup> TIL are uncoupled from humoral immunity. A and B, ELISA data from cohort A ( $n = 40$ ) showing equivalent frequencies of autoantibody responses to (A) NY-ESO-1 and (B) p53 in pretreatment sera from patients with tumors scored as positive (black bars) or negative (white bars) for CD20<sup>+</sup> TIL. The threshold is set at 3.0 SDs from the mean optical density of 30 healthy control samples. C, ELISA data for 6 HGSC patients showing serum autoantibody responses to NY-ESO-1 before primary treatment (Pre; white bars) and 2 to 6 months after primary surgery when tumor burden was lowest according to CA-125 levels (Post; black bars). Data are plotted as reciprocal titers. Representative of 3 independent experiments, each run in triplicate.

#### CD20<sup>+</sup> TIL express cell surface markers characteristic of antigen-presenting cells

The foregoing results suggested that CD20<sup>+</sup> TIL might contribute to tumor immunity through cellular rather than humoral mechanisms. Indeed, in addition to producing

antibodies, B cells can facilitate T-cell responses by serving as APC and by recruiting T cells to affected tissues (42). We therefore assessed whether CD20<sup>+</sup> TIL might serve as APC to T cells, as described in other settings (23, 26, 42, 43). Unfortunately, the low absolute numbers of CD20<sup>+</sup> TIL in human specimens precluded *in vitro* functional analyses. However, sufficient material was available to carry out multiparameter flow cytometry to determine whether CD20<sup>+</sup> TIL express cell-surface molecules involved in antigen presentation. CD20<sup>+</sup> TIL expressed MHC class I (pan-HLA-A, B, and C) and class II (HLA-DR) molecules, as well as CD40 (Fig. 5A). Furthermore, CD20<sup>+</sup> TIL expressed the costimulatory molecules B7-1 (CD80) and B7-2 (CD86), albeit at moderate levels (Fig. 5A). Accordingly, the majority of tumor-infiltrating CD4<sup>+</sup> and CD8<sup>+</sup> T cells displayed an activated effector phenotype (HLA-DR<sup>+</sup>CD45RO<sup>+</sup>CD45-RA<sup>-</sup>CD62L<sup>-</sup>; Fig. 5B). Collectively, our results are consistent with the possibility that CD20<sup>+</sup> TIL serve as APC to T cells in the tumor environment.

#### CD8<sup>+</sup> and CD20<sup>+</sup> TIL colocalize in HGSC

If B cells serve as APC in the tumor environment, they would be expected to be located in close proximity to T cells. To assess this, we carried out 2-color IHC with antibodies to CD8 and CD20. As previously reported, CD8<sup>+</sup> and CD20<sup>+</sup> TIL were found in both tumor stroma and epithelium (Fig. 6A and B). Intriguingly, CD8<sup>+</sup> and CD20<sup>+</sup> lymphocytes were frequently seen in close proximity, often in loosely structured aggregates (Fig. 6A). Such aggregates were even found in tumors with low densities of TIL, suggesting the colocalization of CD20<sup>+</sup> and CD8<sup>+</sup> TIL was an active process. There were numerous examples in which CD8<sup>+</sup> and CD20<sup>+</sup> TIL were directly juxtaposed, consistent with cell-cell interactions (Fig. 6C and D). In summary, these imaging studies indicated that CD8<sup>+</sup> and CD20<sup>+</sup> TIL are frequently colocalized in HGSC, further supporting a possible role for CD20<sup>+</sup> TIL as APC.

#### The combination of CD8<sup>+</sup> and CD20<sup>+</sup> TIL is associated with prolonged survival in HGSC

Finally, we used data from a large previously published cohort (6) to assess the relationship between CD20<sup>+</sup> and CD8<sup>+</sup> TIL and patient survival. CD20<sup>+</sup> and CD8<sup>+</sup> TIL were found in 41% and 84% of cases, respectively. Of the cases that were positive for CD20<sup>+</sup> TIL, almost all were also positive for CD8<sup>+</sup> TIL. Conversely, of the cases that were positive for CD8<sup>+</sup> TIL, approximately half also contained CD20<sup>+</sup> TIL. By Kaplan-Meier analysis, cases that were positive for both CD8<sup>+</sup> and CD20<sup>+</sup> TIL showed markedly greater disease-specific survival compared with those positive for CD8<sup>+</sup> TIL alone (Fig. 6E). Thus, it seems that CD20<sup>+</sup> TIL can potentially enhance the antitumor effect of CD8<sup>+</sup> TIL in ovarian cancer.

#### Discussion

We have investigated potential mechanisms by which CD20<sup>+</sup> TIL contribute to tumor immunity in HGSC,

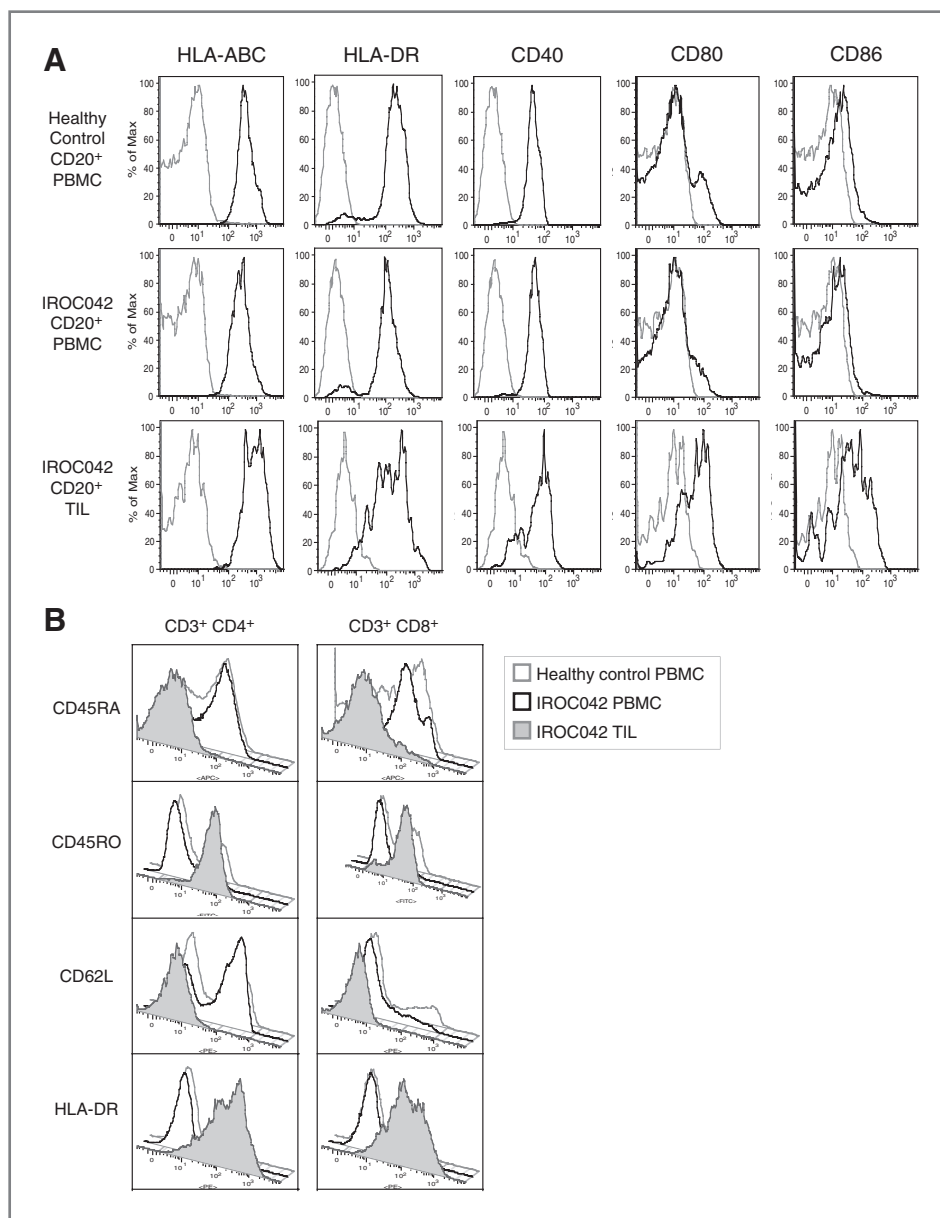


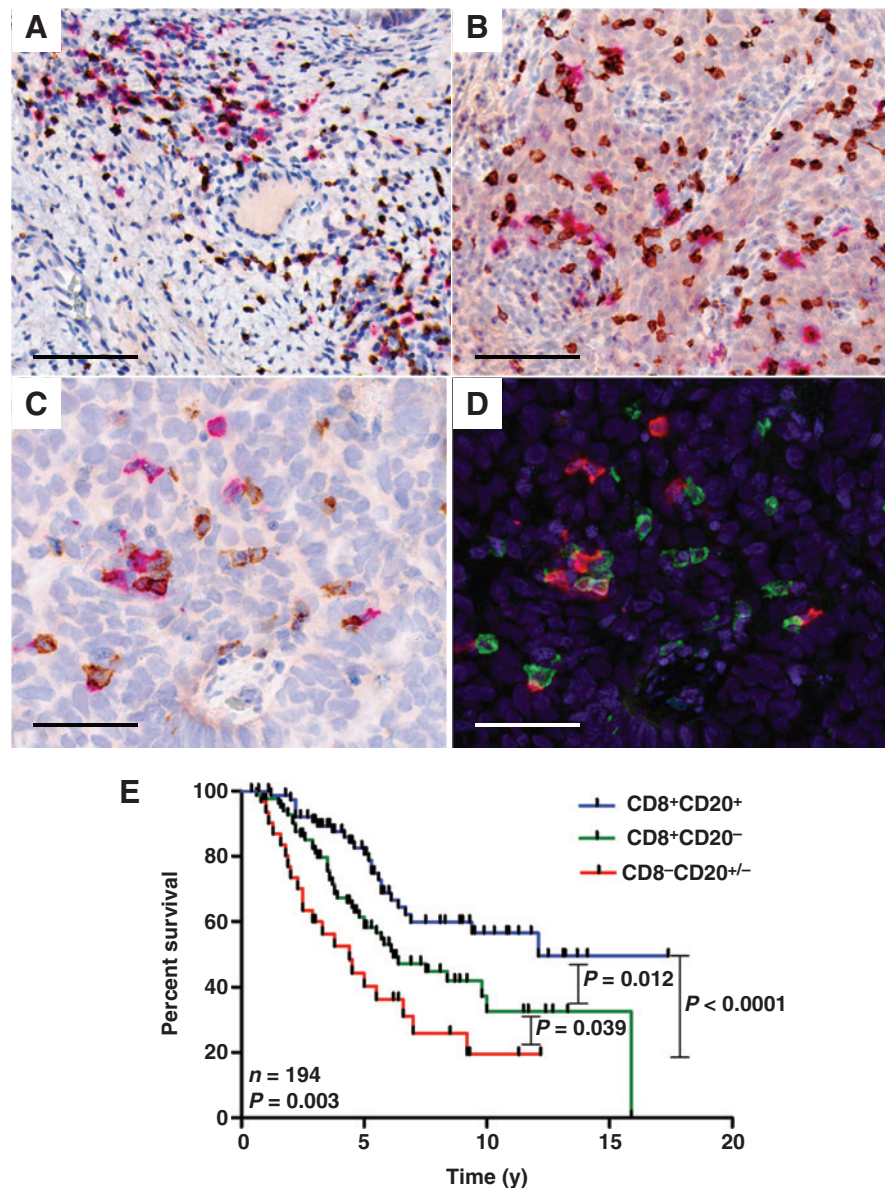
**Figure 5.** CD20<sup>+</sup> TIL have a surface phenotype characteristic of APC, whereas CD4<sup>+</sup> and CD8<sup>+</sup> TIL have a surface phenotype characteristic of activated T cells. A, representative flow cytometry data showing expression of MHC class I (pan-HLA-A, B, C), MHC class II (pan-HLA-DR), CD40, CD80, and CD86 in CD20<sup>+</sup> B cells from healthy control PBMC (top), HGSC patient PBMC (middle), and TIL (bottom). Black lines: specific staining with the indicated antibody. Gray lines: negative controls lacking the indicated antibody. Samples were gated on CD45<sup>+</sup>CD20<sup>+</sup> lymphocytes ( $n = 9$ ). B, representative flow cytometry data showing an activated (HLA-DR<sup>+</sup>CD45RO<sup>+</sup>CD62L<sup>-</sup>) surface phenotype on the majority of CD4<sup>+</sup> (left) and CD8<sup>+</sup> (right) TIL. Samples are gated on CD3<sup>+</sup> lymphocytes ( $n = 9$ ).

thereby promoting prolonged patient survival. CD20<sup>+</sup> TIL showed clear evidence of antigen exposure, including expression of activation markers, class switching to IgG, somatic hypermutation, and oligoclonality. The majority failed to express CD27, suggesting that they belong to a recently described subset of CD27<sup>-</sup> memory B cells (39–41, 44). Despite expressing IgG, CD20<sup>+</sup> TIL showed no correlation with tumor-specific serum autoantibodies and hence seemed to be uncoupled from humoral immunity. Instead, CD20<sup>+</sup> TIL correlated strongly with CD8<sup>+</sup> TIL. The 2 lymphocyte subsets were found in close proximity in tumor tissue, often in loose aggregates. CD20<sup>+</sup> TIL expressed surface markers characteristic of APC, including MHC class I, MHC class II, CD80, and CD86. Furthermore, tumors positive for both CD8<sup>+</sup> and CD20<sup>+</sup> TIL were asso-

ciated with prolonged survival compared with those positive for CD8<sup>+</sup> TIL alone. Collectively, our results support the novel concept that CD20<sup>+</sup> TIL enhance tumor immunity through functional interactions with CD8<sup>+</sup> TIL.

Sequencing of IgG molecules from CD20<sup>+</sup> TIL yielded clear evidence of oligoclonality and somatic hypermutation, which are hallmarks of antigen exposure. The degree of B-cell clonality we measured in HGSC is similar to prior studies in breast cancer and germ cell tumors. Specifically, we found evidence for 11 to 14 B-cell clones in HGSC, compared with 6 to 13 clones in germ cell tumors (18) and 3 to 6 clones in breast cancer (12, 17). Similarly, 58% to 66% of sequences were clonally derived in HGSC, compared with 18% to 79% in germ cell tumors and 30% to 69% in breast cancer. Notably, these are minimal estimates, as it is

**Figure 6.** CD20<sup>+</sup> and CD8<sup>+</sup> TIL colocalize and are associated with prolonged survival in HGSC. A, IHC of HGSC tumor (IROC006) showing CD20<sup>+</sup> TIL (red) and CD8<sup>+</sup> TIL (brown) primarily in stromal regions. B, IHC of a densely infiltrated HGSC tumor (IROC042) showing CD20<sup>+</sup> TIL (red) and CD8<sup>+</sup> TIL (brown) in epithelial and stromal regions. C, high power IHC image of a HGSC tumor (IROC010) showing CD20<sup>+</sup> TIL (red) and CD8<sup>+</sup> TIL (brown) in close proximity. D, the same image as shown in (C), but with false coloring to further contrast the CD20 (red) and CD8 (green) signals. All samples were counterstained with hematoxylin (blue/purple). Original images were taken with a 20× (A and B) or 40× objective (C and D). Scale bars: 100 μm (A and B) or 50 μm (C and D). Representative of 5 tumor samples. E, Kaplan–Meier curves showing that the presence of both CD8<sup>+</sup> and CD20<sup>+</sup> TIL is associated with prolonged disease-specific survival compared with CD8<sup>+</sup> TIL alone or lack of CD8<sup>+</sup> TIL. Primary data is from cohort C (6). Log-rank tests were used to derive *P* values for comparisons between each group and between all 3 groups.



possible that additional less abundant clones were present in all of these studies. In addition to clonality, the degree of somatic hypermutation we observed in HGSC is similar to that reported for breast cancer and germ cell tumors.

What antigens might be recognized by CD20<sup>+</sup> TIL? Although this issue has yet to be addressed in HGSC, prior studies in breast cancer identified 2 antigens recognized by recombinant antibodies derived from tumor-infiltrating B cells: ganglioside D3 and a cleaved form of  $\beta$ -actin that was shown to become exposed on the surface of apoptotic cells (13, 45). These results suggest that CD20<sup>+</sup> TIL responses reflect a breakdown of tolerance to self-proteins, possibly due to apoptosis of tumor cells. Identification of additional antigens recognized by CD20<sup>+</sup> TIL may yield further

insights into the mechanisms by which B-cell responses are triggered and contribute to tumor immunity.

Even though CD20<sup>+</sup> TIL express surface immunoglobulin, we found that they are not associated with serum autoantibodies to the common tumor antigens p53 and NY-ESO-1. This lack of correlation was seen across 2 independent cohorts of patients, as well as within individual patients undergoing cytoreductive surgery and chemotherapy. Although only 2 antigens were assessed, these are the most frequently recognized tumor antigens in HGSC identified to date (19, 20). This finding is consistent with the fact that CD20<sup>+</sup> TIL are associated with prolonged survival in HGSC, whereas serum autoantibodies show little or no positive prognostic signal in most studies (31, 46–48).

Collectively, our data supports the conclusion that serum autoantibodies are produced by cells outside the tumor. Prime candidates are the plasma cells in bone marrow, which are the primary source of serum antibodies in healthy individuals. It remains possible that CD20<sup>+</sup> TIL, and the small populations of germinal center-like B cells and CD38<sup>+</sup> plasmablasts we identified in tumors, are precursors to plasma cells that in turn produce serum antibodies in some patients.

Although CD20<sup>+</sup> TIL exhibit the hallmarks of mature, antigen-experienced B cells, the majority failed to express the conventional memory B-cell marker CD27. CD27<sup>−</sup> memory B cells are present at low numbers in healthy donors (39–41, 44). In patients with systemic lupus erythematosus, the number of CD27<sup>−</sup> memory B cells is elevated in proportion to disease severity (44). To our knowledge, this study is the first to identify CD27<sup>−</sup> memory B cells in cancer. Although the functional differences between CD27<sup>+</sup> and CD27<sup>−</sup> memory B cells have yet to be elucidated, several possibilities can be imagined. Activated helper T cells express CD70, which can ligate CD27 on B cells to induce Ig secretion (35). Perhaps the lack of CD27 expression on CD20<sup>+</sup> TIL allows them to forego antibody production and instead contribute to cellular immunity. Alternatively, the lack of CD27 expression could indicate recent activation of B cells, as exposure of B cells to CD70<sup>+</sup> T cells leads to rapid CD27 downregulation (35). Perhaps the presence of CD27<sup>−</sup> memory B cells reflects a response to CD70 signals by CD4<sup>+</sup> and/or CD8<sup>+</sup> TIL in HGSC.

Using two-color IHC, we showed that CD20<sup>+</sup> TIL are often found in close proximity to CD8<sup>+</sup> TIL (Fig. 6A–D). Moreover, the presence of both CD20<sup>+</sup> and CD8<sup>+</sup> TIL was associated with markedly prolonged patient survival compared with CD8<sup>+</sup> TIL alone (Fig. 6E). These findings suggest that CD20<sup>+</sup> TIL may promote cytolytic antitumor responses. In theory, this could occur through multiple mechanisms. First, CD20<sup>+</sup> TIL could help recruit and retain T cells at the tumor site, facilitating the formation of the lymphoid aggregates we observed (Fig. 6A–D). Indeed, in autoimmunity, allograft rejection, and chronic infection, B cells are central to the formation of so-called tertiary lymphoid structures in affected tissues (28, 49). For example, in a xenograft model of rheumatoid arthritis, depletion of B cells with anti-CD20 antibody led to decreased T-cell activation and infiltration (27). Conversely, depletion of T cells led to disruption of tertiary lymphoid structures and loss of immunoglobulin production by infiltrating B cells (50). Thus, during prolonged immune responses, B cells and T cells can engage in cooperative interactions to maintain a strong presence at the affected site.

Second, CD20<sup>+</sup> TIL could serve as APC in the tumor environment. It is well documented that B cells can present antigens to T cells, including cross-presentation to CD8<sup>+</sup> T cells (51–53). B cells have been shown to serve as APC under a wide variety of physiologic conditions, including autoimmunity and allograft rejection. For example, B cells serve as APC to induce T-cell responses in nonobese diabetic mice (26). Similarly, B cells from multiple sclerosis patients have

been shown to present myelin basic protein to CD4<sup>+</sup> T cells *in vitro* (43). Thus, B cells have the capacity to function as APC in multiple autoimmune disorders and may function similarly in antitumor responses. In support of this notion, we found that CD20<sup>+</sup> TIL express MHC class I and II, as well as the costimulatory molecules CD80 and CD86. Although speculative, the presence of professional APC in the tumor environment may allow for sustained T-cell responses, for example, by providing supportive niches for memory T-cell proliferation. Notably, CD20<sup>+</sup> TIL are far more numerous than immature or mature dendritic cells (as defined by CD1a or CD208 expression, respectively) in immune infiltrates in HGSC (6). Moreover, compared with dendritic cells, B cells have the advantage that B-cell receptor-mediated endocytosis facilitates concentration of small quantities of specific antigens, which may allow the amplification of responses to tumor antigens expressed at low levels. To definitively show that CD20<sup>+</sup> TIL serve as APC in the tumor environment, it will be necessary to identify their cognate antigens and assess recognition by CD4<sup>+</sup> and CD8<sup>+</sup> TIL.

Our findings have implications for the immunotherapy of cancer. Most cancer vaccines are modeled on acute viral infections, which are characterized by large yet transient T-cell responses. By contrast, in autoimmunity or allograft rejection, T-cell responses are sustained over many months or years and involve cooperative interactions with colocalized B cells. Thus, it may be possible to generate more potent, sustained T-cell responses in the tumor environment by promoting the infiltration of tumor-reactive B cells. In support of this idea, adoptive transfer of activated B cells has been shown to induce tumor-specific T-cell immunity in murine models (54). Thus, improved understanding of the functional phenotype of CD20<sup>+</sup> TIL, their target antigens, and their mechanism of recruitment to target tissues may facilitate the design of more effective immunotherapies for the treatment of cancer.

## Disclosure of Potential Conflicts of Interest

No potential conflicts of interest were disclosed.

## Authors' Contributions

**Conception and design:** J.S. Nielsen, N.J. Nesslinger, B.H. Nelson

**Development of methodology:** J.S. Nielsen, K. Milne, N.J. Nesslinger

**Acquisition of data (provided animals, acquired and managed patients, provided facilities, etc.):** J.S. Nielsen, R.A. Sahota, K. Milne, S.E. Kost, N.J. Nesslinger, P.H. Watson

**Analysis and interpretation of data (e.g., statistical analysis, biostatistics, computational analysis):** J.S. Nielsen, R.A. Sahota, K. Milne, P.H. Watson, B.H. Nelson

**Writing, review, and/or revision of the manuscript:** J.S. Nielsen, R.A. Sahota, K. Milne, S.E. Kost, N.J. Nesslinger, P.H. Watson, B.H. Nelson

**Administrative, technical, or material support (i.e., reporting or organizing data, constructing databases):** J.S. Nielsen, R.A. Sahota

**Study supervision:** J.S. Nielsen, B.H. Nelson

## Acknowledgments

The authors thank the patients and healthy controls who provided specimens for our research as well as Alvin Ng, Jill Brandon, Adam Girardin, Kristy Dillon, and Winnie Sun for technical assistance.

## Grant Support

This study was supported by the BC Cancer Agency Tumour Tissue Repository, Victoria, BC, a member of the Canadian Tumor Repository

Network, U. S. Department of Defense grant #00486221, the BC Cancer Foundation, and a fellowship from the Canadian Institutes of Health Research (J.S. Nielsen).

The costs of publication of this article were defrayed in part by the payment of page charges. This article must therefore be hereby marked

advertisement in accordance with 18 U.S.C. Section 1734 solely to indicate this fact.

Received January 23, 2012; revised April 10, 2012; accepted April 20, 2012; published OnlineFirst May 2, 2012.

## References

- Kobel M, Kalloger SE, Huntsman DG, Santos JL, Swenerton KD, Seidman JD, et al. Differences in tumor type in low-stage versus high-stage ovarian carcinomas. *Int J Gynecol Pathol* 2010;29:203–11.
- Colombo N, Peiretti M, Parma G, Lapresa M, Mancari R, Carinelli S, et al. Newly diagnosed and relapsed epithelial ovarian carcinoma: ESMO Clinical Practice Guidelines for diagnosis, treatment and follow-up. *Ann Oncol* 2010;21 Suppl 5:v23–30.
- Nelson BH. The impact of T-cell immunity on ovarian cancer outcomes. *Immunol Rev* 2008;222:101–16.
- Zhang L, Conejo-Garcia JR, Katsaros D, Gimotty PA, Massobrio M, Regnani G, et al. Intratumoral T cells, recurrence, and survival in epithelial ovarian cancer. *N Engl J Med* 2003;348:203–13.
- Hamanishi J, Mandai M, Iwasaki M, Okazaki T, Tanaka Y, Yamaguchi K, et al. Programmed cell death 1 ligand 1 and tumor-infiltrating CD8<sup>+</sup> T lymphocytes are prognostic factors of human ovarian cancer. *Proc Natl Acad Sci U S A* 2007;104:3360–5.
- Milne K, Kobel M, Kalloger SE, Barnes RO, Gao D, Gilks CB, et al. Systematic analysis of immune infiltrates in high-grade serous ovarian cancer reveals CD20, FoxP3 and TIA-1 as positive prognostic factors. *PLoS One* 2009;4:e6412.
- Sato E, Olson SH, Ahn J, Bundy B, Nishikawa H, Qian F, et al. Intraepithelial CD8<sup>+</sup> tumor-infiltrating lymphocytes and a high CD8<sup>+</sup>/regulatory T cell ratio are associated with favorable prognosis in ovarian cancer. *Proc Natl Acad Sci U S A* 2005;102:18538–43.
- Hwang WT, Adams SF, Tahirovic E, Hagemann IS, Coukos G. Prognostic significance of tumor-infiltrating T cells in ovarian cancer: a meta-analysis. *Gynecol Oncol* 2012;124:192–8.
- Al-Shibli KI, Donnem T, Al-Saad S, Persson M, Bremnes RM, Busund LT. Prognostic effect of epithelial and stromal lymphocyte infiltration in non-small cell lung cancer. *Clin Cancer Res* 2008;14:5220–7.
- Nedergaard BS, Ladekarl M, Nyengaard JR, Nielsen K. A comparative study of the cellular immune response in patients with stage IB cervical squamous cell carcinoma. Low numbers of several immune cell subtypes are strongly associated with relapse of disease within 5 years. *Gynecol Oncol* 2008;108:106–11.
- Schmidt M, Bohm D, von Tonne C, Steiner E, Puhl A, Pilch H, et al. The humoral immune system has a key prognostic impact in node-negative breast cancer. *Cancer Res* 2008;68:5405–13.
- Coronella JA, Telleman P, Kingsbury GA, Truong TD, Hays S, Jungmans RP. Evidence for an antigen-driven humoral immune response in medullary ductal breast cancer. *Cancer Res* 2001;61:7889–99.
- Hansen MH, Nielsen H, Ditzel HJ. The tumor-infiltrating B cell response in medullary breast cancer is oligoclonal and directed against the autoantigen actin exposed on the surface of apoptotic cancer cells. *Proc Natl Acad Sci U S A* 2001;98:12659–64.
- Hansen MH, Nielsen HV, Ditzel HJ. Translocation of an intracellular antigen to the surface of medullary breast cancer cells early in apoptosis allows for an antigen-driven antibody response elicited by tumor-infiltrating B cells. *J Immunol* 2002;169:2701–11.
- Nzula S, Going JJ, Stott DI. Antigen-driven clonal proliferation, somatic hypermutation, and selection of B lymphocytes infiltrating human ductal breast carcinomas. *Cancer Res* 2003;63:3275–80.
- Simsa P, Teillaud JL, Stott DI, Toth J, Kotlan B. Tumor-infiltrating B cell immunoglobulin variable region gene usage in invasive ductal breast carcinoma. *Pathol Oncol Res* 2005;11:92–7.
- Wang Y, Ylera F, Boston M, Kang SG, Kutok JL, Klein-Szanto AJ, et al. Focused antibody response in plasma cell-infiltrated non-medullary (NOS) breast cancers. *Breast Cancer Res Treat* 2007;104:129–44.
- Willis SN, Mallozzi SS, Rodig SJ, Cronk KM, McArdel SL, Caron T, et al. The microenvironment of germ cell tumors harbors a prominent antigen-driven humoral response. *J Immunol* 2009;182:3310–7.
- Gnjatic S, Ritter E, Buchler MW, Giese NA, Brors B, Frei C, et al. Seromic profiling of ovarian and pancreatic cancer. *Proc Natl Acad Sci U S A* 2010;107:5088–93.
- Stone B, Schummer M, Paley PJ, Thompson L, Stewart J, Ford M, et al. Serologic analysis of ovarian tumor antigens reveals a bias toward antigens encoded on 17q. *Int J Cancer* 2003;104:73–84.
- Rodriguez-Pinto D. B cells as antigen presenting cells. *Cell Immunol* 2005;238:67–75.
- Tumanov A, Kuprash D, Lagarkova M, Grivennikov S, Abe K, Shakhov A, et al. Distinct role of surface lymphotoxin expressed by B cells in the organization of secondary lymphoid tissues. *Immunity* 2002;17:239–50.
- Chan OT, Hannum LG, Haberman AM, Madaio MP, Shlomchik MJ. A novel mouse with B cells but lacking serum antibody reveals an antibody-independent role for B cells in murine lupus. *J Exp Med* 1999;189:1639–48.
- Lehnhardt A, Mengel M, Pape L, Ehrlich JH, Offner G, Strehlau J. Nodular B-cell aggregates associated with treatment refractory renal transplant rejection resolved by rituximab. *Am J Transplant* 2006;6:847–51.
- Sarwal M, Chua MS, Kambham N, Hsieh SC, Satterwhite T, Masek M, et al. Molecular heterogeneity in acute renal allograft rejection identified by DNA microarray profiling. *N Engl J Med* 2003;349:125–38.
- Serreze DV, Fleming SA, Chapman HD, Richard SD, Leiter EH, Tisch RM. B lymphocytes are critical antigen-presenting cells for the initiation of T cell-mediated autoimmune diabetes in nonobese diabetic mice. *J Immunol* 1998;161:3912–8.
- Takemura S, Klimiuk PA, Braun A, Goronzy JJ, Weyand CM. T cell activation in rheumatoid synovium is B cell dependent. *J Immunol* 2001;167:4710–8.
- Yanaba K, Bouaziz JD, Matsushita T, Magro CM, St Clair EW, Tedder TF. B-lymphocyte contributions to human autoimmune disease. *Immunol Rev* 2008;223:284–99.
- Zarkhin V, Kambham N, Li L, Kwok S, Hsieh SC, Salvatierra O, et al. Characterization of intra-graft B cells during renal allograft rejection. *Kidney Int* 2008;74:664–73.
- Clarke B, Tinker AV, Lee CH, Subramanian S, van de Rijn M, Turbin D, et al. Intraepithelial T cells and prognosis in ovarian carcinoma: novel associations with stage, tumor type, and BRCA1 loss. *Mod Pathol* 2009;22:393–402.
- Milne K, Barnes RO, Girardin A, Mawer MA, Nesslinger NJ, Ng A, et al. Tumor-infiltrating T cells correlate with NY-ESO-1-specific autoantibodies in ovarian cancer. *PLoS One* 2008;3:e3409.
- Brochet X, Lefranc MP, Giudicelli V. IMGT/V-QUEST: the highly customized and integrated system for IG and TR standardized V-J and V-D-J sequence analysis. *Nucleic Acids Res* 2008;36:W503–8.
- Lefranc MP, Giudicelli V, Ginestoux C, Jabado-Michaloud J, Folch G, Bellahcene F, et al. IMGT, the international ImMunoGeneTics information system. *Nucleic Acids Res* 2009;37:D1006–12.
- Stockert E, Jager E, Chen YT, Scanlan MJ, Gout I, Karbach J, et al. A survey of the humoral immune response of cancer patients to a panel of human tumor antigens. *J Exp Med* 1998;187:1349–54.
- Agematsu K, Nagumo H, Yang FC, Nakazawa T, Fukushima K, Ito S, et al. B cell subpopulations separated by CD27 and crucial collaboration of CD27<sup>+</sup> B cells and helper T cells in immunoglobulin production. *Eur J Immunol* 1997;27:2073–9.
- Klein U, Rajewsky K, Kuppers R. Human immunoglobulin (Ig)M+IgD<sup>+</sup> peripheral blood B cells expressing the CD27 cell surface antigen carry somatically mutated variable region genes: CD27 as a general marker for somatically mutated (memory) B cells. *J Exp Med* 1998;188:1679–89.

37. Sanz I, Wei C, Lee FE, Anolik J. Phenotypic and functional heterogeneity of human memory B cells. *Semin Immunol* 2008;20:67–82.
38. Berkowska MA, Driessen GJ, Bikos V, Grosserichter-Wagener C, Stamatopoulos K, Cerutti A, et al. Human memory B cells originate from three distinct germinal center-dependent and -independent maturation pathways. *Blood* 2011;118:2150–8.
39. Ehrhardt GR, Hsu JT, Gartland L, Leu CM, Zhang S, Davis RS, et al. Expression of the immunoregulatory molecule FcRH4 defines a distinctive tissue-based population of memory B cells. *J Exp Med* 2005;202:783–91.
40. Fecteau JF, Cote G, Neron S. A new memory CD27-IgG+ B cell population in peripheral blood expressing VH genes with low frequency of somatic mutation. *J Immunol* 2006;177:3728–36.
41. Wirths S, Lanzavecchia A. ABCB1 transporter discriminates human resting naive B cells from cycling transitional and memory B cells. *Eur J Immunol* 2005;35:3433–41.
42. Nelson BH. CD20+ B cells: the other tumor-infiltrating lymphocytes. *J Immunol* 2010;185:4977–82.
43. Harp CT, Lovett-Racke AE, Racke MK, Frohman EM, Monson NL. Impact of myelin-specific antigen presenting B cells on T cell activation in multiple sclerosis. *Clin Immunol* 2008;128:382–91.
44. Wei C, Anolik J, Cappione A, Zheng B, Pugh-Bernard A, Brooks J, et al. A new population of cells lacking expression of CD27 represents a notable component of the B cell memory compartment in systemic lupus erythematosus. *J Immunol* 2007;178:6624–33.
45. Kotlan B, Simsa P, Teillaud JL, Fridman WH, Toth J, McKnight M, et al. Novel ganglioside antigen identified by B cells in human medullary breast carcinomas: the proof of principle concerning the tumor-infiltrating B lymphocytes. *J Immunol* 2005;175:2278–85.
46. Gadducci A, Ferdeghini M, Buttitta F, Cosio S, Fanucchi A, Annicchiarico C, et al. Assessment of the prognostic relevance of serum anti-p53 antibodies in epithelial ovarian cancer. *Gynecol Oncol* 1999;72:76–81.
47. Mayerhofer K, Tempfer C, Kucera E, Hefler L, Zeisler H, Kainz C, et al. Humoral p53 antibody response is a prognostic parameter in ovarian cancer. *Anticancer Res* 1999;19:875–8.
48. Vogl FD, Frey M, Kreienberg R, Runnebaum IB. Autoimmunity against p53 predicts invasive cancer with poor survival in patients with an ovarian mass. *Br J Cancer* 2000;83:1338–43.
49. Bystry RS, Aluvihare V, Welch KA, Kallikourdis M, Betz AG. B cells and professional APCs recruit regulatory T cells via CCL4. *Nat Immunol* 2001;2:1126–32.
50. Kang YM, Zhang X, Wagner UG, Yang H, Beckenbaugh RD, Kurtin PJ, et al. CD8 T cells are required for the formation of ectopic germinal centers in rheumatoid synovitis. *J Exp Med* 2002;195:1325–36.
51. Gnjjatic S, Atanackovic D, Matsuo M, Jager E, Lee SY, Valmori D, et al. Cross-presentation of HLA class I epitopes from exogenous NY-ESO-1 polypeptides by nonprofessional APCs. *J Immunol* 2003;170:1191–6.
52. Ahmadi T, Flies A, Efebera Y, Sherr DH. CD40 Ligand-activated, antigen-specific B cells are comparable to mature dendritic cells in presenting protein antigens and major histocompatibility complex class I- and class II-binding peptides. *Immunology* 2008;124:129–40.
53. de Wit J, Souwer Y, Jorritsma T, Klaasse Bos H, ten Brinke A, Neefjes J, et al. Antigen-specific B cells reactivate an effective cytotoxic T cell response against phagocytosed *Salmonella* through cross-presentation. *PLoS One* 2010;5:e13016.
54. Li Q, Lao X, Pan Q, Ning N, Yet J, Xu Y, et al. Adoptive transfer of tumor reactive B cells confers host T-cell immunity and tumor regression. *Clin Cancer Res* 2011;17:4987–95.

**Supplementary Figure 1: B cells in HGSC tumors exhibit oligoclonal and somatically hypermutated immunoglobulin sequences.** Immunoglobulin genes were sequenced from three HGSC tumors and compared with germline sequences. Identical sequences or sequences containing only a single difference were excluded. Remaining sequences were defined as clonal if V-D-J junctions were identical. Tables represent gene usage and clonal groups from each tumor.

IROC010				IROC015				IROC025			
Clone	V gene	D gene	J gene	Clone	V gene	D gene	J gene	Clone	V gene	D gene	J gene
153-A12	IGHV1-3	IGHD2-8	IGHJ5	156-C02	IGHV1-2	IGHD4-17	IGHJ4	159-F12	IGHV1-2	IGHD6-19	IGHJ4
153-C07	IGHV1-3	IGHD2-8	IGHJ5	156-G10	IGHV1-2	IGHD4-17	IGHJ4	159-B09	IGHV1-2	IGHD6-19	IGHJ4
153-F04	IGHV1-3	IGHD2-8	IGHJ5	156-C09	IGHV1-8	IGHD5-12	IGHJ4	159-C02	IGHV1-2	IGHD6-19	IGHJ4
153-E06	IGHV1-3	IGHD5-12	IGHJ4	156-D11	IGHV1-8	IGHD5-12	IGHJ4	159-A10	IGHV1-46	IGHD6-19	IGHJ5
153-D12	IGHV1-3	IGHD5-12	IGHJ4	156-D06	IGHV1-18	IGHD5-12	IGHJ3	159-E02	IGHV1-46	IGHD6-19	IGHJ5
153-A01	IGHV1-18	IGHD5-12	IGHJ4	156-H03	IGHV1-18	IGHD5-12	IGHJ3	159-E04	IGHV1-46	IGHD6-19	IGHJ5
153-A02	IGHV1-18	IGHD5-12	IGHJ4	156-A01	IGHV1-18	IGHD5-12	IGHJ3	159-B07	IGHV2-5	IGHD3-22	IGHJ4
153-A07	IGHV1-18	IGHD5-12	IGHJ4	156-H11	IGHV1-18	IGHD5-12	IGHJ3	159-D03	IGHV2-5	IGHD3-22	IGHJ4
153-H08	IGHV1-18	IGHD5-12	IGHJ4	156-C06	IGHV1-18	IGHD5-12	IGHJ3	159-A11	IGHV2-70	IGHD4-17	IGHJ6
153-H12	IGHV1-18	IGHD5-12	IGHJ4	156-F04	IGHV1-46	IGHD5-12	IGHJ6	159-C09	IGHV2-70	IGHD4-17	IGHJ6
154-E09	IGHV3-23	IGHD6-19	IGHJ6	156-A12	IGHV1-46	IGHD5-12	IGHJ6	160-B10	IGHV3-11	IGHD3-3	IGHJ3
154-F06	IGHV3-23	IGHD6-19	IGHJ6	156-B01	IGHV1-46	IGHD5-12	IGHJ6	160-E10	IGHV3-11	IGHD3-3	IGHJ3
154-F08	IGHV3-23	IGHD6-19	IGHJ6	156-A09	IGHV2-70	IGHD1-7	IGHJ6	160-H01	IGHV3-11	IGHD6-6	IGHJ4
154-G08	IGHV3-23	IGHD6-19	IGHJ6	156-A10	IGHV2-70	IGHD1-7	IGHJ6	160-E02	IGHV3-11	IGHD6-6	IGHJ4
154-A06	IGHV3-23	IGHD6-19	IGHJ6	156-D05	IGHV2-70	IGHD1-7	IGHJ6	160-G04	IGHV3-11	IGHD6-6	IGHJ4
154-C03	IGHV3-23	IGHD6-19	IGHJ6	156-D10	IGHV2-70	IGHD1-7	IGHJ6	160-D05	IGHV3-15	IGHD3-22	IGHJ4
155-C09	IGHV4-30	IGHD2-2	IGHJ5	156-A02	IGHV2-70	IGHD3-16	IGHJ6	160-E04	IGHV3-15	IGHD3-22	IGHJ4
155-E03	IGHV4-30	IGHD2-2	IGHJ5	156-G11	IGHV2-70	IGHD3-16	IGHJ6	160-D10	IGHV3-15	IGHD3-22	IGHJ4
155-B11	IGHV4-31	IGHD2-8	IGHJ6	157-C04	IGHV3-33	IGHD6-19	IGHJ4	160-F08	IGHV3-15	IGHD3-22	IGHJ4
155-F11	IGHV4-31	IGHD2-8	IGHJ6	157-E12	IGHV3-33	IGHD6-19	IGHJ4	160-G07	IGHV3-15	IGHD3-22	IGHJ4
155-D12	IGHV4-31	IGHD3-10	IGHJ6	158-B02	IGHV4-34	IGHD3-10	IGHJ5	161-B01	IGHV4-4	IGHD5-5	IGHJ2
155-F02	IGHV4-31	IGHD3-10	IGHJ6	158-E02	IGHV4-34	IGHD3-10	IGHJ5	161-B07	IGHV4-4	IGHD5-5	IGHJ2
155-G08	IGHV4-31	IGHD3-10	IGHJ6	158-C04	IGHV4-34	IGHD3-10	IGHJ5	161-A10	IGHV4-4	IGHD6-19	IGHJ5
155-C04	IGHV4-31	IGHD3-22	IGHJ4	158-D08	IGHV4-34	IGHD3-10	IGHJ5	161-A11	IGHV4-4	IGHD6-19	IGHJ5
155-D04	IGHV4-31	IGHD3-22	IGHJ4	158-F03	IGHV4-34	IGHD3-10	IGHJ5	161-C05	IGHV4-4	IGHD6-19	IGHJ5
155-D09	IGHV4-31	IGHD3-22	IGHJ4	158-C01	IGHV4-34	IGHD3-10	IGHJ5	160-C06	IGHV5-51	IGHD2-15	IGHJ3
155-E06	IGHV4-31	IGHD3-22	IGHJ4	158-B06	IGHV4-34	IGHD3-10	IGHJ5	160-C06	IGHV5-51	IGHD2-15	IGHJ3
155-G10	IGHV4-31	IGHD3-22	IGHJ4	157-D03	IGHV5-51	IGHD3-10	IGHJ3	160-C08	IGHV5-51	IGHD3-22	IGHJ6
155-H08	IGHV4-31	IGHD3-22	IGHJ4	157-D12	IGHV5-51	IGHD3-10	IGHJ3	160-G09	IGHV5-51	IGHD3-22	IGHJ6
155-E02	IGHV4-34	IGHD3-10	IGHJ4	157-B05	IGHV5-51	IGHD7-27	IGHJ4	160-A12	IGHV5-51	IGHD4-23	IGHJ4
155-G11	IGHV4-34	IGHD3-10	IGHJ4	157-B07	IGHV5-51	IGHD7-27	IGHJ4	160-A02	IGHV5-51	IGHD4-23	IGHJ4
155-E04	IGHV4-34	IGHD6-19	IGHJ6	157-B08	IGHV5-51	IGHD7-27	IGHJ4	160-B07	IGHV5-51	IGHD4-23	IGHJ4
155-B10	IGHV4-34	IGHD6-19	IGHJ6	157-B10	IGHV5-51	IGHD7-27	IGHJ4	160-E09	IGHV5-51	IGHD4-23	IGHJ4
155-C11	IGHV4-34	IGHD6-19	IGHJ6	157-D09	IGHV5-51	IGHD7-27	IGHJ4	160-H06	IGHV5-51	IGHD4-23	IGHJ4
154-C05	IGHV5-51	IGHD3-10	IGHJ4	157-G05	IGHV5-51	IGHD7-27	IGHJ4	160-D04	IGHV5-51	IGHD4-23	IGHJ4
154-C05	IGHV5-51	IGHD3-10	IGHJ4	157-G09	IGHV5-51	IGHD7-27	IGHJ4	160-H02	IGHV5-51	IGHD4-23	IGHJ4
154-C05	IGHV5-51	IGHD3-10	IGHJ4	157-H04	IGHV5-51	IGHD7-27	IGHJ4	161-C01	IGHV6-1	IGHD1-14	IGHJ3
154-C05	IGHV5-51	IGHD3-10	IGHJ4	157-H05	IGHV5-51	IGHD7-27	IGHJ4	161-D10	IGHV6-1	IGHD1-14	IGHJ3
154-A04	IGHV5-51	IGHD3-10	IGHJ6								
154-F04	IGHV5-51	IGHD3-10	IGHJ6								
154-D04	IGHV5-51	IGHD4-17	IGHJ5								
154-G03	IGHV5-51	IGHD4-17	IGHJ5								
154-B10	IGHV5-51	IGHD5-5	IGHJ4								
154-B10	IGHV5-51	IGHD5-5	IGHJ4								

**Supplementary Table 1. Clinical characteristics of patient cohort A.**

<b>No. of patients</b>	40
<b>Age at surgery, median (range)</b>	66 (44-79)
<b>Debulking Status</b>	
Optimal (no visible residual)	2 (5%)
Minimal Residual (<1cm residual disease)	10 (25%)
Suboptimal (>1cm residual disease)	28 (70%)
<b>Chemotherapy regimen</b>	
Carboplatin/paclitaxel	24 (60%)
Carboplatin only	15 (37.5%)
No chemotherapy	1 (2.5%)
<b>Stage</b>	
2	2 (5%)
3	31 (77.5%)
4	6 (15%)
Unknown	1 (2.5%)
<b>Grade</b>	
3	40 (100%)
<b>Status</b>	
Alive	13 (32.5%)
Dead	27 (67.5%)
<b>Follow-up time in yrs, median (range)</b>	1.9 (0.1-3.8)

**Supplementary Table 2. Antibodies used for flow cytometry.**

<b>Antigen</b>	<b>Fluorochrome</b>	<b>Clone</b>	<b>Supplier</b>
CD3	FITC	HIT3a	BD Biosciences, Mississauga, ON, Canada
CD3	PE-Cy7	SK7	BD Biosciences
CD4	APC-H7	RPA-T4	BD Biosciences
CD8	PerCP-Cy5.5	RPA-T8	eBioscience, San Diego, CA
CD20	APC-H7	2H7	BD Biosciences
CD27	PE	M-T271	BD Biosciences
CD38	PerCP-Cy5.5	HIT2	BD Biosciences
CD40	FITC	5C3	BD Biosciences
CD45	PE-Cy7	HI30	eBioscience
CD45RA	APC	HI100	BD Biosciences
CD45RO	FITC	UCHL-1	eBioscience
CD56	APC	B159	BD Biosciences
CD62L	PE	Dreg 56	BD Biosciences
CD80	PE-Cy5	L307.4	BD Biosciences
CD86	PE-Cy5	2331 (FUN-1)	BD Biosciences
CD138	PE	DL-101	eBioscience
HLA-ABC	PE	W6/32	eBioscience
HLA-DR	FITC	LN3	eBioscience
HLA-DR	PE	L243 (G46-6)	BD Biosciences
IgD	FITC	IA6-2	BD Biosciences
IgG	PE-Cy7	G18-145	BD Biosciences
IgM	APC	G20-127	BD Biosciences

**Supplementary Table 3. CA125 levels and NY-ESO-1 autoantibody titres before (Pre) and after (Post) primary surgery and chemotherapy for the 6 HGSC patients shown in Figure 4C. Titres represent mean values from three independent experiments.**

Patient	CD20-TIL status	CA125		NY-ESO-1 reciprocal titre	
		Pre	Post	Pre	Post
IROC008	CD20-	2,388	1,096	12,800	3,200
IROC013	CD20-	273	5	273,067	6,400
IROC033	CD20-	6,572	17	2,867,200	19,200
IROC060	CD20+	4,037	Not available	409,600	204,800
IROC065	CD20+	592	57	1,167	4,800
IROC072	CD20+	184	6	409,600	19,200

## Review

## The Prognostic Value of FoxP3+ Tumor-Infiltrating Lymphocytes in Cancer: A Critical Review of the Literature

Ronald J. deLeeuw<sup>1,2</sup>, Sara E. Kost<sup>1,2</sup>, Juzer A. Kakal<sup>1</sup>, and Brad H. Nelson<sup>1,2,3</sup>

## Abstract

CD8+ tumor-infiltrating lymphocytes (TIL) are associated with survival in a variety of cancers. A second subpopulation of TIL, defined by forkhead box protein P3 (FoxP3) expression, has been reported to inhibit tumor immunity, resulting in decreased patient survival. On the basis of this premise, several groups are attempting to deplete FoxP3+ T cells to enhance tumor immunity. However, recent studies have challenged this paradigm by showing that FoxP3+ T cells exhibit heterogeneous phenotypes and, in some cohorts, are associated with favorable prognosis. These discrepant results could arise from differences in study methodologies or the biologic properties of specific cancer types. Here, we conduct the first systematic review of the prognostic significance of FoxP3+ T cells across nonlymphoid cancers (58 studies from 16 cancers). We assessed antibody specificity, cell-scoring strategy, multivariate modeling, use of single compared with multiple markers, and tumor site. Two factors proved important. First, when FoxP3 was combined with one additional marker, double-positive T cells were generally associated with poor prognosis. Second, tumor site had a major influence. FoxP3+ T cells were associated with poor prognosis in hepatocellular cancer and generally good prognosis in colorectal cancer, whereas other cancer types were inconsistent or understudied. We conclude that FoxP3+ T cells have heterogeneous properties that can be discerned by the use of additional markers. Furthermore, the net biologic effects of FoxP3+ T cells seem to depend on the tumor site, perhaps reflecting microenvironmental differences. Thus, depletion of FoxP3+ T cells might enhance tumor immunity in some patient groups but be detrimental in others. *Clin Cancer Res*; 18(11); 1–8. ©2012 AACR.

## Introduction

Many studies across a wide variety of human cancers have shown a clear association between the presence of tumor-infiltrating lymphocytes (TIL) and patient survival (1–4). To further understand this phenomenon, additional immune markers have been used to subdivide CD3+ T cells into functional subsets, with special emphasis on cytotoxic (e.g., CD8+, nucleolysin TIA-1 isoform p40+) and regulatory [e.g., CD4+, interleukin 2 receptor subunit alpha (CD25)+, FoxP3+] phenotypes (3, 5). Whereas TIL-expressing cytotoxic markers are generally associated with favorable prognosis, TIL-expressing regulatory markers (referred to as Tregs) were initially reported to correlate with poor prognosis (5). This finding fit with the general notion that Tregs

suppress adaptive immune responses and led many groups to pursue strategies to deplete Tregs from patients with cancer as a means to enhance tumor immunity (6–8).

In the past decade, much effort has been devoted to finding molecular markers that uniquely define Tregs. Initially, these cells were characterized as CD4+ and CD25<sup>high</sup> (9). Further investigation revealed that Tregs express and functionally depend on the transcription factor forkhead box protein P3 (FoxP3; ref. 10). Indeed, humans and mice that lack an intact *FOXP3* gene suffer a severe autoimmune syndrome known as immune dysregulation/polyendocrinopathy/enteropathy/X-linked syndrome in humans or the *Scurfy* phenotype in mice (10, 11). Given its essential role in Treg development and function, FoxP3 became a popular single marker for Treg studies in cancer. Intriguingly, studies of the prognostic value of FoxP3+ T cells have led to highly discrepant findings. In some studies, tumor-infiltrating FoxP3+ T cells have been associated with poor prognosis, consistent with the initial hypothesis that FoxP3+ Tregs inhibit antitumor immunity. In contrast, other studies have found that FoxP3+ T cells are associated with a favorable prognosis.

How can these widely discrepant prognostic claims be explained? On the one hand, they could reflect technical differences among studies, including the specific FoxP3 antibody used, scoring strategy, and statistical methods. Alternatively, the differing claims could reflect biologic

**Authors' Affiliations:** <sup>1</sup>Trev and Joyce Deeley Research Centre, British Columbia Cancer Agency; <sup>2</sup>Department of Biochemistry and Microbiology, University of Victoria, Victoria; <sup>3</sup>Department of Medical Genetics, University of British Columbia, Vancouver, British Columbia, Canada

**Note:** Supplementary data for this article are available at Clinical Cancer Research Online (<http://clincancerres.aacrjournals.org/>).

**Corresponding Author:** Brad Nelson, Trev and Joyce Deeley Research Centre, British Columbia Cancer Agency, 2410 Lee Avenue, Victoria, BC V8R 6V5, Canada. Phone: 250-519-5700; Fax: 250-519-2004; E-mail: [bnelson@bccancer.bc.ca](mailto:bnelson@bccancer.bc.ca)

**doi:** 10.1158/1078-0432.CCR-11-3216

©2012 American Association for Cancer Research.

### Translational Relevance

Although forkhead box protein P3+ (FoxP3+) T cells are conventionally thought to suppress tumor immunity, this idea has been challenged by recent studies showing that, in some patient cohorts, tumor-infiltrating FoxP3+ T cells are associated with favorable prognosis. To investigate this apparent discrepancy, we did a comprehensive review of the literature on the prognostic significance of tumor-infiltrating FoxP3+ T cells in human cancer. We conclude that FoxP3 is inadequate as a single functional or prognostic marker. Moreover, the prognostic significance of FoxP3+ T cells can vary according to tumor site. Thus, the original view that FoxP3+ T cells invariably suppress tumor immunity is oversimplified. We require better understanding of the functional subtypes of FoxP3+ T cells and their biologic properties in different tumor microenvironments if we wish to rationally modulate their behavior to enhance tumor immunity.

factors. For example, it is conceivable that FoxP3+ T cells exhibit conventional regulatory (i.e., inhibitory) properties in some contexts but not others. Alternatively, FoxP3+ T cells may be consistently regulatory in nature but appear as favorable prognostic markers in some cancers because of their association with tumor-infiltrating CD8+ T cells or other effectors (12, 13). Others have suggested that, in colorectal and gastric cancers, FoxP3+ T cells may inhibit tumor-promoting inflammatory responses to microbes, which could explain their association with favorable outcomes in these and similar contexts (14). Finally, emerging evidence indicates that FoxP3 expression encompasses a heterogeneous population of cells that contain both regulatory T cells, which produce cytokines such as TGF- $\beta$ 1 and interleukin 10, and nonregulatory T cells, which may express interferon gamma and interleukin 17 (15–19; reviewed in ref. 20). Given these various possibilities, it seems reasonable to question whether depletion of Tregs based on FoxP3 expression is likely to be beneficial or detrimental to patients with cancer.

To investigate this controversy, we did a comprehensive and critical review of the literature on tumor-infiltrating FoxP3+ T cells and prognosis in human cancer. Articles for review were identified during a PubMed search using the terms "FoxP3" and "cancer" and were vetted by title and abstract by one of the authors (R.J. deLeeuw). Several selection criteria were applied. First, we excluded studies of lymphoid cancers, because the immunologic nature of these malignancies makes it difficult to assess whether FoxP3+ T cells are acting directly on tumor cells or indirectly on antitumor effector lymphocytes. Second, we excluded studies that only correlated FoxP3+ T cells with late-stage disease as opposed to patient survival. Third, we included only those studies that measured FoxP3 expression by immunohistochemistry (IHC) or immunofluorescence to

ensure that the intratumoral location of FoxP3+ cells was known. Finally, we reviewed a given data set only once, excluding secondary or tertiary studies that referred to a previously published data set.

In the end, we reviewed 58 studies encompassing 16 different cancer types (Table 1), including bladder (19), breast (21–28), cervical (29, 30), colorectal (12, 31–39), endometrial (40–42), gastric (14, 43–46), head and neck (47), hepatocellular (48–52), lung (53, 54), melanoma (55–58), mesothelial (59), oral (4, 60–63), ovarian (2, 3, 13, 64–67), pancreatic (68), renal (69, 70), and vulvar cancers (Supplementary Table S1; ref. 71). The reported prognostic value of FoxP3+ T cells in these 58 studies ranged from poor ( $n = 23$ ), to neutral ( $n = 23$ ), to good ( $n = 12$ ). To better understand why the prognostic value of FoxP3+ T cells varies so widely, we assessed each study for technical factors (including the specific FoxP3 antibody used, scoring strategy, and the use of multivariate modeling) and biologic factors (including the use of additional markers to define Tregs and the tumor site studied).

### Antibody Specificity

Different FoxP3 antibodies can yield different staining patterns, indicating that some antibodies may have suboptimal sensitivity or specificity (72, 73). Although 18 of the 58 reviewed studies failed to state which specific FoxP3 antibody was used, within the remaining 40 studies, 11 different FoxP3 antibodies were used (Table 1). The most commonly used antibody was a monoclonal designated 236A/E7. In the 23 studies that used 236A/E7, the prognostic significance of FoxP3+ T cells ranged from poor ( $n = 10$ ), to neutral ( $n = 8$ ), to good ( $n = 5$ ). Given that a single FoxP3 antibody can yield prognostic results this disparate, it seems that FoxP3 prognostic variability is not solely attributable to antibody selection.

### Cell-Scoring Strategy

We investigated 4 aspects of the scoring strategies used to categorize tumors as positive or negative for FoxP3+ T cells: cutoff points, intratumoral location, use of tissue microarrays compared with whole sections, and computerized compared with manual counting (Table 1). Although there is no standard cutoff point for TIL studies, 32 out of 58 of the reviewed studies used the median number of FoxP3+ T cells as the cutoff point. Within these 32, the distribution among poor, neutral, and good prognostic claims was 16, 11, and 5 studies, respectively. The remaining studies used a variety of scoring strategies, including the presence compared with absence of FoxP3+ T cells, the mean number of FoxP3+ T cells, or other criteria. A fairly even distribution among poor, neutral, and good prognostic claims was observed regardless of the cutoff point used (Table 1). Thus, differing scoring strategies do not account for the variable claims of FoxP3 prognostic significance.

TIL can reside in tumor epithelium, stroma, or both, and this may influence their prognostic significance. Among the 58 reviewed studies, 15 did not discriminate between the

**Table 1.** Characteristics of 58 studies

	Poor	Neutral	Good
FoxP3 prognosis claim	23	23	12
Specific antibody			
Clone 42	1		
Custom	1		
BioLegend	3	1	
Abcam	6	4	1
mAbcam22509	2	1	1
Novus Biologicals		1	
FJK-16s		1	
206D		1	
eBioscience		2	
236A/E7	10	8	5
mAbcam22510		2	1
PCH101		2	1
259D			1
eBio7979			1
221D/D3			1
Scoring strategy			
Cutoff point			
Absence and/or presence	1	3	3
Mean cutoff	1	3	1
Median cutoff	16	11	5
Other cutoff	5	6	3
Counting location			
General count	5	5	5
Tumor only	8	7	4
Tumor and stroma	10	11	3
Tissue used			
Whole sections	16	17	7
Tissue microarray	7	6	5
Counting strategy			
Investigator(s)	16	14	8
Computer program		4	2
Not reported	7	5	2
Multivariate correction for stage or grade			
Yes: 42	20	11	11
No: 16	3	12	1
Multivariate correction for other TIL subsets			
Yes: 8	2	3	3
No: 50	21	20	9
Use of multiple markers			
Yes: 8	4	4	
No: 50	19	19	12
Tumor site			
Hepatocellular	5		
Cervical	2		
Head and neck	1		
Pancreatic	1		

*(Continued on the following page)***Table 1.** Characteristics of 58 studies (Cont'd)

	Poor	Neutral	Good
FoxP3 prognosis claim	23	23	12
Renal	1	1	
Lung	1	1	
Endometrial	1	2	
Melanoma	2	2	
Breast	5	1	2
Mesothelioma		1	
Vulvar		1	
Oral	1	3	1
Gastric	2	1	2
Ovarian	1	4	2
Bladder			1
Colorectal		6	4

NOTE: Study *N* mean (range): 219 (30–1,445).

epithelial and stromal location of FoxP3+ T cells and, instead, provided a general count; 19 counted only FoxP3+ T cells in the epithelium; and 24 counted FoxP3+ T cells from epithelial and stromal compartments independently (Table 1). Regardless of the location of enumerated FoxP3+ T cells, a fairly even distribution was seen among poor, neutral, and good prognostic claims.

We next examined the use of tumor tissue microarrays (TMA) compared with whole sections (Table 1). TMAs were used in 18 of the 58 studies, and prognostic claims ranged from poor ( $n = 7$ ), to neutral ( $n = 6$ ), to good ( $n = 5$ ). A similar range of prognostic claims was seen with studies using whole tissue sections. Regarding cell counting, 38 studies used manual counting by one or more investigators, 6 studies used a computer-based quantification method, and 14 studies did not state the counting method (Table 1). Studies that used manual counting showed an unbiased spread among poor ( $n = 16$ ), neutral ( $n = 14$ ), and good ( $n = 8$ ) prognostic claims, regardless of the number of investigators who carried out cell counting. Definitive conclusions could not be drawn regarding the use of computerized counting, as only 6 studies used such methods, 3 of which involved colorectal cancer (see below).

### Multivariate Correction for Stage or Grade of Disease

In principle, the density of FoxP3+ T cells could reflect the stage and/or grade of disease, which could influence prognosis. Of the 45 studies that correlated FoxP3+ T cells to stage and/or grade, 25 found a significant association between FoxP3+ T cells and the stage and/or grade of disease, with 11 reporting a  $P$ -value  $\leq 0.001$  (Supplementary Table S1). A potential confounding effect is that the quantity of TIL can influence nodal staging, especially in colorectal cancer (74). Nonetheless, these studies support the possibility that FoxP3+ T cells could simply serve as a marker of more advanced disease.

This issue was addressed in 42 studies by use of multivariate models that included stage, grade, and other clinicopathologic features (Table 1). Among these studies, the prognostic significance of FoxP3+ T cells ranged from poor ( $n = 20$ ), to neutral ( $n = 11$ ), to good ( $n = 11$ ). Notably, in 4 studies, FoxP3+ T cells were a significant univariate prognostic indicator, only to be removed during multivariate analysis. Of the 16 studies that did not use multivariate analysis, the potentially confounding effects of stage and grade were mitigated in most by the fact that (i) FoxP3+ T cells showed no prognostic significance even in univariate analysis or (ii) only specific stages or grades of disease were included in the study. In summary, even though FoxP3+ T cells are frequently associated with the stage and/or grade of disease, we found that this factor was well controlled in most studies and does not account for the variability of FoxP3 prognostication.

### Multivariate Correction for Other Tumor-Infiltrating Lymphocyte Subsets

FoxP3+ T cells are usually found together with other TIL subsets, which can make it difficult to discern their independent prognostic effect. Although multivariate analysis can solve this problem, it requires that all TIL subtypes significant in univariate analysis be included in the multivariate model. In the 8 studies that included all TIL subsets in multivariate analysis, the prognostic value of FoxP3+ T cells ranged from poor ( $n = 2$ ), to neutral ( $n = 3$ ), to good ( $n = 3$ ; Table 1). Thus, although the number of studies is low, it seems that the prognostic significance of FoxP3+ T cells is not solely attributable to the presence of other TIL subpopulations.

Several studies made prognostic claims on the basis of the ratio of FoxP3+ T cells to other lymphocyte subsets, including CD3+/FoxP3+ ( $n = 2$ ), CD4+/CD25+/FoxP3+ ( $n = 1$ ), CD68+/FoxP3+ ( $n = 2$ ), CD8+/FoxP3+ or FoxP3+/CD8+ ( $n = 18$ ), CD8+/CCR4+/FoxP3+ ( $n = 1$ ), FoxP3+/CD4+ ( $n = 2$ ), FoxP3+/CD3+/CD45RO+ ( $n = 1$ ), and Granzyme-B+/FoxP3+ ( $n = 1$ ; Supplementary Table S1). Among these 28 studies, prognostic claims for FoxP3+ TIL ranged from poor ( $n = 12$ ), to neutral ( $n = 11$ ), to good ( $n = 5$ ). Thus, the use of lymphocyte ratios has been inconsistently applied and yielded inconsistent prognostic claims.

### Clinical Significance and Publication Bias

We next evaluated whether the magnitude of the prognostic effect was similar for studies claiming good compared with poor prognosis. Of the 58 studies, 32 reported multivariate hazard ratios for overall survival. A funnel plot revealed no significant difference between the magnitude of hazard ratios for studies claiming poor compared with good prognosis (Fig. 1). Furthermore, there was no evidence of publication bias, as the studies were evenly distributed throughout the plot.

### Use of Multiple Markers to Define FoxP3+ T Cells

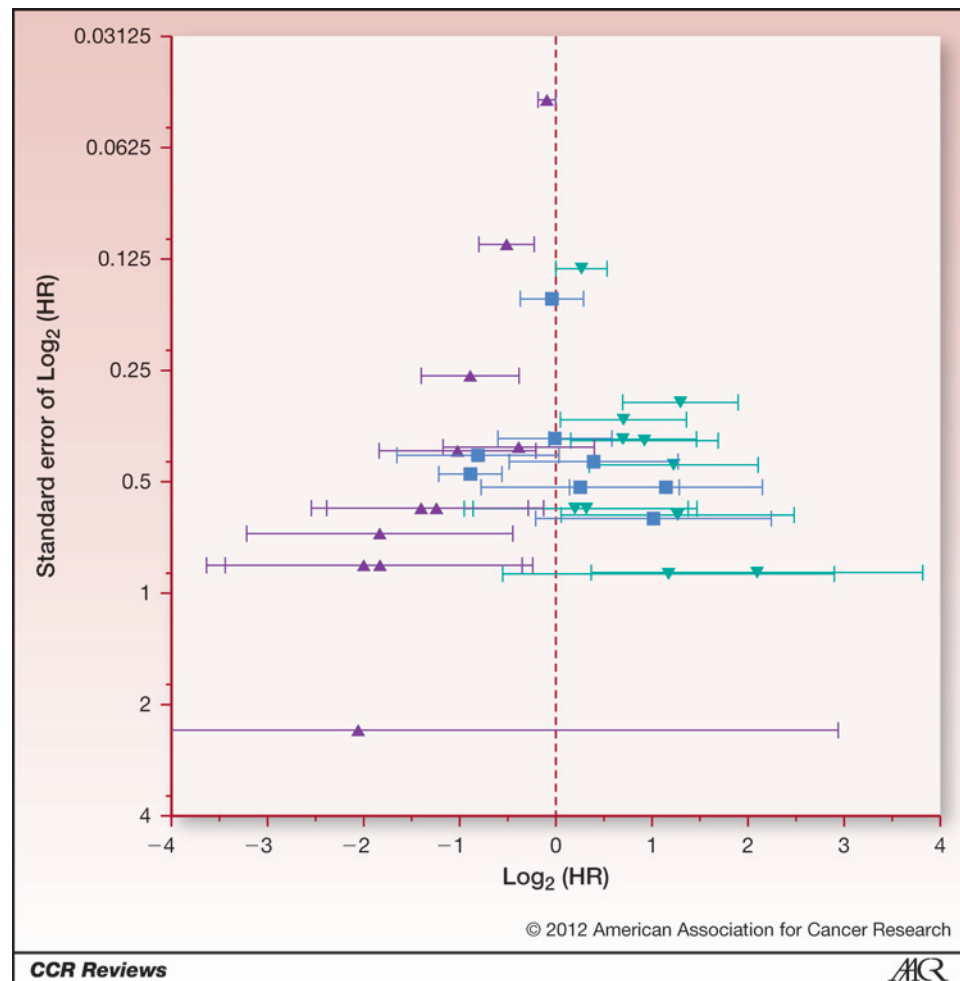
Although FoxP3 was originally thought to uniquely define conventional CD4+ Tregs (75), more recent studies indicate that, in some circumstances, FoxP3 can also be expressed by effector T cells (16, 18). We assessed whether studies that subdivided FoxP3+ T cells using a second marker yield more consistent prognostic results. Of the 58 reviewed studies, 50 used FoxP3 as a sole marker, which resulted in variable prognostic claims ranging from poor ( $n = 19$ ), to neutral ( $n = 19$ ), to good ( $n = 12$ ; Table 1). The remaining 8 studies measured at least one marker in addition to FoxP3, including CD4, CD8, CD25, and C-C chemokine receptor 4 (CCR4). Four of these 8 studies showed that FoxP3+ T cells that coexpressed a second marker were associated with poor prognosis. The remaining 4 claimed that the identified subset did not have any prognostic significance. Of note, none of the 8 studies claimed an association with good prognosis.

On the basis of the above findings, we investigated more closely which markers were used in addition to FoxP3. Shah and colleagues used 2-color IHC to identify both CD4+FoxP3+ and CD8+FoxP3+ T cells in cervical cancer. Intriguingly, they found CD8+FoxP3+ T cells at a mean number of 3.32 per high-power field and CD4+FoxP3+ T cells at a mean number of 11.45 per high-power field (30). Thus, had they used FoxP3 as a single marker, only ~75% of the cells they measured would have been CD4+ T cells, which underscores the fact that not all FoxP3+ T cells are conventional Tregs. In another study, Watanabe and colleagues used coexpression of CCR4 to delineate a subset of FoxP3-expressing T cells in oral cancer (62). An average of 58% of FoxP3+ cells were found to coexpress CCR4. Whereas total FoxP3+ T cells had no prognostic value (similar to 3 other studies of oral cancer; refs. 60, 61, 63), CCR4+FoxP3+ T cells showed a highly significant association with survival. These studies highlight the importance of using additional markers to account for the heterogeneity of FoxP3+ T cells.

### Tumor Site and Subtype

It is conceivable that the biologic and prognostic effect of FoxP3+ T cells depends on microenvironmental context, in which case, tumor site and histologic and/or molecular subtype may be important factors. Indeed, when tumor site was taken into consideration, we found clear prognostic associations in some cases. For example, the 5 studies of hepatocellular cancer unanimously concluded that FoxP3+ T cells are associated with a poor prognosis (Table 1). Conversely, 4 out of 10 studies investigating colorectal cancer concluded that FoxP3+ T cells correlated with a good prognosis, whereas the remaining 6 studies found no prognostic association. In considering colorectal cancer, Ladoire and colleagues recently hypothesized that the favorable prognostic effect of FoxP3+ T cells may reflect their ability to suppress tumor-promoting inflammatory responses to gut microbes (76).

**Figure 1.** Analysis of clinical significance and publication bias. The figure shows a funnel plot of log-transformed hazard ratios (HR) compared with standard error for the reviewed studies. Each symbol represents one study: ▼, poor prognostic claim; ▲, good prognostic claim; □, neutral prognostic claim. Bars represent 95% confidence intervals.



In contrast to the above examples, the prognostic significance of FoxP3+ T cells remains controversial in several other cancers. In breast cancer, the reported prognostic effect of FoxP3+ T cells ranges from poor ( $n = 5$ ), to neutral ( $n = 1$ ), to good ( $n = 2$ ). Although ovarian cancer was one of the first tumor sites in which CD4+ Tregs were associated with poor prognosis (5), subsequent studies using FoxP3 as a marker are split among poor ( $n = 1$ ), neutral ( $n = 4$ ), and good ( $n = 2$ ) prognostic claims. Similarly, studies looking at gastric cancers show a split among poor ( $n = 2$ ), neutral ( $n = 1$ ), and good ( $n = 2$ ) prognostic claims. For the remaining 10 tumor sites, the number of published studies is insufficient to make definitive conclusions about the prognostic significance of FoxP3+ T cells.

In addition to tissue of origin, tumors can be classified based on their molecular features, as discussed recently by Ogino and colleagues (77). Hence, it is conceivable that the variability of FoxP3+ T cell prognostication could be attributable to the inherent molecular heterogeneity within tumor types. In support of this idea, the prognostic value of FoxP3+ T cells is stronger in mismatch repair-proficient colorectal cancer compared with mismatch repair-deficient colorectal cancer (31). Similarly, FoxP3+ T cells are prog-

nostically significant in estrogen receptor (ER)+ but not ER- breast cancer (22, 27). In uveal melanoma, FoxP3+ T cells provide prognostic significance in cyclooxygenase-2+ cases (58). Although few in number, these studies suggest that the molecular subtype of tumors may influence the prognostic value of FoxP3 T cells.

## Conclusions

Having critically reviewed the literature on the prognostic value of FoxP3+ T cells, we can make several recommendations for future studies. (i) We recommend that prognostic marker studies follow a standard reporting structure, such as the REMARK criteria (78). (ii) In many cancers, FoxP3+ T cells are highly correlated with the stage and grade of disease; therefore, it is important to correct for these and other appropriate clinicopathologic factors. (iii) FoxP3+ T cells are invariably found with other lymphocytes; therefore, all TIL subsets with prognostic value should be included in multivariate models. (iv) The use of multiple markers to identify functional subsets of FoxP3+ T cells can lead to greater clarity about their prognostic value. (v) The prognostic value of FoxP3+ T cells seems to depend significantly on tumor site and possibly molecular subtype, suggesting

that the biologic properties of FoxP3<sup>+</sup> T cells are influenced by the tumor microenvironment in which they reside. Overall, this study provides a cautionary note for the concept of depleting FoxP3<sup>+</sup> cells from patients with cancer as a means to enhance tumor immunity. Our findings suggest that this strategy may be beneficial for some tumor sites (e.g., liver) but detrimental to others (e.g., colorectal). Improved understanding of the different FoxP3<sup>+</sup> T cell subsets in human cancer will likely enable the development of more precise and effective immunotherapies.

### Disclosure of Potential Conflicts of Interest

No potential conflicts of interest were disclosed.

### References

- Galon J, Costes A, Sanchez-Cabo F, Kirilovsky A, Mlecnik B, Lagorce-Pagès C, et al. Type, density, and location of immune cells within human colorectal tumors predict clinical outcome. *Science* 2006;313:1960–4.
- Leffers N, Gooden MJ, de Jong RA, Hoogeboom BN, ten Hoor KA, Hollema H, et al. Prognostic significance of tumor-infiltrating T-lymphocytes in primary and metastatic lesions of advanced stage ovarian cancer. *Cancer Immunol Immunother* 2009;58:449–59.
- Sato E, Olson SH, Ahn J, Bundy B, Nishikawa H, Qian F, et al. Intraepithelial CD8<sup>+</sup> tumor-infiltrating lymphocytes and a high CD8<sup>+</sup>/regulatory T cell ratio are associated with favorable prognosis in ovarian cancer. *Proc Natl Acad Sci U S A* 2005;102:18538–43.
- Zhang YL, Li J, Mo HY, Qiu F, Zheng LM, Qian CN, et al. Different subsets of tumor infiltrating lymphocytes correlate with NPC progression in different ways. *Mol Cancer* 2010;9:4.
- Curiel TJ, Coukos G, Zou L, Alvarez X, Cheng P, Mottram P, et al. Specific recruitment of regulatory T cells in ovarian carcinoma fosters immune privilege and predicts reduced survival. *Nat Med* 2004;10:942–9.
- Barnett B, Kryczek I, Cheng P, Zou W, Curiel TJ. Regulatory T cells in ovarian cancer: biology and therapeutic potential. *Am J Reprod Immunol* 2005;54:369–77.
- Morse MA, Hobeika AC, Osada T, Serra D, Niedzwiecki D, Lyerly HK, et al. Depletion of human regulatory T cells specifically enhances antigen-specific immune responses to cancer vaccines. *Blood* 2008;112:610–8.
- Powell DJ Jr, Attia P, Ghetie V, Schindler J, Vitetta ES, Rosenberg SA. Partial reduction of human FOXP3<sup>+</sup> CD4<sup>+</sup> T cells in vivo after CD25-directed recombinant immunotoxin administration. *J Immunother* 2008;31:189–98.
- Shevach EM. CD4<sup>+</sup> CD25<sup>+</sup> suppressor T cells: more questions than answers. *Nat Rev Immunol* 2002;2:389–400.
- Sakaguchi S, Yamaguchi T, Nomura T, Ono M. Regulatory T cells and immune tolerance. *Cell* 2008;133:775–87.
- Sakaguchi S, Ono M, Setoguchi R, Yagi H, Hori S, Fehervari Z, et al. Foxp3<sup>+</sup> CD25<sup>+</sup> CD4<sup>+</sup> natural regulatory T cells in dominant self-tolerance and autoimmune disease. *Immunol Rev* 2006;212:8–27.
- Correale P, Rotundo MS, Del Vecchio MT, Remondo C, Migali C, Ginanneschi C, et al. Regulatory (FoxP3<sup>+</sup>) T-cell tumor infiltration is a favorable prognostic factor in advanced colon cancer patients undergoing chemo or chemimmunotherapy. *J Immunother* 2010;33:435–41.
- Milne K, Kaloger SE, Barnes RO, Gao D, Gilks CB, et al. Systematic analysis of immune infiltrates in high-grade serous ovarian cancer reveals CD20, FoxP3 and TIA-1 as positive prognostic factors. *PLoS ONE* 2009;4:e6412.
- Haas M, Dimmler A, Hohenberger W, Grabenbauer GG, Niedobitek G, Distel LV. Stromal regulatory T-cells are associated with a favourable prognosis in gastric cancer of the cardia. *BMC Gastroenterol* 2009;9:65.
- Martin F, Ladoire S, Mignot G, Apetoh L, Ghiringhelli F. Human FOXP3 and cancer. *Oncogene* 2010;29:4121–9.
- Miyara M, Yoshioka Y, Kitoh A, Shima T, Wing K, Niwa A, et al. Functional delineation and differentiation dynamics of human CD4<sup>+</sup> T cells expressing the FoxP3 transcription factor. *Immunity* 2009;30:899–911.
- Strauss L, Bergmann C, Szczepanski M, Gooding W, Johnson JT, Whiteside TL. A unique subset of CD4<sup>+</sup>CD25<sup>high</sup>Foxp3<sup>+</sup> T cells secreting interleukin-10 and transforming growth factor-beta1 mediates suppression in the tumor microenvironment. *Clin Cancer Res* 2007;13:4345–54.
- Thornton AM, Korty PE, Tran DQ, Wohlfert EA, Murray PE, Belkaid Y, et al. Expression of Helios, an Ikaros transcription factor family member, differentiates thymic-derived from peripherally induced Foxp3<sup>+</sup> T regulatory cells. *J Immunol* 2010;184:3433–41.
- Winerdal ME, Marits P, Winerdal M, Hasan M, Rosenblatt R, Tolf A, et al. FOXP3 and survival in urinary bladder cancer. *BJU Int* 2011;108:1672–8.
- Whiteside TL. Immune responses to malignancies. *J Allergy Clin Immunol* 2010;125[Suppl 2]:S272–83.
- Aruga T, Suzuki E, Saji S, Horiguchi S, Horiguchi K, Sekine S, et al. A low number of tumor-infiltrating FOXP3-positive cells during primary systemic chemotherapy correlates with favorable anti-tumor response in patients with breast cancer. *Oncol Rep* 2009;22:273–8.
- Bates GJ, Fox SB, Han C, Leek RD, Garcia JF, Harris AL, et al. Quantification of regulatory T cells enables the identification of high-risk breast cancer patients and those at risk of late relapse. *J Clin Oncol* 2006;24:5373–80.
- de Kruijff EM, van Nes JG, Sajet A, Tummers QR, Putter H, Osanto S, et al. The predictive value of HLA class I tumor cell expression and presence of intratumoral Tregs for chemotherapy in patients with early breast cancer. *Clin Cancer Res* 2010;16:1272–80.
- Ladoire S, Arnould L, Apetoh L, Coudert B, Martin F, Chauffert B, et al. Pathologic complete response to neoadjuvant chemotherapy of breast carcinoma is associated with the disappearance of tumor-infiltrating foxp3<sup>+</sup> regulatory T cells. *Clin Cancer Res* 2008;14:2413–20.
- Ladoire S, Arnould L, Mignot G, Coudert B, Rébé C, Chalmin F, et al. Presence of Foxp3 expression in tumor cells predicts better survival in HER2-overexpressing breast cancer patients treated with neoadjuvant chemotherapy. *Breast Cancer Res Treat* 2011;125:65–72.
- Liu F, Lang R, Zhao J, Zhang X, Pringle GA, Fan Y, et al. CD8<sup>+</sup> cytotoxic T cell and FOXP3<sup>+</sup> regulatory T cell infiltration in relation to breast cancer survival and molecular subtypes. *Breast Cancer Res Treat* 2011;130:645–55.
- Mahmoud SM, Paish EC, Powe DG, Macmillan RD, Lee AH, Ellis IO, et al. An evaluation of the clinical significance of FOXP3<sup>+</sup> infiltrating cells in human breast cancer. *Breast Cancer Res Treat* 2011;127:99–108.
- Yan M, Jene N, Byrne D, Millar EK, O'Toole SA, McNeil CM, et al. Recruitment of regulatory T cells is correlated with hypoxia-induced

### Authors' Contributions

**Conception and design:** R.J. deLeeuw, B.H. Nelson

**Development of methodology:** B.H. Nelson

**Acquisition of data:** R.J. deLeeuw, S.E. Kost, J.A. Kakal

**Analysis and interpretation of data:** R.J. deLeeuw, S.E. Kost, B.H. Nelson

**Writing, review, and/or revision of the manuscript:** R.J. deLeeuw, S.E. Kost, J.A. Kakal, B.H. Nelson

**Study supervision:** R.J. deLeeuw, B.H. Nelson

### Grant Support

British Columbia Cancer Foundation, Canadian Institutes of Health Research, and National Science and Engineering Research Council of Canada.

Received December 13, 2011; revised March 16, 2012; accepted March 25, 2012; published OnlineFirst April 17, 2012.

- CXCR4 expression, and is associated with poor prognosis in basal-like breast cancers. *Breast Cancer Res* 2011;13:R47.
29. Jordanova ES, Gorter A, Ayachi O, Prins F, Durrant LG, Kenter GG, et al. Human leukocyte antigen class I, MHC class I chain-related molecule A, and CD8+/regulatory T-cell ratio: which variable determines survival of cervical cancer patients? *Clin Cancer Res* 2008;14:2028–35.
  30. Shah W, Yan X, Jing L, Zhou Y, Chen H, Wang Y. A reversed CD4/CD8 ratio of tumor-infiltrating lymphocytes and a high percentage of CD4 (+)FOXP3(+) regulatory T cells are significantly associated with clinical outcome in squamous cell carcinoma of the cervix. *Cell Mol Immunol* 2011;8:59–66.
  31. Frey DM, Droeser RA, Viehl CT, Zlobec I, Lugli A, Zingg U, et al. High frequency of tumor-infiltrating FOXP3(+) regulatory T cells predicts improved survival in mismatch repair-proficient colorectal cancer patients. *Int J Cancer* 2010;126:2635–43.
  32. Grabenbauer GG, Lahmer G, Distel L, Niedobitek G. Tumor-infiltrating cytotoxic T cells but not regulatory T cells predict outcome in anal squamous cell carcinoma. *Clin Cancer Res* 2006;12:3355–60.
  33. Lee WS, Park S, Lee WY, Yun SH, Chun HK. Clinical impact of tumor-infiltrating lymphocytes for survival in stage II colon cancer. *Cancer* 2010;116:5188–99.
  34. Loddenkemper C, Schernus M, Noutsias M, Stein H, Thiel E, Nagorsen D. In situ analysis of FOXP3+ regulatory T cells in human colorectal cancer. *J Transl Med* 2006;4:52.
  35. Noshok K, Baba Y, Tanaka N, Shima K, Hayashi M, Meyerhardt JA, et al. Tumour-infiltrating T-cell subsets, molecular changes in colorectal cancer, and prognosis: cohort study and literature review. *J Pathol* 2010;222:350–66.
  36. Salama P, Phillips M, Grieco F, Morris M, Zeps N, Joseph D, et al. Tumor-infiltrating FOXP3+ T regulatory cells show strong prognostic significance in colorectal cancer. *J Clin Oncol* 2009;27:186–92.
  37. Sinicrope FA, Rego RL, Ansell SM, Knutson KL, Foster NR, Sargent DJ. Intraepithelial effector (CD3+)/regulatory (FoxP3+) T-cell ratio predicts a clinical outcome of human colon carcinoma. *Gastroenterology* 2009;137:1270–9.
  38. Suzuki H, Chikazawa N, Tasaka T, Wada J, Yamasaki A, Kitaura Y, et al. Intratumoral CD8(+) T/FOXP3 (+) cell ratio is a predictive marker for survival in patients with colorectal cancer. *Cancer Immunol Immunother* 2010;59:653–61.
  39. Zeestraten EC, Van Hoesel AQ, Speetjens FM, Menon AG, Putter H, van de Velde CJ, et al. FoxP3- and CD8-positive infiltrating immune cells together determine clinical outcome in colorectal cancer. *Cancer Microenviron* 2011 Jul 6. [Epub ahead of print].
  40. de Jong RA, Leffers N, Boezen HM, ten Hoor KA, van der Zee AG, Hollema H, et al. Presence of tumor-infiltrating lymphocytes is an independent prognostic factor in type I and II endometrial cancer. *Gynecol Oncol* 2009;114:105–10.
  41. Giatromanolaki A, Bates GJ, Koukourakis MI, Sivridis E, Gatter KC, Harris AL, et al. The presence of tumor-infiltrating FOXP3+ lymphocytes correlates with intratumoral angiogenesis in endometrial cancer. *Gynecol Oncol* 2008;110:216–21.
  42. Yamagami W, Susumu N, Tanaka H, Hirasawa A, Banno K, Suzuki N, et al. Immunofluorescence-detected infiltration of CD4+FOXP3+ regulatory T cells is relevant to the prognosis of patients with endometrial cancer. *Int J Gynecol Cancer* 2011;21:1628–34.
  43. Mizukami Y, Kono K, Kawaguchi Y, Akaike H, Kamimura K, Sugai H, et al. Localisation pattern of Foxp3+ regulatory T cells is associated with clinical behaviour in gastric cancer. *Br J Cancer* 2008;98:148–53.
  44. Perrone G, Ruffini PA, Catalano V, Spino C, Santini D, Mureto P, et al. Intratumoral FOXP3-positive regulatory T cells are associated with adverse prognosis in radically resected gastric cancer. *Eur J Cancer* 2008;44:1875–82.
  45. Shen Z, Zhou S, Wang Y, Li RL, Zhong C, Liang C, et al. Higher intratumoral infiltrated Foxp3+ Treg numbers and Foxp3+/CD8+ ratio are associated with adverse prognosis in resectable gastric cancer. *J Cancer Res Clin Oncol* 2010;136:1585–95.
  46. Wang B, Xu D, Yu X, Ding T, Rao H, Zhan Y, et al. Association of intra-tumoral infiltrating macrophages and regulatory T cells is an independent prognostic factor in gastric cancer after radical resection. *Ann Surg Oncol* 2011;18:2585–93.
  47. Sun DS, Zhao MQ, Xia M, Li L, Jiang YH. The correlation between tumor-infiltrating Foxp3+ regulatory T cells and cyclooxygenase-2 expression and their association with recurrence in resected head and neck cancers. *Med Oncol* 2011 Mar 22. [Epub ahead of print]. PubMed
  48. Chen KJ, Zhou L, Xie HY, Ahmed TE, Feng XW, Zheng SS. Intratumoral regulatory T cells alone or in combination with cytotoxic T cells predict prognosis of hepatocellular carcinoma after resection. *Med Oncol* 2011 Jun 16. [Epub ahead of print]. PubMed
  49. Gao Q, Qiu SJ, Fan J, Zhou J, Wang XY, Xiao YS, et al. Intratumoral balance of regulatory and cytotoxic T cells is associated with prognosis of hepatocellular carcinoma after resection. *J Clin Oncol* 2007;25:2586–93.
  50. Kobayashi N, Hiraoka N, Yamagami W, Ojima H, Kanai Y, Kosuge T, et al. FOXP3 +regulatory T cells affect the development and progression of hepatocarcinogenesis. *Clin Cancer Res* 2007;13:902–11.
  51. Sasaki A, Tanaka F, Mimori K, Inoue H, Kai S, Shibata K, et al. Prognostic value of tumor-infiltrating FOXP3+ regulatory T cells in patients with hepatocellular carcinoma. *Eur J Surg Oncol* 2008;34:173–9.
  52. Zhou J, Ding T, Pan W, Zhu LY, Li L, Zheng L. Increased intratumoral regulatory T cells are related to intratumoral macrophages and poor prognosis in hepatocellular carcinoma patients. *Int J Cancer* 2009;125:1640–8.
  53. Shimizu K, Nakata M, Hiram Y, Yukawa T, Maeda A, Tanemoto K. Tumor-infiltrating Foxp3+ regulatory T cells are correlated with cyclooxygenase-2 expression and are associated with recurrence in resected non-small cell lung cancer. *J Thorac Oncol* 2010;5:585–90.
  54. Tao H, Mimura Y, Aoe K, Kobayashi S, Yamamoto H, Matsuda E, et al. Prognostic potential of FOXP3 expression in non-small cell lung cancer cells combined with tumor-infiltrating regulatory T cells. *Lung Cancer* 2012;75:95–101.
  55. Hillen F, Baeten CI, van de Winkel A, Creyten D, van der Schaft DW, Winnepenninckx V, et al. Leukocyte infiltration and tumor cell plasticity are parameters of aggressiveness in primary cutaneous melanoma. *Cancer Immunol Immunother* 2008;57:97–106.
  56. Ladányi A, Mohos A, Somlai B, Liskay G, Gilde K, Fejos Z, et al. FOXP3+ cell density in primary tumor has no prognostic impact in patients with cutaneous malignant melanoma. *Pathol Oncol Res* 2010;16:303–9.
  57. Miracco C, Mourmouras V, Biagioli M, Rubegni P, Mannucci S, Monciatti I, et al. Utility of tumour-infiltrating CD25+FOXP3+ regulatory T cell evaluation in predicting local recurrence in vertical growth phase cutaneous melanoma. *Oncol Rep* 2007;18:1115–22.
  58. Mougialakos D, Johansson CC, Trocme E, Ali-Ericsson C, Economou MA, Larsson O, et al. Intratumoral forkhead box P3-positive regulatory T cells predict poor survival in cyclooxygenase-2-positive uveal melanoma. *Cancer* 2010;116:2224–33.
  59. Anraku M, Cunningham KS, Yun Z, Tsao MS, Zhang L, Keshavjee S, et al. Impact of tumor-infiltrating T cells on survival in patients with malignant pleural mesothelioma. *J Thorac Cardiovasc Surg* 2008;135:823–9.
  60. Distel LV, Fickenscher R, Dietel K, Hung A, Iro H, Zenk J, et al. Tumour infiltrating lymphocytes in squamous cell carcinoma of the oro- and hypopharynx: prognostic impact may depend on type of treatment and stage of disease. *Oral Oncol* 2009;45:e167–74.
  61. Pretscher D, Distel LV, Grabenbauer GG, Wittlinger M, Buettner M, Niedobitek G. Distribution of immune cells in head and neck cancer: CD8+ T-cells and CD20+ B-cells in metastatic lymph nodes are associated with favourable outcome in patients with oro- and hypopharyngeal carcinoma. *BMC Cancer* 2009;9:292.
  62. Watanabe Y, Katou F, Ohtani H, Nakayama T, Yoshie O, Hashimoto K. Tumor-infiltrating lymphocytes, particularly the balance between CD8 (+) T cells and CCR4(+) regulatory T cells, affect the survival of patients with oral squamous cell carcinoma. *Oral Surg Oral Med Oral Pathol Oral Radiol Endod* 2010;109:744–52.
  63. Zingg U, Montani M, Frey DM, Dirnhofer S, Esterman AJ, Went P, et al. Tumour-infiltrating lymphocytes and survival in patients with adenocarcinoma of the oesophagus. *Eur J Surg Oncol* 2010;36:670–7.

64. Adams SF, Levine DA, Cadungog MG, Hammond R, Facciabene A, Olvera N, et al. Intraepithelial T cells and tumor proliferation: impact on the benefit from surgical cytoreduction in advanced serous ovarian cancer. *Cancer* 2009;115:2891–902.
65. Barnett JC, Bean SM, Whitaker RS, Kondoh E, Baba T, Fujii S, et al. Ovarian cancer tumor infiltrating T-regulatory (T(reg)) cells are associated with a metastatic phenotype. *Gynecol Oncol* 2010;116:556–62.
66. Pölcher M, Braun M, Friedrichs N, Rudlowski C, Bercht E, Fimmers R, et al. Foxp3(+) cell infiltration and granzyme B(+)/Foxp3(+) cell ratio are associated with outcome in neoadjuvant chemotherapy-treated ovarian carcinoma. *Cancer Immunol Immunother* 2010;59:909–19.
67. Shah CA, Allison KH, Garcia RL, Gray HJ, Goff BA, Swisher EM. Intratumoral T cells, tumor-associated macrophages, and regulatory T cells: association with p53 mutations, circulating tumor DNA and survival in women with ovarian cancer. *Gynecol Oncol* 2008;109:215–9.
68. Hiraoka N, Onozato K, Kosuge T, Hirohashi S. Prevalence of FOXP3+ regulatory T cells increases during the progression of pancreatic ductal adenocarcinoma and its premalignant lesions. *Clin Cancer Res* 2006;12:5423–34.
69. Li JF, Chu YW, Wang GM, Zhu TY, Rong RM, Hou J, et al. The prognostic value of peritumoral regulatory T cells and its correlation with intratumoral cyclooxygenase-2 expression in clear cell renal cell carcinoma. *BJU Int* 2009;103:399–405.
70. Siddiqui SA, Frigola X, Bonne-Annee S, Mercader M, Kuntz SM, Krambeck AE, et al. Tumor-infiltrating Foxp3-CD4+CD25+ T cells predict poor survival in renal cell carcinoma. *Clin Cancer Res* 2007;13:2075–81.
71. de Jong RA, Toppen NL, Ten Hoor KA, Boezen HM, Kema IP, Hollema H, et al. Status of cellular immunity lacks prognostic significance in vulvar squamous carcinoma. *Gynecol Oncol* 2012;125:186–93.
72. Tran DQ, Ramsey H, Shevach EM. Induction of FOXP3 expression in naive human CD4+FOXP3 T cells by T-cell receptor stimulation is transforming growth factor-beta dependent but does not confer a regulatory phenotype. *Blood* 2007;110:2983–90.
73. Woo YL, Sterling J, Crawford R, van der Burg SH, Coleman N, Stanley M. FOXP3 immunohistochemistry on formalin-fixed paraffin-embedded tissue: poor correlation between different antibodies. *J Clin Pathol* 2008;61:969–71.
74. Ogino S, Noshio K, Irahara N, Meyerhardt JA, Baba Y, Shima K, et al. Lymphocytic reaction to colorectal cancer is associated with longer survival, independent of lymph node count, microsatellite instability, and CpG island methylator phenotype. *Clin Cancer Res* 2009;15:6412–20.
75. Kryczek I, Liu R, Wang G, Wu K, Shu X, Szeliga W, et al. FOXP3 defines regulatory T cells in human tumor and autoimmune disease. *Cancer Res* 2009;69:3995–4000.
76. Ladoire S, Martin F, Ghiringhelli F. Prognostic role of FOXP3+ regulatory T cells infiltrating human carcinomas: the paradox of colorectal cancer. *Cancer Immunol Immunother* 2011;60:909–18.
77. Ogino S, Galon J, Fuchs CS, Dranoff G. Cancer immunology—analysis of host and tumor factors for personalized medicine. *Nat Rev Clin Oncol* 2011;8:711–9.
78. McShane LM, Altman DG, Sauerbrei W, Taube SE, Gion M, Clark GM. Statistics Subcommittee of NCI-EORTC Working Group on Cancer Diagnostics. REporting recommendations for tumor MARKer prognostic studies (REMARK). *Breast Cancer Res Treat* 2006;100:229–35.